GEORGIA INSTITUTE OF TECHNOLOGY — OFFICE OF CONTRACT ADMINISTRATION

PROJECT ADMINISTRATION DATA SHEET

[X] ORIGINAL [ ] REVISION NO. _____

Project No. E-16-681 R6111-0A0 GTRC/~~GTX~~ DATE 4 / 14 / 86

Project Director: Dr. A.J. Calise School/~~SAK~~ AE

Sponsor: NASA Langley Research Center Hampton, VA 23665-5225

Type Agreement: Grant No. NAG-1-660

Award Period: From 3/11/86 To ~~3/10/87~~ 7/31/87 (Performance) ~~3/10/87~~ 7/31/87 (Reports)

Sponsor Amount:	This Change	Total to Date
Estimated:	$ 196,642.00	$ 196,642.00
Funded:	$ 58,000.00	$ 58,000.00

Cost Sharing Amount: $ 5,883.00 Cost Sharing No: E-16-385 F6111-0A0

Title: Singular Perturbation Analysis of AOTV Related Trajectory Optimization Problems

ADMINISTRATIVE DATA OCA Contact R. Dennis Farmer X4820

1) Sponsor Technical Contact:	2) Sponsor Admin/Contractual Matters:
Dr. Christopher Gracey	Mr. John F. Royall
GCD M/S 489	NASA Langley Research Center
NASA Langley Research Center	Mail Stop 126
Hampton, VA 23665	Hampton, VA 23665-5225
(804) 865-4681	(804) 865-3215

Defense Priority Rating: N/A Military Security Classification: UNCLASSIFIED

(or) Company/Industrial Proprietary: N/A

RESTRICTIONS

See Attached NASA Supplemental Information Sheet for Additional Requirements.

Travel: Foreign travel must have prior approval – Contact OCA in each case. Domestic travel requires sponsor approval where total will exceed greater of $500 or 125% of approved proposal budget category.

Equipment: Title vests with Georgia Tech if less than $1,000.00, greater than $1,000.00 Sponsor retains the right to retain title, However, none proposed.

COMMENTS:

Contract OCA Subcontracts to initiate Subcontracting Agreements.

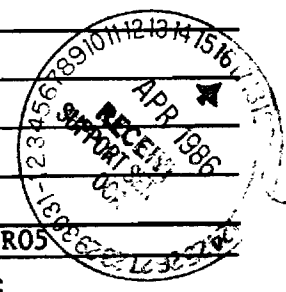

COPIES TO: SPONSOR'S I. D. NO. 02.105.001.86.R05

Project Director
Research Administrative Network
Research Property Management
Accounting
Procurement/EES Supply Services
Research Security Services
Reports Coordinator (OCA)
Research Communications (2)
GTRC
Library
Project File
Other

GEORGIA INSTITUTE OF TECHNOLOGY
OFFICE OF CONTRACT ADMINISTRATION

PROJECT SUMMARY
CLOSEOUT COMPLETE

Closeout Complete Date ********

Project No. E-16-681 Center No. R6111-0A0

Project Director CALISE A J School/Lab AE

Sponsor NASA/LANGLEY RESEARCH CTR, VA

Contract/Grant No. NAG 1-660 Contract Entity GTRC

Prime Contract No.

Title SINGULAR PERTURB ANALY OF AOTV RELATED TRAJECTORY OPTIMIZATION PROBLEMS

Effective Completion Date 900131 (Performance) 900131 (Reports)

Closeout Actions:	Y/N	Date Submitted
Final Invoice or Copy of Final Invoice	Y	
Final Report of Inventions and/or Subcontracts	Y	
Government Property Inventory & Related Certificate	Y	890710
Classified Material Certificate	N	
Release and Assignment	N	
Other	N	

Comments

Subproject Under Main Project No.

Continues Project No.

Distribution:

Project Director	Y
Administrative Network Representative	Y
GTRI Accounting/Grants and Contracts	Y
Procurement/Supply Services	Y
Research Property Managment	Y
Research Security Services	N
Reports Coordinator (OCA)	Y
GTRC	Y
Project File	Y
Other	N
	N

E-1601

SINGULAR PERTURBATION ANALYSIS OF AOTV RELATED TRAJECTORY OPTIMIZATION PROBLEMS

PROGRESS REPORT

14 April - 30 October, 1986

November 1986

Research Supported by NASA - Langley Research Center

NASA Grant No. NAG-1-660

Principal Investigator: Dr. Anthony J. Calise
Research Assistant: Mr. Gyoung Bae
NASA Grant Monitor: Dr. Christopher Gracey

Georgia Institute of Technology
School of Aerospace Engineering
Atlanta, GA 30332

Table of Contents

SUMMARY

Research during this period has concentrated on the problem of aeroassisted orbital plane change. This maneuver requires the use of three impulses - one to deorbit, one to reorbit and one to recircularize at the new orbit. The orbit plane change is effected entirely in the atmosphere through the use of lift and bank angle control. For circular orbits of nearly equal radii, it can be shown that the fuel consumption is minimized by minimizing the energy loss in the atmospheric portion of the trajectory. The research explores the use of singular perturbation theory to develop an optimal guidance law for the atmospheric portion.

The results to date indicate that singular perturbation methods can be applied; however, a difficult terminal boundary analysis is required. The reduced solution models only the heading rate dynamics, and produces a realistic profile (altitude versus energy) and control to be flown. A large terminal boundary layer is required to match the terminal constraint on altitude. Most of our effort has been directed at approximate methods for solving the terminal boundary layer equations. The equations result from an analysis of altitude and flight path angle dynamics on the same time scale. A nonlinear control law was derived which produces near optimal results. However, the current solution is difficult to implement because it requires two switches in the control solution that are heading and altitude dependent. In general, the solution is very sensitive to switching times. We propose two alternatives to be investigated during the next reporting period. The first relies on a linearization of the necessary conditions about the reduced solution and the second will examine the analysis of altitude and flight path angle dynamics on separate boundary layers.

1. PROBLEM FORMULATION

The following three state model has been the subject of our current research

$$\dot{\psi} = C_L^* \rho S V \lambda \sin\mu / 2m\cos\gamma \tag{1}$$

$$\varepsilon\dot{h} = V\sin\gamma \tag{2}$$

$$\varepsilon\dot{\gamma} = C_L^* \rho S V(\lambda\cos\mu + M\cos\gamma)/2m \tag{3}$$

where

$$M(h,V) = (2m/C_L^* S)[1-\bar{\mu}/V^2 r]/\rho r \tag{4}$$

$$r = r_s + h \tag{5}$$

and $\bar{\mu}$ is the gravitational constant. The objective is to minimize the energy loss

$$J = -\int_0^{t_f} \dot{E}\, dt \tag{6}$$

where E is the total energy per unit mass

$$E = V^2/2 - \bar{\mu}/r < 0 \tag{7}$$

The expression for the energy rate in (6) is

$$\dot{E} = -C_D^* (1 + \lambda^2)\rho S V^3/4m \tag{8}$$

where a parabolic drag polar form is used to define the drag coefficient

$$C_D = C_{Do} + KC_L^2 \tag{9}$$

In the above equations the superscript * denotes the lift and drag coefficient values at maximum L/D

$$C_L^* = (C_{Do}/K)^{1/2} \qquad C_D^* = 2C_{Do} \tag{10}$$

The controls are bank angle (μ) and the normalized lift coefficient

$$\lambda = C_L/C_L^* \tag{11}$$

Note that in this formulation we treat E as constant, but account for the energy loss through the performance index.

In [1] the sensible atmosphere is assumed to occur at h_o = 200,000 ft. The starting velocity and flight path angle (V_o,γ_o) are derived using a deorbit impulse ΔV_1 from circular orbit at h_c = 100 nm, which is optimized for the atmospheric maneuver of interest. The initial heading angle is taken as zero. In the SPT formulation, altitude appears as a control variable in the reduced problem. The optimal solution has the form

$$h^* = h(E) \tag{12}$$

For comparison purposes, in this study the starting energy is chosen to match that of [1], and h_o, V_o are derived from (7) and (12). From conservation of energy this results in the same deorbit impulse, but slightly different values for h_o, V_o. The initial flight path angle is derived from conservation of angular momentum.

$$\gamma_o = -\cos^{-1}[(r_s + h_c)(V_c - \Delta V_1)/(r_s + h_o)V] \tag{13}$$

where r_s is the mean earth radius and $V_c = [\bar{\mu}/(r_s+h)]^{1/2}$. The vehicle begins the maneuver with a mass m_c and, as a result of the deorbit impulse, the mass for the atmospheric portion is given by

$$m = m_c \exp(-\Delta V_1/C) \tag{14}$$

where C is the characteristic velocity. The terminal conditions are:

$$h(t_f) = 200{,}000 \text{ ft}, \quad \psi(t_f) = \psi_f > 0 \tag{15}$$

Since the condition on $h(t_f)$ is lost in the reduced solution (12), a terminal boundary layer correction is required.

2. SINGULAR PERTURBATION ANALYSIS

2.1 Reduced Problem

Setting $\varepsilon = 0$ in (1-3) the necessary conditions for optimality become

$$H_o = \lambda_\psi \dot{\psi} - \dot{E} = 0 \tag{16}$$

$$\gamma = 0 \qquad \lambda\cos\mu = -M \tag{17}$$

$$\mu_o, h_o = \arg\min_{h,\mu} \{\dot{\psi}/\dot{E}\} \tag{18}$$

It can be shown that this results in the following reduced solution:

$$\lambda_o = (1 + 2M_o^2)^{1/2} \tag{19}$$

$$\sin\mu_o = [(1 + M_o^2)/(1 + 2M_o^2)]^{1/2} \tag{20}$$

$$h_o = \arg \min_h \{V^2(1 + M^2)^{1/2}\}|_{E = \text{const.}} \tag{21}$$

where M_o is the value of M for $h = h_o$. The quadrant for the bank angle in (20) is resolved based on the following inequalities:

$$0 < \mu_o < \pi/2 \text{ for } M < 0 \tag{22}$$

$$\pi/2 < \mu_o < \pi \text{ for } M > 0 \tag{23}$$

It can be seen from the above solution that M plays a crucial role in the solution process. In [1], M was treated as a constant in the dynamics.

Since most of the energy is kinetic, V is weakly dependent on h for constant E. This can readily be seen from (7) and (5) where changes in h give rise to small changes in r. Thus, the minimization in (21) results in a value for M very close to zero. The interpretation is that the maneuver should be performed at an altitude where gravitational and centripetal forces nearly cancel one another. For M small, it can be seen from (19,20) that the maneuver is performed at near maximum L/D and at near 90 of bank angle. These results are in good agreement with the results in [1]. Figure 1 compares the altitude profiles derived from (21) with the true optimal profile taken from [1]. The need for a terminal boundary layer analysis is evident in this figure. However, if the vehicle was not required to exit the atmosphere, the reduced solution may be sufficiently accurate.

2.2 Boundary Layer Problem

A boundary layer analysis is required to obtain a guidance law that will both follow the altitude profile defined by (21) (initial boundary layer) and

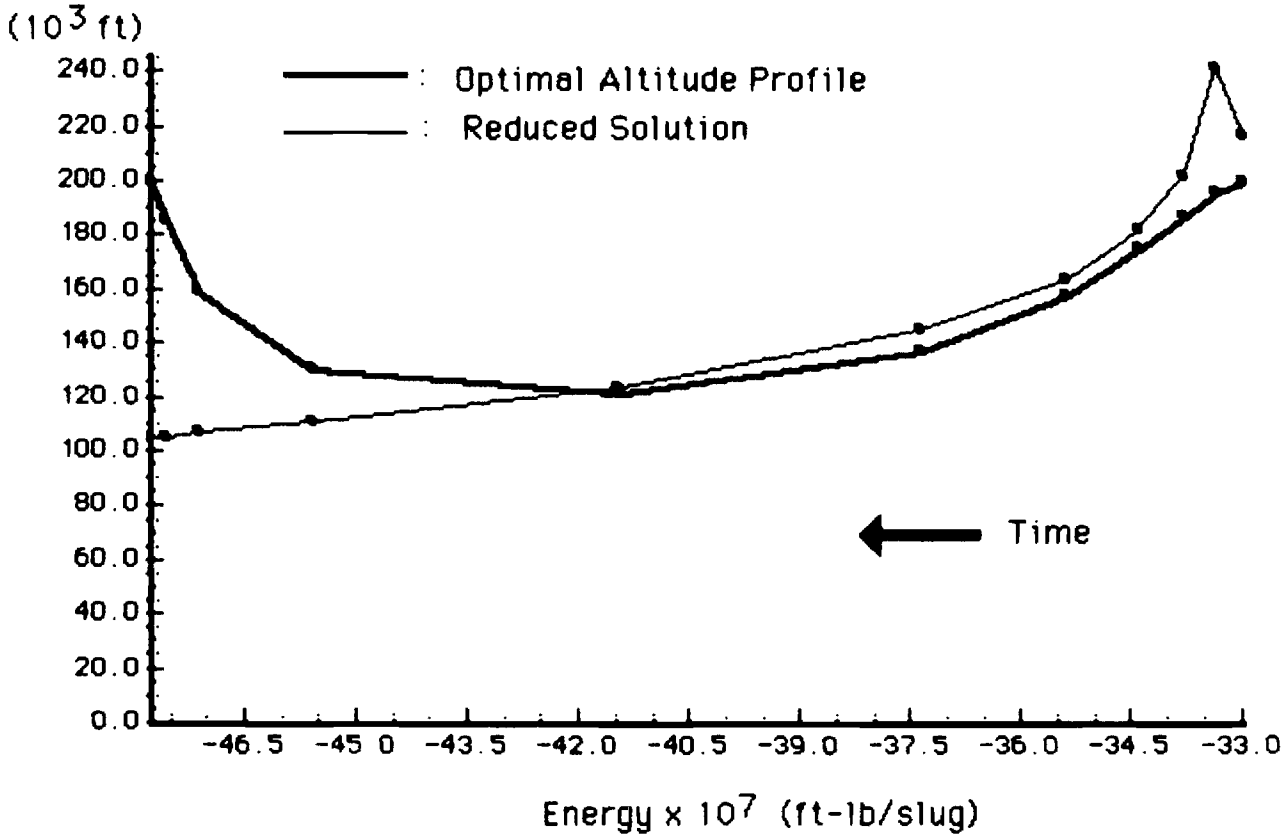

Figure 1. Comparison of the reduced solution with the true optimal profile.

satisfy the terminal constraint on altitude (terminal boundary layer). The necessary conditions in the boundary layer are:

$$H_{BL} = \lambda_\psi^o \dot{\psi} + \lambda_h V\sin\gamma + \lambda_\gamma \dot{\gamma} - \dot{E} = 0 \tag{24}$$

$$\partial H_{BL}/\partial L_1 = 0, \qquad \partial H_{BL}/\partial L_2 = 0 \tag{25}$$

where λ_ψ^o is determined in the reduced solution from (16)

$$\lambda_\psi^o = \dot{E}^o/\dot{\psi}^o \tag{26}$$

using the solutions for λ_o, μ_o and h_o. In (25), L_1 and L_2 represent the horizontal and vertical components of lift coefficient

$$L_1 = \lambda\sin\mu \qquad L_2 = \lambda\cos\mu \tag{27}$$

which are now used as control variables in place of λ and μ.

The first condition in (25) results in

$$L_1^* = (V_o/V)^2(1 + M_o)^{1/2}/\cos\gamma \tag{28}$$

where M_o, V_o are the values of M and V corresponding to $h = h_o$ for the current value of E. This solution approaches the corresponding reduced solution as h approaches h_o.

The second condition in (25) yields

$$L_2^* = -(C_L^*/C_D^*V^2)\lambda_\gamma \tag{29}$$

which can also be shown to approach the reduced solution as h approaches h_o,

where

$$\lambda_\gamma^o = C_D^* V_o^2 M_o / C_L^* \tag{30}$$

Unfortunately, evaluation of λ_γ needed in (29) requires the solution of a two-point boundary value problem. When close to the reduced solution it may be possible to use (30), which results in the following expression for flight path angle rate

$$\dot{\gamma} = C_L^* \rho S V (M\cos\gamma - V_o^2 M_o / V^2)/2m \tag{31}$$

For γ near zero and h near h_o, (31) simplifies to

$$\dot{\gamma} = C_L^* \rho S V_o (M - M_o) \tag{32}$$

To obtain a feedback solution for the general case we neglected the second term in (24). This was done on the basis that $\lambda_h^o = 0$ and γ is small over the entire optimal trajectory. This results in the following explicit solution for L_2

$$L_2^* = -M\cos\gamma \pm (M^2\cos^2\gamma - L_1^2 + 1)^{1/2} \tag{33}$$

The first term on the right hand side of (33) is simply the lift required to maintain zero flight path angle rate. The second term is always > 0 and asymptotically approaches zero as $h \to h_o$ and $\gamma \to o$. Thus this solution also asymptotically approaches the reduced solution. Both solutions in (33) satisfy the conditions that H_{BL} is minimized and $H_{BL} = 0$. During the initial boundary layer the + sign is used when $h < h_o$ to generate a positive flight path angle rate, and the minus sign used when $h > h_o$. The corresponding

value of the costate variable is

$$\lambda_\gamma^* = (\lambda_\psi^o \dot{\psi} - \dot{E}^*)/\dot{\gamma}^* \tag{34}$$

which approaches an indeterminate form (0/0) as $h \to h_o$ and $\gamma \to 0$. The + sign is used to initiate the terminal boundary layer.

At this time repeated trial runs are required to determine the switching time so that the desired final heading is achieved when the altitude reaches 200,000 ft. Also, a characteristic of these profiles is that L_1 remains close to 1.0 throughout, while M grows to a large negative number near the end (on the order of -2.0). This is due to the presence of ρ in the denominator of (4). Thus there is every indication that the sign should be switched again in (33) prior to the end of the trajectory so that L_2 again becomes small. This is also a general characteristic of the optimal profiles in [1].

From (29) it is apparent that L_2 should be a continuous function of time. There is a discontinuity that occurs at the switch to the terminal boundary layer which is a consequence of the singular perturbation approximation. A second discontinuity occurs at the second switch which is a consequence of neglecting the second term in (24). However, it was observed that the second term in (33) passes through a minimum during the ascent phase, and the second switch was executed at that time to minimize the discontinuity. It is felt that this should more closely approximate the true solution if we were able to retain the second term in (24) in the analysis, and still preserve an explicit solution for L_2.

A comparison of the resulting flight path with that in [1] for a 40 plane change is illustrated in Figure 2. Table 1 compares the impulses required for the maneuver. Note that the singular perturbation solution

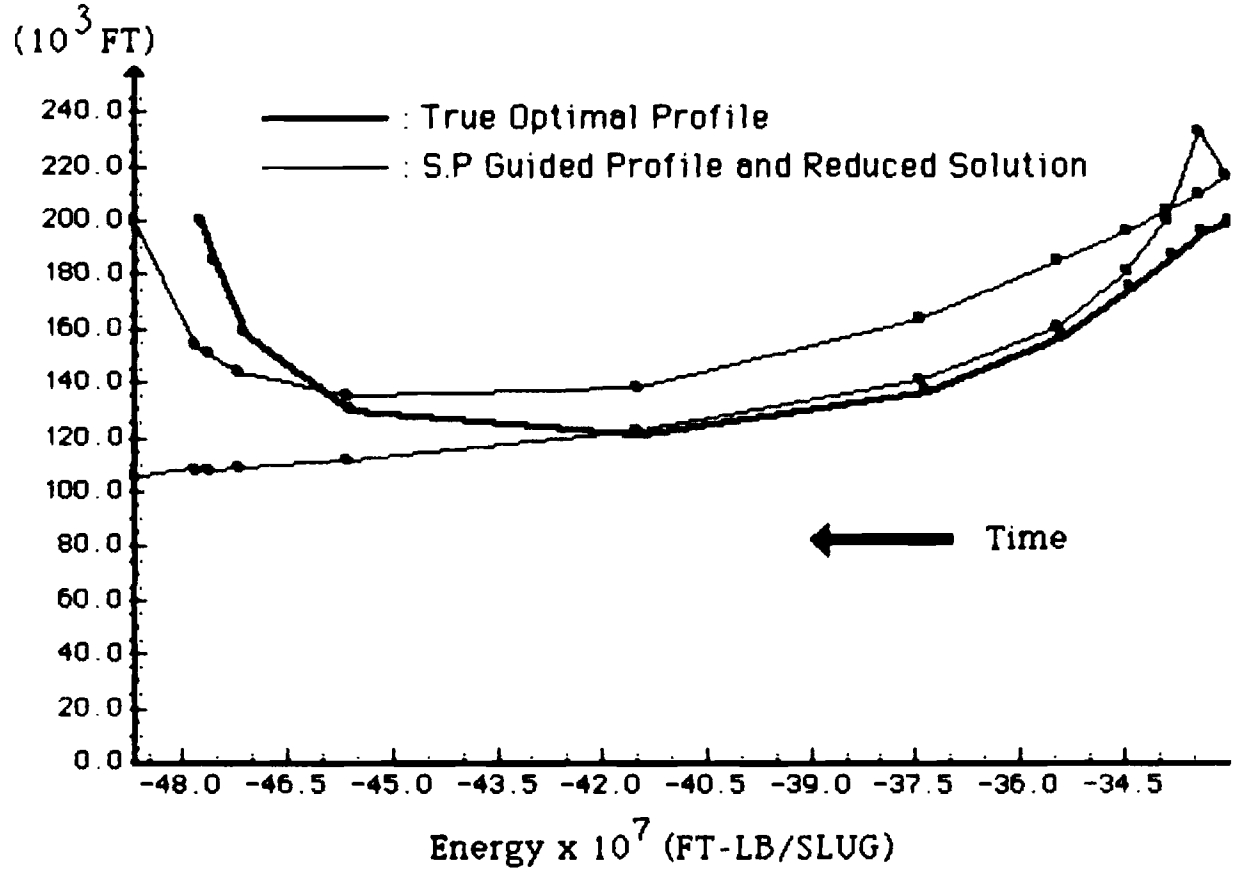

Figure 2. Comparison of the guided S.P. solution with the reduced solution and the true optimal profile.

TABLE 1

COMPARISON OF TOTAL IMPULSE AND FUEL FRACTION
REQUIRED FOR A 40^0 PLANE CHANGE MANEUVER

GUIDANCE LAWS	DEORBIT IMPULSE (ft/s)	BOOST IMPULSE (ft/s)	REORBIT IMPULSE (ft/s)	TOTAL IMPULSE (ft/s)	FUEL FRACTION
OPTIMAL	125.	6470.	177.	6772.	.49
S.P. SOLUTION	126.	6642.	214.	6982.	.50
GUIDED SOLUTION	374.	7651.	122.	8147.	.56
SINGLE IMPULSE	*	*	*	17497.	.83

results in a fuel fraction close to the true optimal solution, and is considerably better than the guided solution in [1]. A comparison to the fuel fraction needed for a purely impulsive maneuver is also given which clearly demonstrates the advantage of aero-assisted orbital transfer.

3. FUTURE WORK

During the next reporting period we plan to investigate two alternatives to constructing a boundary layer solution. The first is based on a linearization of the necessary conditions in the boundary layer to obtain a linear feedback solution without neglecting the second term in (24) This method has been previously used in [2]. The second approach analyzes the altitude and flight path angle dynamics in separate layers [3]. This approach also will yield a feedback solution form, but one which is nonlinear.

REFERENCES

1. Hull, D.G., Giltner, J.M., Speyer, J.L., and Mapar, J., "Minimum Energy-Loss Guidance for Aero-Assisted Orbital Plane Change", J. of Guidance and Control, Vol. 8, No. 4, July-Aug., 1985.

2. Ardema, M.D., "Linearization of the Boundary Layer Equations of the Minimum Time-to-Climb Problem", J. of Guidance and Control, Vol. 2, No. 5, Sept.-Oct., 1979.

3. Calise, A.J., "Optimization of Aircraft Altitude and Flight-Path Angle Dynamics", J. of Guidance and Control, Vol. 7, No. 1, Jan.-Feb., 1984.

SINGULAR PERTURBATION ANALYSIS OF AOTV-RELATED TRAJECTORY OPTIMIZATION PROBLEMS

PROGRESS REPORT

1 September - 30 July, 1987

July 1987

Research Supported by NASA - Langley Research Center

NASA Grant No. NAG-1-660

Principal Investigator: Dr. Anthony J. Calise
Research Assistant: Mr. Gyong Bae
NASA Grant Monitor: Dr. Christopher Gracey

Georgia Institute of Technology
School of Aerospace Engineering
Atlanta, Georgia 30332-0150

TABLE OF CONTENTS

LIST OF FIGURES

SECTION 1.
SUMMARY OF RESEARCH ACCOMPLISHMENTS

Research during this year has concentrated on the problem of aero-assisted orbital plane change. This maneuver requires the use of three impulses - one to deorbit, one to reorbit, and one to recircularize at the new orbit. The orbit plane change is effected entirely in the atmosphere through the use of lift and bank-angle control. For circular orbits of nearly equal radii, it can be shown that fuel consumption is minimized by minimizing the energy loss in the atmospheric portion of the trajectory. The research explored the use of singular perturbation theory to develop an optimal guidance law for the atmospheric portion.

The results to date indicate that singular perturbation methods can be applied; however, a difficult terminal boundary analysis is required. The reduced solution models only the heading rate dynamics, and produces a realistic profile (altitude versus energy) and control to be flown. A large terminal boundary layer is required to match the terminal constraint on altitude. Most of our effort has been directed at approximate methods for solving the boundary layer equations.

The boundary layer equations result from an analysis of altitude and flight path angle dynamics on the same time scale. A nonlinear control law was derived which produces near-optimal results. However, the current solution is difficult to implement because it requires two switches in the control solution that are heading and altitude dependent. In general, the solution is very sensitive to switching times. The results will appear in a special issue on Optimal Trajectories and Guidance of Hypervelocity Vehicles in the Journal of Astronautical Sciences [1]. The results have also been reported in our midterm progress report [2].

During the second half of this year's effort, we have investigated a linearization of the necessary conditions about the reduced solution along the lines described in [3]. However, while this approach produces excellent results for the initial boundary layer, we have not been able to find a useful way of invoking the terminal constraints in the terminal boundary layer solution. The primary problem is that the terminal boundary layer dynamics are unstable forward in time. The results of this research activity

has been submitted for presentation in the AIAA Atmospheric Flight Mechanics Conference [4], treating only the problem of heading change with minimum energy loss and with terminal altitude free. This avoids the issue of a terminal boundary layer. This paper is included in Appendix A.

During this period we have also been successful in generating optimal trajectories using a multiple shooting code provided by the DFVLR in West Germany. We found the code to be highly efficient when properly initialized. the reduced solution from the singular perturbation analysis was used as a starting point for multiple shooting. Since this work was only recently completed and not documented in [4], a discussion of the results is included in Section 2.

Section 3 outlines a new approach which attempts to invoke the terminal constraint on altitude indirectly as part of the problem formulation, thereby avoiding the need for a terminal boundary layer in the singular perturbation analysis. While we are still in the exploratory stages with this line of investigation, preliminary results do indicate that this will be a promising approach. Recommendations for research during the next reporting period are also contained in this section.

SECTION 2.
MULTIPLE SHOOTING RESULTS

Multiple shooting is a technique for solving two-point boundary value problems. In order to use this technique in optimal control formulations, it is first necessary to eliminate the control in terms of the state and adjoint variables. For free terminal time problems, an additional state is artificially introduced which represents the free terminal time, and the condition that the Hamiltonian be zero is invoked as an additional terminal constraint. The program provided by the DFVLR requires that the user supply subroutines for defining the state and adjoint derivatives and boundary conditions. A data file is also required to define the initial guess of state and adjoint values at selected grid points along the profile. Success in obtaining a converged solution unfortunately depends a great deal on the quality of the initial guess. When the algorithm does converge, it does so with few iterations, and to an extreme level of accuracy limited only by the level of machine precision available. Our experience with the code is that the reduced solution from the singular perturbation analysis provides a good starting guess.

In this section we present results related to the problem of optimal heading change with free terminal altitude. This is the same problem dealt with in Appendix A in a singular perturbation context. An exponential atmosphere was used to simplify the derivative expressions for the adjoint variables. Figures 1 - 3 provide a comparison of the trajectory and control profiles. It is interesting to note that the optimal control consists of a maneuver at maximum L/D with a bank angle close to 90 degrees. While the trajectory profiles and flight times are appreciably different, loss in optimality of the guided trajectory (SP solution) was only 0.4 percent of the energy loss for the numerically optimized profile. This indicates that there is very little sensitivity of performance to the exact profile that is flown, so long as it is flown at near max L/D and 90 degrees of bank angle. However, these results do validate the reduced order modeling results obtained through singular perturbation analysis. Although the results shown are for a single-entry condition, similar results were obtained for several other combinations of initial conditions.

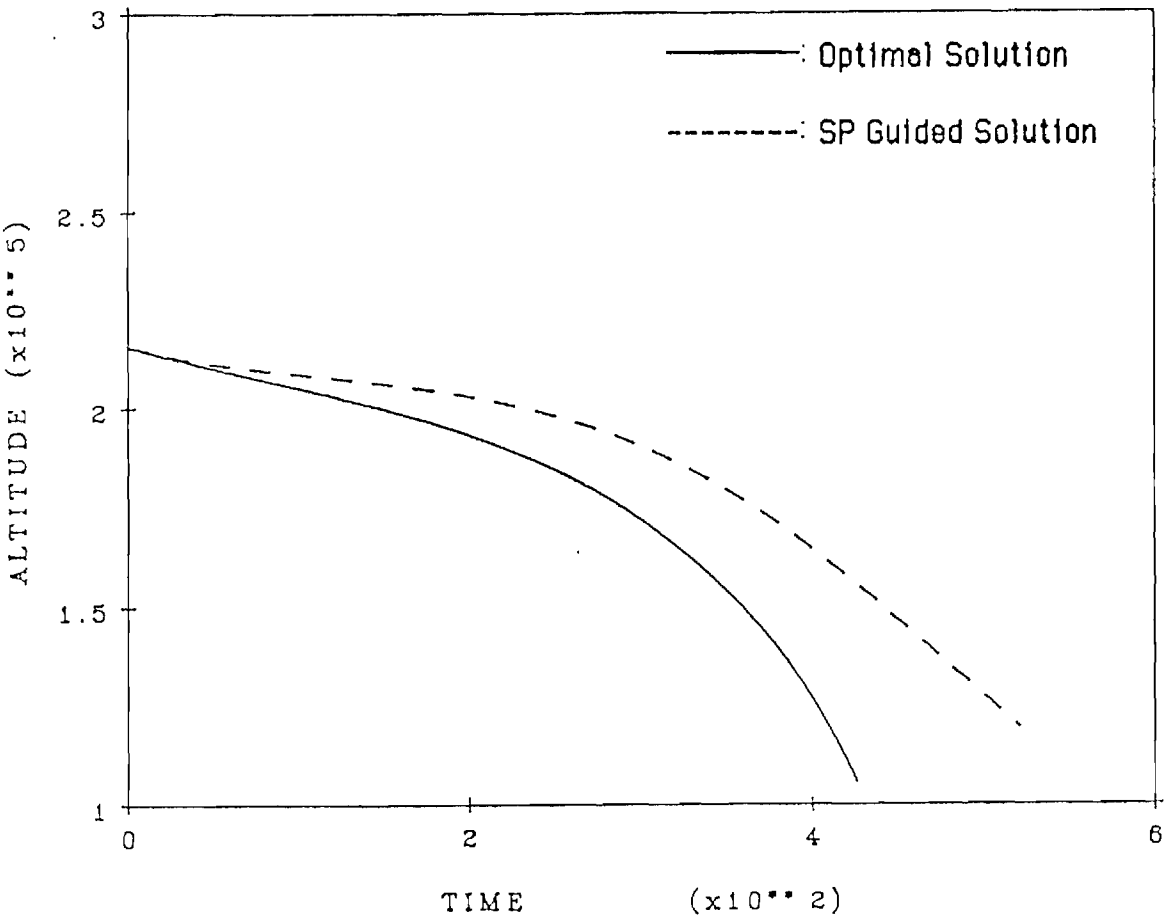

Figure 1. Comparison of the altitude profile for the optimal solution and the SP guided solution.

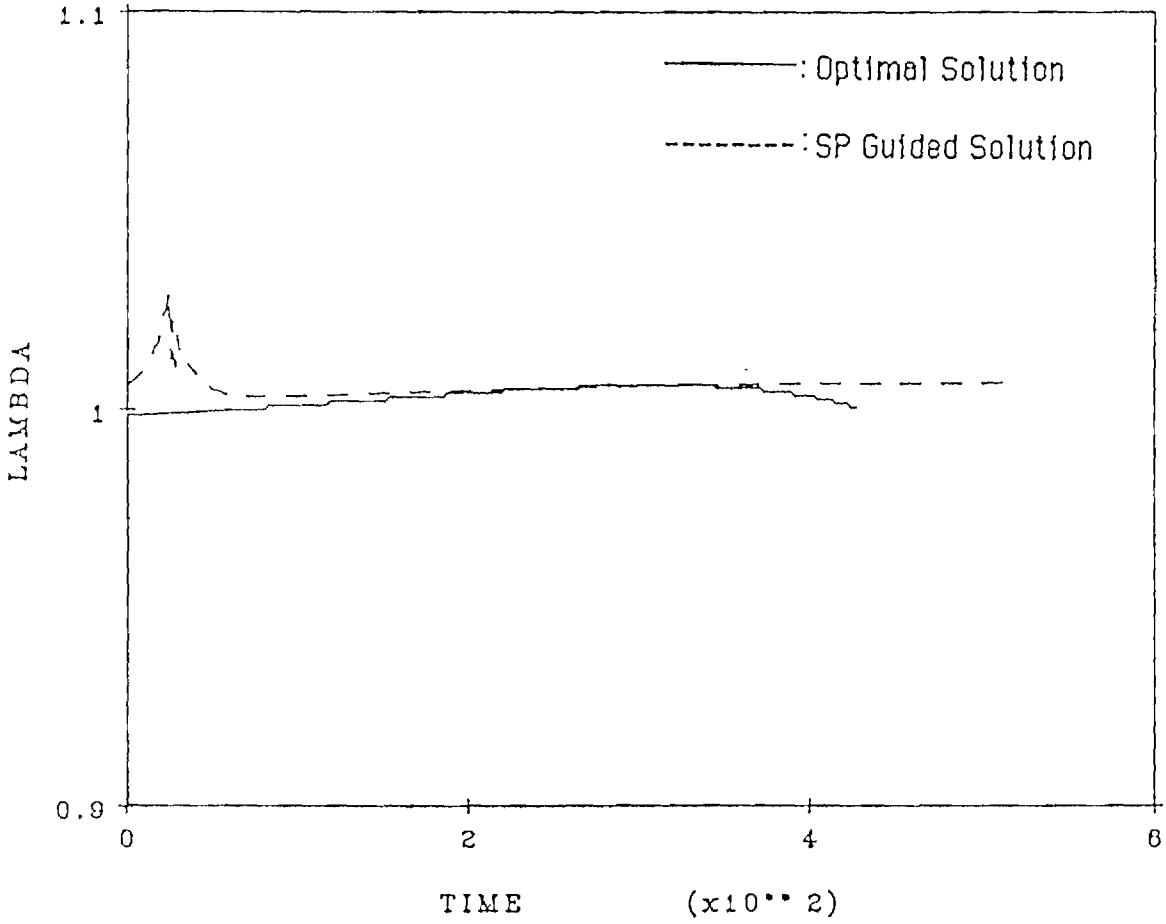

Figure 2. Comparison of the normalized lift coefficient time histories.

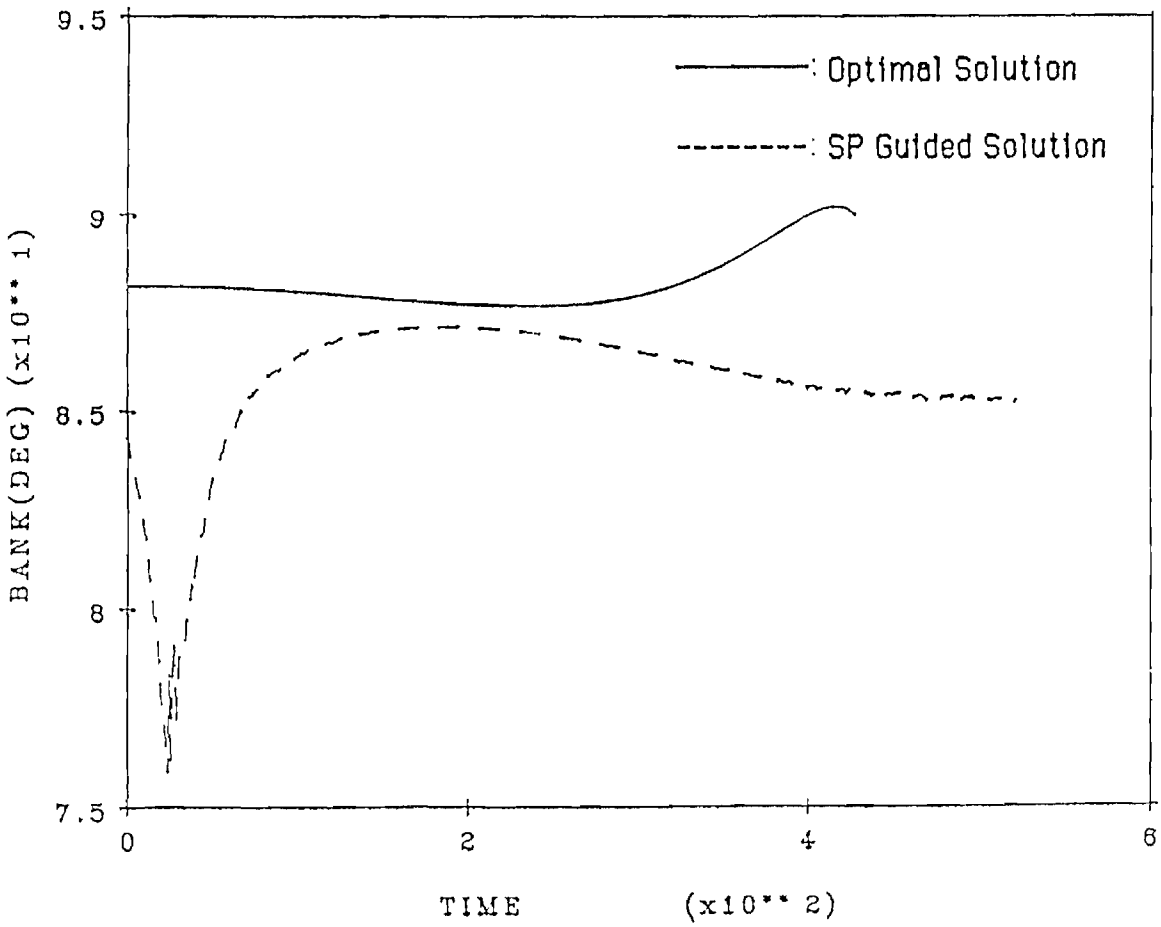

Figure 3. Comparison of the bank angle time histories.

SECTION 3.

A NEW ANALYSIS APPROACH FOR ENFORCING A TERMINAL ALTITUDE CONSTRAINT

Based on the results to date it seems essential to avoid problem formulations that require a large terminal boundary layer correction. That is, the essential features of the total altitude profile should be captured in the reduced solution where altitude appears as a control variable.

An approach that we are currently investigating uses a penalty function in the performance index to represent the terminal constraint on altitude. The performance index has the form

$$J = -\int_0^{t_f} [\dot{E} - \nu(\delta h/\delta\psi)^2\dot{\psi}]\, dt \tag{1}$$

where

$$\delta h = h - h_f, \qquad \delta\psi = \psi - \psi_f \tag{2}$$

h_f is the final altitude and ψ_f is the final heading. Since the objective is to minimize J, the second term in (1) will cause the optimal-altitude profile in the reduced solution to approach the desired terminal altitude as the heading approaches the specified final heading. Since there is now no terminal constraint on altitude, only an initial boundary layer analysis for this problem formulation is required. Achieving the desired terminal altitude simultaneously as the final heading is reached is the most difficult aspect of the orbit plane change problem. The approaches in [5-7] all rely on an integration of the state and co-state dynamics over the entire trajectory, based on the approximation that M (Loh's constant) is indeed constant. Use of the performance index in (1) is a singular perturbation context achieves the same effect without introducing this approximation, but at the cost of distorting the index of performance.

The parameter, ν, should be chosen so that the profile remains essentially like that obtained in the initial boundary layer solutions obtained to date, with the effect of the second term felt later in the trajectory. One way to achieve this end is to select ν on the basis of several trial runs for a moderate plane change so that the terminal velocity is maximized, and then

to hold it fixed for other plane changes. The value of this approach can then be evaluated based on simulations for a range of plane changes and comparison to numerically optimized solutions. We plan to apply the multiple shooting code for the comparison studies.

The analysis in [4] was repeated for the performance index in (1). The effect of the weighting parameter on the reduced solution and the resulting guided solution is illustrated in Figures 4 and 5. Figure 4 shows that the objective of incorporating a terminal altitude constraint as part of the reduced solution is achieved through the use of (1) as the index of performance. Also, the trajectory shaping is strongly influenced by the choice of the weighting parameter. The resulting simulated trajectories of Figure 5 appear reasonable; however, the corresponding lift coefficient profiles are not attainable. This is shown in Figure 6, where the lift coefficient profile corresponding $\nu = 1.5 \times 10^{-4}$ approaches 5.0 near the end of the profile. The corresponding bank-angle profile approaches 0°, as shown in Figure 7. It should also be pointed-out that this value of the weighting parameter resulted in minimum energy loss, and that the resulting total impulse for the total maneuver was slightly improved over the result for the SP-guided solution in our first progress report [2].

During the next reporting period we would like to further pursue this line of investigation by constraining the normalized lift coefficient to 1.0. It has been demonstrated in [5] that the optimal profiles exhibit this characteristic. This should insure an achievable control profile. We would also like to further evaluate the multiple shooting code by exercising it for the orbital plane change problem. This will remove the need to constrain our comparisons to the results in [5] in future work. This has been a persistent problem to date since we have had difficulty in matching the atmospheric and aerodynamic modeling that was used in that study.

In addition to the above line of investigation, we would like to begin addressing some of the other topics that appeared in our original three-year research proposal [8]. These include direct methods of enforcing state and control constraints, and the interaction between these constraints and vehicle design parameters. We would also like to address issues related to sensitivity to such factors as entry flight path angle, atmospheric uncertainties, and guidance error sources. Other problem formulations for future

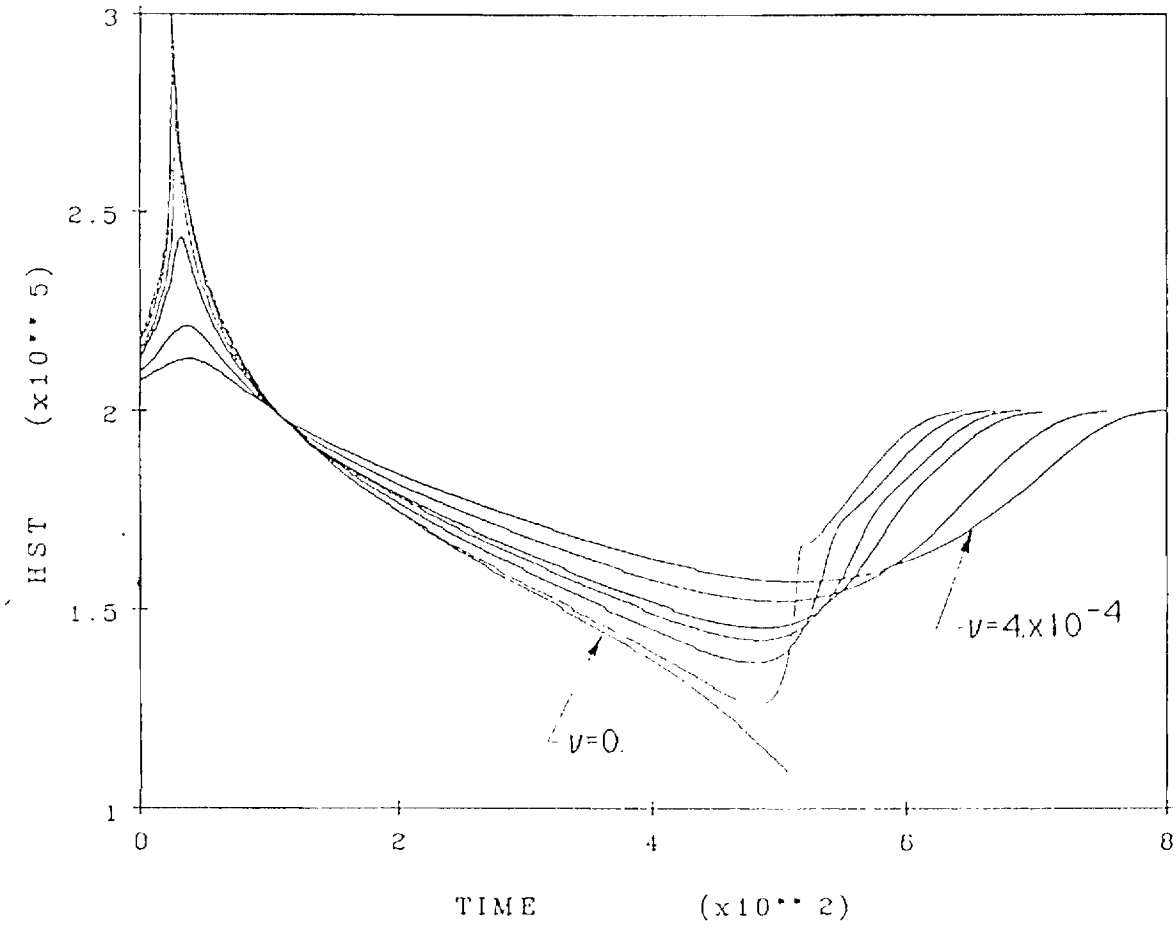

Figure 4. SP reduced solution profiles for values of $\nu = 0, 10^{-5}, 5\times10^{-5}, 10^{-4}, 1.5\times10^{-4}, 3\times10^{-4}$ and 4×10^{-4}.

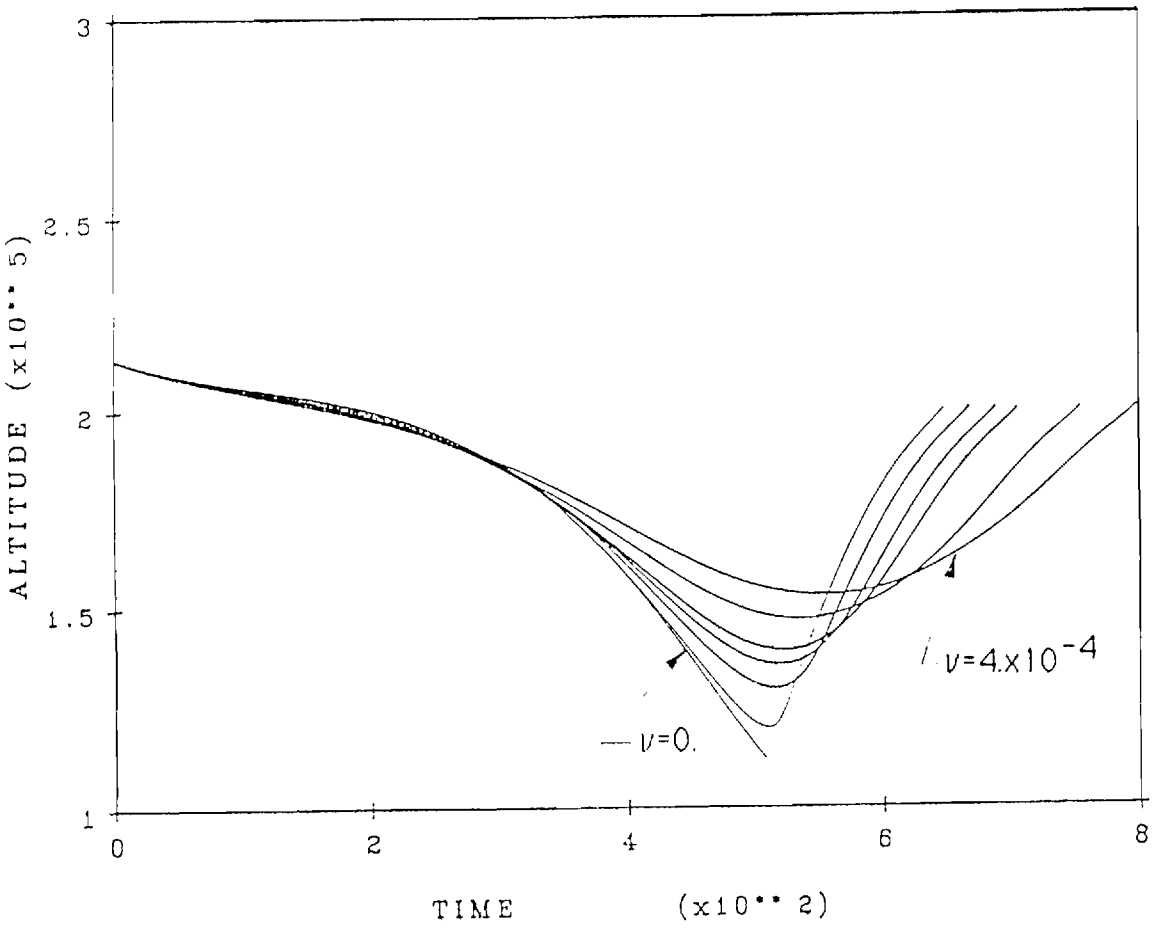

Figure 5. Guided solution profiles for values of ν = 0, 10^{-5}, $5x10^{-5}$, 10^{-4}, $1.5x10^{-4}$, $3x10^{-4}$ and $4x10^{-4}$.

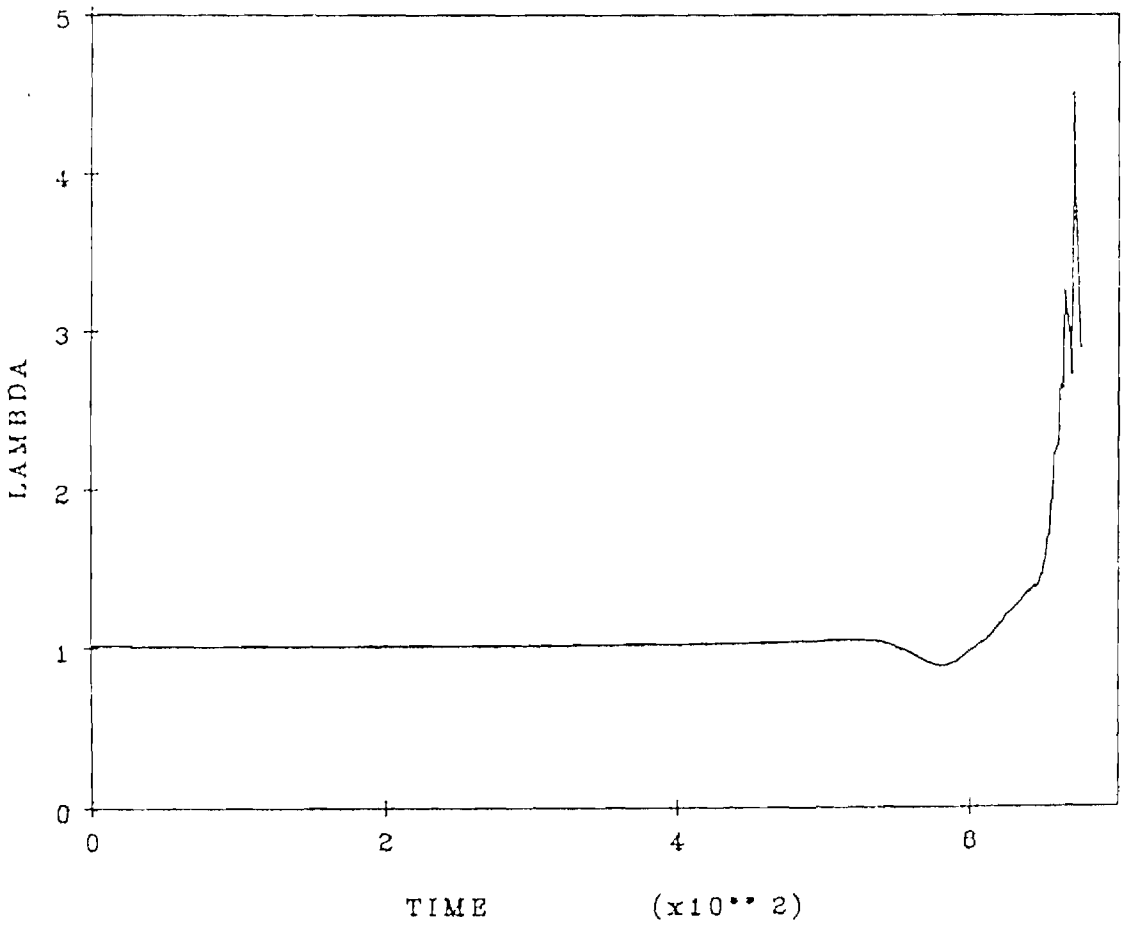

Figure 6 Normalized lift coefficient time history for $\nu = 1.5 \times 10^{-4}$.

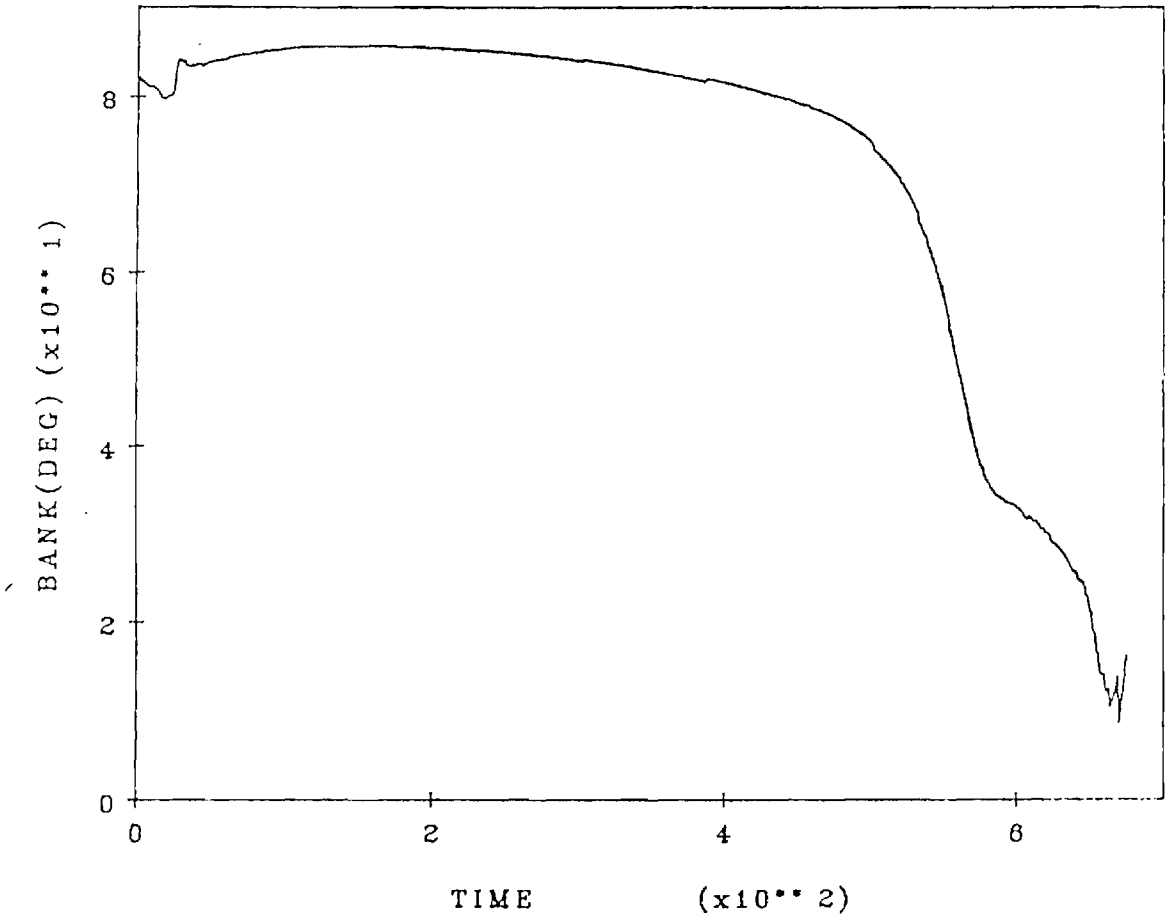

Figure 7 Bank angle time history for $\nu = 1.5 \times 10^{-4}$.

space transportation systems, such as coplanar orbit transfer, and re-entry guidance for maximum lateral range may take priority, and will be selected in coordination with the NASA grant monitor to insure their relevance to current and future NASA programs.

REFERENCES

1. Calise, A.J., "Singular Perturbation Analysis of the Atmospheric Orbital Plane Change Problem," submitted to the J. of Astro. Sci., Nov., 1986.

2. Calise, A.J., Bae, G., "Singular Perturbation Analysis of AOTV Related Trajectory Optimization Problems," Progress Report for the Period 14 April - 30 Oct., Nov., 1986.

3. Ardema, M.D., "Linearization of the Boundary Layer Equation of the Minimum Time-to Climb Problem," J. of Guid. and Cont., Vol. 2, No. 5, Sept.-Oct., 1979.

4. Calise, A.J., Bae, G., "Optimal Heading Change with Minimum Energy Loss for a Hypersonic Gliding Vehicle," submitted to the AIAA Atmospheric Flight Mechanics Conf., August, 1987.

5. Hull, D.G., Giltner, J.M., Speyer, J.L., and Mapar, J., "Minimum Energy-Loss Guidance for Aero-Assisted Orbital Plane Change, J. of Guid. and Cont., Vol. 8, No. 4, July-Aug., 1985.

6. Hull, D.G., McClendon, J.R., and Speyer, J.L., "Improved Aero-Assisted Plane Change Using Successive Approximation," AIAA Atmospheric Flight Mechanics Conf., Williamsburg, VA, Aug., 1986.

7. Hull, D.G., McClendon, J.R., and Speyer, J.L., "Aero-Assisted Orbital Plane Change Using an Elliptic Drag Polar, AIAA Aerospace Sciences Meeting, Reno, NV, Jan., 1986.

8. Calise, A.J., Research Proposal submitted by Georgia Tech Research Corporation, Oct., 1985.

APPENDIX A.

OPTIMAL HEADING CHANGE WITH MINIMUM ENERGY LOSS FOR A HYPERSONIC GLIDING VEHICLE

Anthony J. Calise* and Gyoung H. Bae**
Georgia Institute of Technology
Aerospace Engineering
Atlanta, GA 30332

February, 1987

ABSTRACT

A three state model is presented for analyzing the problem of optimal changes in heading with minimum energy loss for a hypersonic gliding vehicle. A further model order reduction to a single state model is examined using singular perturbation theory. The optimal solution for the reduced problem defines an optimal altitude profile dependent on the current energy of the vehicle, and the corresponding optimal lift and bank angle. A separate boundary layer analysis, based on an expansion of the necessary conditions about the reduced solution, is used to account for altitude and flight path angle dynamics and to derive a guidance law in feedback form. The guidance law is evaluated for a hypothetical vehicle.

INTRODUCTION

This paper addresses the problem of developing analytical methods for optimal guidance of hypersonic vehicles. Energy state approximations combined with singular perturbation theory (SPT) have been proven useful in aircraft trajectory optimization, both in obtaining algebraic control solutions and in satisfying trajectory and control constraints[1-4]. However, the underlying flat earth and constant gravitational field assumptions in aircraft modeling do not apply to hypersonic vehicles. Moreover, the use of SPT requires an inherent time scale separation in the problem formulation for successful application. It is not known at this time if SPT can be applied to hypersonic vehicle control optimization. The intent of this paper is to explore this possibility for a simple problem formulation.

The problem of optimal atmospheric heading change with minimum energy loss has application to maneuvering reentry vehicle guidance, and to aeroassisted orbit transfer vehicles (AOTV's). In this simple problem formulation, we ignore terminal constraints on both altitude and flight path angle, and thus avoid the issue of a terminal boundary layer correction. However, comparisons can be made to the initial portion of an AOTV optimal maneuver, and to the general characteristics of these optimal profiles. References 5-7 typify the studies that have been performed on the problem of optimal aeroassisted orbital plane change. For circular orbits of nearly equal radii, it can be shown that fuel consumption is minimized by minimizing the energy loss in the atmospheric portion of the trajectory.

This paper presents a problem formulation suitable for singular perturbation analysis. The reduced and boundary layer solutions are examined and compared to the general characteristics of the numerical solutions given in Ref. 7 for the AOTV problem.

PROBLEM FORMULATION

In [7] it has been shown that the cross range angle for the orbital plane change trajectory that minimizes energy loss is negligibly small. Capitalizing on this fact, it is possible to reduce the equations of motion for flight over a nonrotating spherical Earth to the following four state model:

$$\dot{h} = V\sin\gamma \tag{1}$$

$$\dot{V} = -C_D^*(1+\lambda^2)\rho SV^2/4m - \bar{\mu}\sin\gamma/r^2 \tag{2}$$

$$\dot{\gamma} = (C_L^*\rho SV/2m)(\lambda\cos\mu+M\cos\gamma) \tag{3}$$

$$\dot{\psi} = C_L^*\lambda\rho SV\sin\mu/2m\cos\gamma \tag{4}$$

where

$$C_D = C_{Do} + KC_L^2 \tag{5}$$

$$M(h,V) = (2m/C_L^*S)[1-\bar{\mu}/V^2r]/\rho r \tag{6}$$

and $\bar{u}$ is the gravitational constant. In these equations the superscript * denotes the maximum lift-to drag values:

$$C_L^* = (C_{Do}/K)^{1/2} \qquad C_D^* = 2C_{Do} \tag{7}$$

and λ is the normalized lift coefficient

$$\lambda = C_L/C_L^* \tag{8}$$

The equation for V in (2) includes the gravity term, which was neglected in [7]. The control variables are λ and the bank angle (μ). Under the hypothesis that the cross range angle is small, ψ closely approximates the change in orbit inclination.

*Professor, Senior Member AIAA
**Graduate Research Assistant

Boundary Conditions

In [7] the sensible atmosphere is assumed to occur at h_o = 200,000 ft. The starting velocity and flight path angle are derived using a deorbit impulse ΔV_1 from circular orbit at h_c = 100 nm, which is optimized for the atmospheric maneuver of interest. The initial heading angle is taken as zero. In the SPT formulation, altitude appears as a control variable. The optimal solution appears in the form

$$h^* = h(E) \tag{9}$$

where E is the total energy per unit mass

$$E = V^2/2 - \bar{\mu}/r < 0 \tag{10}$$

For comparison purposes, in this paper the starting energy is chosen to match that of [7], and h(0), V(0) are derived from (9) and (10). From conservation of energy this results in the same deorbit impulse. The initial flight path angle is derived from conservation of angular momentum.

$$\gamma(0) = -\cos^{-1}[(r_s+h_c)(V_c-\Delta V_1)/(r_s+h_o)V_o] \tag{11}$$

where r_s is the mean earth radius and $V_c=[\bar{\mu}/(r_s+h_c]^{1/2}$ is the circular velocity. The vehicle begins the maneuver with a mass m_c and, as a result of the deorbit impulse, the mass for the atmospheric portion is given by

$$m = m_c \exp(-\Delta V_1/C) \tag{12}$$

where C is the characteristic velocity. The terminal condition is taken as:

$$\psi(t_f) = \psi_f > 0 \tag{13}$$

There are no terminal constraints on altitude and flight path angle.

Optimal Control Problem

The objective is to minimize the energy lost in maneuvering to a specified heading. Regarding energy as a slow variable, and altitude and flight path angle as fast variables, the following three state model was adopted for singular perturbation analysis:

$$\dot{\psi} = C_L^* \rho SV\lambda \sin\mu/2m\cos\gamma \tag{14}$$

$$\varepsilon\dot{h} = V\sin\gamma \tag{15}$$

$$\varepsilon\dot{\gamma} = C_L^* \rho SV(\lambda\cos\mu+M\cos\gamma)/2m \tag{16}$$

The objective is to minimize

$$J = -\int_o^{t_f} \dot{E}dt \tag{17}$$

where

$$\dot{E} = -C_D^*(1+\lambda^2)\rho SV^3/4m \tag{18}$$

Note that in the above formulation E is regarded as constant in the dynamics, but that changes in energy are accounted for in the performance index. Thus, V (wherever it appears) must be regarded as a function of h and E in accordance with (10). The perturbation parameter ε is introduced to signify the presence of fast dynamics, and is nominally equal 1.0. We seek a reduced and zero order boundary layer solution about ε = 0, in accordance with the procedures detailed in [2-4].

SINGULAR PERTURBATION ANALYSIS

Reduced Problem

Setting ε = 0 in (14-16) the necessary conditions for optimality become:

$$H_o = \lambda_\psi \dot{\psi} - \dot{E} = 0 \tag{19}$$

$$\gamma = 0 \qquad \lambda\cos\mu = -M \tag{20}$$

$$\mu_o,\ h_o = \arg\min_{h,\mu} \{\dot{\psi}/\dot{E}\} \tag{21}$$

It can be shown that this results in the following reduced solution:

$$\lambda_o = (1 + 2M_o^2)^{1/2} \tag{22}$$

$$\sin\mu_o = [(1 + M_o^2)/(1 + 2M_o^2)]^{1/2} \tag{23}$$

$$h_o = \arg\min_{h} \{V^2(1 + M^2)^{1/2}\}\big|_{E = \text{const.}} \tag{24}$$

where M_o is the value of M for $h = h_o$. The quadrant for the bank angle in (23) is resolved based on the following inequalities:

$$0 < \mu_o < \pi/2 \text{ for } M_o < 0 \tag{25}$$

$$\pi/2 < \mu_o < \pi \text{ for } M_o > 0 \tag{26}$$

It can be seen from the above solution that M plays a crucial role in the solution process. In [7], M was treated as a constant in the dynamics.

Since most of the energy is kinetic, V is weakly dependent on h for constant E. This can readily be seen from (10) where changes in h give rise to small changes in r. Thus, the minimization in (24) results in a value for M very close to zero. The interpretation is that the maneuver should be performed at an altitude where gravitational and centripetal forces nearly cancel one another. For M small, it can be seen from (22,23) that the maneuver is performed at near maximum L/D and at near 90^{o} of bank angle. These results are in good agreement with the results in [7]. Figure 1 compares the altitude profiles derived from (24) with the true optimal profile taken from [7]. The need for a terminal boundary layer analysis is evident in this figure. However, if the vehicle was not required to exit the atmosphere, the reduced solution may be sufficiently accurate.

Boundary Layer Problem

A boundary layer analysis is required to obtain a guidance law that will both follow the altitude profile defined by (24) (initial boundary layer) and satisfy the terminal constraint on altitude (terminal boundary layer). The necessary conditions in the boundary layer are:

$$H_{BL} = \lambda_{\psi}^{o}\dot{\psi} + \lambda_h V\sin\gamma + \lambda_\gamma \dot{\gamma} - \dot{E} = 0 \qquad (27)$$

$$\partial H_{BL}/\partial L_1 = 0, \qquad \partial H_{BL}/\partial L_2 = 0 \qquad (28)$$

where λ_{ψ}^{o} is determined in the reduced solution from (19)

$$\lambda_{\psi}^{o} = \dot{E}^{o}/\dot{\psi}^{o} \qquad (29)$$

using the solutions for λ_o, μ_o and h_o. In (28), L_1 and L_2 represent the horizontal and vertical components of lift coefficient

$$L_1 = \lambda\sin\mu \qquad L_2 = \lambda\cos\mu \qquad (30)$$

which are now used as control variables in place of λ and μ.

The first condition in (28) results in

$$L_1^{*} = (V_o/V)^{2}(1 + M_o)^{1/2}/\cos\gamma \qquad (31)$$

where M_o, V_o are the values of M and V corresponding to $h = h_o$ for the current value of E. This solution approaches the corresponding reduced solution as h approaches h_o.

The second condition in (28) yields

$$L_2^{*} = -(C_L^{*}/C_D^{*}V^{2})\lambda_\gamma \qquad (32)$$

which can also be shown to approach the reduced solution as h approaches h_o, where

$$\lambda_\gamma^{o} = C_D^{*} V_o^{2} M_o/C_L^{*} \qquad (33)$$

Unfortunately, evaluation of λ_γ needed in (32) requires the solution of a two-point boundary value problem. When close to the reduced solution it may be possible to use (33), which results in the following expression for flight path angle rate

$$\dot{\gamma} = C_L^{*}\rho SV(M\cos\gamma - V_o^{2}M_o/V^{2})/2m \qquad (34)$$

For γ near zero and h near h_o, (34) simplifies to

$$\dot{\gamma} = C_L^{*}\rho SV_o(M-M_o)/2m \qquad (35)$$

Expansion of the Boundary Layer Problem

To obtain a feedback solution for L_2 we consider an expansion of the boundary layer necessary conditions of (27,28) together with the state and costate dynamics expressed in the stretched time scale $\tau = t/\varepsilon$:

$$dh/d\tau = V\sin\gamma, \qquad d\lambda_h/d\tau = -\partial H_{BL}/\partial h \qquad (36)$$

$$d\gamma/d\tau = C_{L\rho}^{*}SV(L_2+M\cos\gamma)/2m, \quad d\lambda\gamma/d\tau = -\partial H_{BL}/\partial\gamma \qquad (37)$$

Substituting for L_1 and L_2 from (31,32), equations (36,37) are expanded about the reduced solutions equilibrium conditions:

$$\bar{h} = h_o(E), \qquad \bar{\gamma} = 0 \qquad (38)$$

$$\bar{\lambda}_h = 0 \quad , \qquad \bar{\lambda}_\gamma = -C_D^{*}M_oV_o^{2}/C_L^{*} \qquad (39)$$

where the value for $\bar{\lambda}_\gamma$ follows from (32) with $L_2^{*} = -M_o$ ($\dot{\gamma} = 0$ in the reduced solution). This results in the following linear perturbation equations:

$$\begin{bmatrix}\delta h'\\ \gamma'\\ \lambda'_h\\ \delta\lambda'_\gamma\end{bmatrix} = \begin{bmatrix}0 & V_o & 0 & 0\\ K_1 & 0 & 0 & K_2\\ K_3 & 0 & 0 & -K_1\\ 0 & K_4 & -V_o & 0\end{bmatrix}\begin{bmatrix}\delta h\\ \gamma\\ \lambda\\ \delta\lambda_\gamma\end{bmatrix} \qquad (40)$$

where

$$K_1 = [V^{2}r^{2}-(\beta V^{2}+\bar{\mu})r+2\beta\bar{\mu}]/\beta Vr^{3} - 2\bar{\mu}^{2}/V^{3}r^{4} - C_L^{*}S\bar{\mu}M\rho/mVr^{2} \qquad (41)$$

$$K_2 = -C_L^* S\rho/2mC_D^* V \tag{42}$$

$$K_3 = -\partial^2 H_{BL}/\partial h^2 \leq 0 \tag{43}$$

$$K_4 = C_D^* S\rho V^3(1+2M^2)/2m \tag{44}$$

The expressions in (41-44) are evaluated at $h = h_o$, and β is the scale height for an exponential atmospheric model at $h = h_o$. The term in (43) is complicated to express analytically, but can easily be evaluated numerically taking into account the fact that $\partial H_{BL}/\partial h$ evaluated at $h = h_o$ is zero.

The eigenvalues of (40) are arranged symmetrically about the imaginary axis, and occur in complex conjugate pairs. Since the boundary layer dynamics are stable forward in time, the state vector in (40) can be expressed as

$$x = k_1\vec{a} + k_2\vec{b} \tag{45}$$

where $x^T = [\delta h, \gamma, \lambda_h, \delta\lambda_\gamma]$, and $\vec{a},\vec{b}$ are the real and imaginary parts of the eigenvectors associated with the stable eigenvalues. Knowing δh and γ, it is a simple exercise to solve for k_1, k_2, λ_h and $\delta\lambda_\gamma$. Then L_2^* in (32) can be evaluated for

$$\lambda_\gamma = \bar{\lambda}_\gamma + \delta\lambda_\gamma \tag{46}$$

Equations (31,32) and (46) thus constitute a feedback control law.

NUMERICAL RESULTS

Figures 2 and 3 illustrate the altitude and heading profiles that result from using the guidance law derived in the preceding section with the dynamics as defined in (1-4). Also shown in Fig. 2 is the reduced solution altitude profile from (24) for comparison purposes. Note the asymptotic behavior of the boundary layer dynamics.

CONCLUSIONS

The paper illustrates the use of model order reduction and singular perturbation analysis to derive a guidance law for a hypervelocity vehicle. The problem formulation was simplified to avoid the issue of a terminal boundary analysis required to satisfy terminal constraints on altitide and flight path angle. However, the results do indicate that these methods are effective in gaining insight to the nature of the optimal profiles for maneuverng in the atmosphere, and for developing suboptimal guidance strategies. Future research will address the problem of added terminal constraints.

Acknowledgement

This research was supported by NASA Langley under Grant No. NAG-1-660.

References

1. Bryson, A.E., Desai, M.N., and Hoffman, W.C., "Energy-State Approximation in Performance Optimization of Supersonic Aircraft," Journal of Aircraft, Vol. 6, No. 6, Nov.-Dec., 1968, pp. 481-488.

2. Calise, A.J., "Singular Perturbation Methods for Variational Problems in Aircraft Flight", IEEE Trans. on A.C., Vol. AC-21, No. 3, June 1976, pp. 345-353.

3. Calise, A.J., "Extended Energy Management Methods for Flight Performance Optimization", AIAA Journal, Vol. 15, No. 3, 1977, pp. 314-321.

4. Calise, A.J., "Singular Perturbation Techniques for On-Line Optimal Flight-Path Control", AIAA Journal of Guidance and Control, Vol. 4, No. 4, 1981, pp. 398-405.

5. Joosten, B.K. and Pierson, B.L., "Minimum-Fuel Aerodynamic Orbital Plane Change Maneuvers," AIAA 19th Aerospace Sciences Meeting, St. Louis, Missouri, January 12-15, 1981.

6. Hull, D.G. and Speyer, J.L., "Optimal Reentry and Plane-Change Trajectories," Journal of Astron. Sciences, Vol. XXX, No. 2, April-June 1982, pp. 117-130

7. Hull, D.G., Giltner, J.M., Speyer, J.L., and Mapar, J., "Minimum Energy-Loss Guidance for Aero-Assisted Orbital Plane Change," AIAA Journal of Guidance, Control, and Dynamics, Vol. 8, No. 4, July-August, 1985, pp. 487-493.

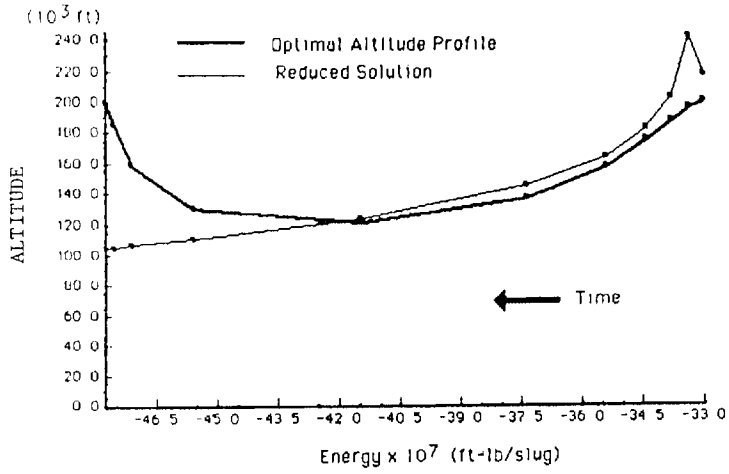

Fig. 1 Comparison of the reduced solution with the true optimal solution.

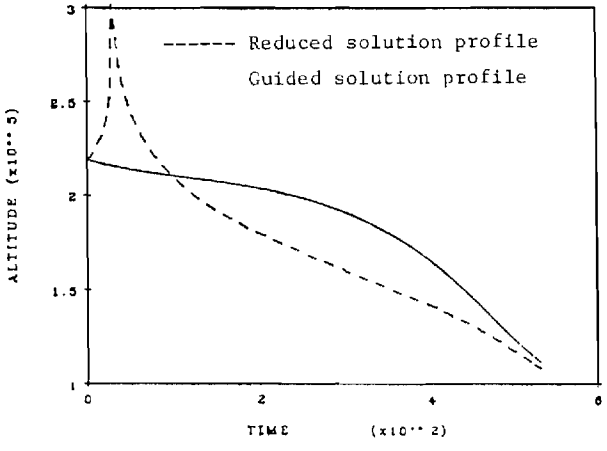

Fig. 2 Comparison of the guided altitude profile with the reduced solution profile.

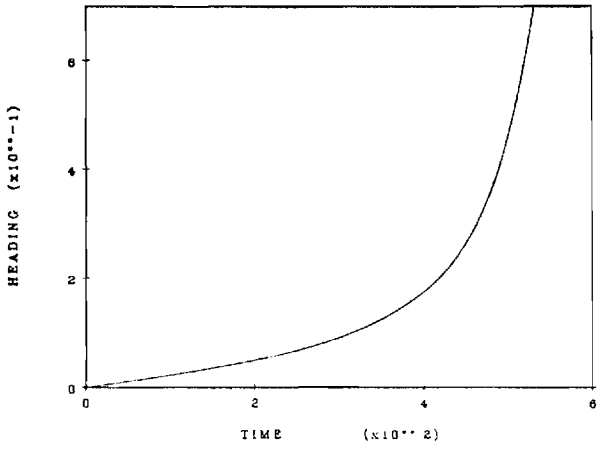

Fig. 3 Heading profile for the guided solution.

SINGULAR PERTURBATION ANALYSIS OF AOTV-RELATED TRAJECTORY OPTIMIZATION PROBLEMS

PROGRESS REPORT

1 August - 30 November, 1987

December 1987

Research Supported by NASA - Langley Research Center

NASA Grant No. NAG-1-660

Principal Investigator: Dr. Anthony J. Calise
Research Assistant: Mr. Gyong Bae
NASA Grant Monitor: Dr. Daniel Moerder

Georgia Institute of Technology
School of Aerospace Engineering
Atlanta, Georgia 30332-0150

TABLE OF CONTENTS

LIST OF FIGURES

LIST OF TABLES

SECTION 1
SUMMARY OF RESEARCH ACCOMPLISHMENTS

Research to date has concentrated on the problem of aeroassisted orbital plane change. The results reported earlier [1,2] indicate the usefulness of singular perturbation theory is developing analytic guidance solutions. However, a difficult terminal boundary layer (TBL) analysis is required to satisfy the terminal constraint on altitude. All of these results have also appeared in the open literature [3,4]. Unfortunately, we have not been able to explicitly solve the TBL problem in closed form, since it requires a forward integration of the equations of motion to invoke the terminal constraint. This report documents a suboptimal control solution for the vertical component of lift, which is based on a predictive/corrective type guidance law. this guidance law provides a highly accurate method of controlling terminal heading and altitude with nearly minimum energy loss. The horizontal component of lift is based on the earlier results reported in [2,4].

Section 2 presents the rational and derivation of the guidance law, which is used to both initiate the TBL maneuver and to define the vertical component of lift. Numerical results that demonstrate the performance of the total guidance algorithm are contained in Section 3. Included in this section are comparisons to numerically computed optimal trajectories from [5].

SECTION 2
A SUBOPTIMAL GUIDANCE LAW

As a point of reference, we first summarize the equations of motion that are the subject of this research:

$$\dot{h} = V\sin\gamma \tag{1}$$

$$\dot{V} = -C_D^*(1+\lambda^2)\rho SV^2/4m - \bar{\mu}\sin\gamma/r^2 \tag{2}$$

$$\dot{\gamma} = (C_L^* \rho SV/2m)(\lambda \cos\mu + M\cos\gamma) \tag{3}$$

$$\dot{\psi} = C_L^* \rho SV\lambda \sin\mu/2m\cos\gamma \tag{4}$$

where

$$C_D = C_{Do} + KC_L^2 \tag{5}$$

$$M(h,V) = (2m/C_L^* S)[1-\bar{\mu}/V^2 r]/\rho r \tag{6}$$

and $\bar{u}$ is the gravitational constant. In these equations the superscript * denotes the maximum lift-to-drag values:

$$C_L^* = (C_{Do}/K)^{1/2} \qquad C_D^* = 2C_{Do} \tag{7}$$

and λ is the normalized lift coefficient

$$\lambda = C_L/C_L^* \tag{8}$$

As reported in [1,4], the reduced solution defines the optimal altitude for maneuvering as a function of vehicle energy, which is defined by the following function minimization

$$h_o = \arg \min_h \{V^2(1+M^2)^{1/2}\} \tag{9}$$

where

$$E = V^2/2 - \bar{\mu}/r < 0 \tag{10}$$

The corresponding optimal horizontal and vertical lift components are defined in a separate boundary analysis, where it is shown that

$$L_1^* = \lambda^* \sin\mu^* = (V_0/V)^2(1+M_0)^{1/2}/\cos\gamma \tag{11}$$

$$L_2^* = \lambda^* \cos\mu^* = -(C_L^*/C_D^* V^2)\lambda_\gamma \tag{12}$$

The difficulty lies in the fact that λ_γ in (12) is unknown. In [4], it is shown that λ_γ can be accurately estimated during the initial boundary layer using a linearized analysis of the necessary conditions. However, to date, we have not been successful in providing a closed form solution to the TBL solution. Note that (11) is valid throughout, and represents a closed form guidance law. Below we present a guidance algorithm for defining L_2 in the TBL. It is a predictive/corrective type guidance law constructed to maintain L_2 as small as possible during the TBL maneuver while satisfying terminal constraints on altitude and heading. This algorithm both determines when the TBL should be initiated, and the guidance algorithm for defining L_2 in the TBL.

Despite the fact that $L_2(t)$ is difficult to predict, it is possible to accurately predict the final velocity. The expression for energy rate is given by

$$\dot{E} = C_D^*(1+\lambda^2)\rho S V^3/4m \tag{13}$$

Combining (4), (10), and (13), and using the fact that $\lambda \simeq 1$, $\mu \simeq \pi/2$, $r \simeq$ constant $= \bar{r}$, and $\gamma \simeq 0$, throughout the optimal trajectory [1], results in

$$dE/d\psi = -2(C_D^*/C_L^*)(E+\mu/\bar{r}) \tag{14}$$

Integrating (14) gives a relationship between velocity and heading along the the optimal path

$$V^2(t) = V^2(0)\exp\{K^*\psi(t)\}, \qquad K^* = 2C_D^*/C_L^* \tag{15}$$

which, in particular, can be used to estimate $V(t_f)$ given ψ_f.

The guidance law for the TBL is based on the fact that L_2 should be kept small, and that the vertical plane motion of the vehicle is largely determined by the gravity force at high altitudes. This is evident from the (3), where we note that to maintain near constant flight path angle requires

$$L_2 \simeq -M \tag{16}$$

For a typical re-entry from a 100 nm circular orbit and for a 40° plane change maneuver, (15) can be used to show that the value of M is on the order of -3 to -4 near the end of the trajectory, which would imply an angle of attack three to four times the maximum lift-to-drag value. This unrealistically large value implies that a major part of the TBL maneuver should occur at the bottom of the trajectory, with only minor corrections allowed during the climbing phase. Thus, a predictive/corrective form of guidance law was selected. To simplify the problem of predicting the forward motion, it was assumed that the TBL maneuver consists of two sub-arcs. The first is a constant flight path angle rate pull-up maneuver, followed by a second arc in which the vehicle flies solely under the influence of gravity. This motion is independent of what is simultaneously taking place in the horizontal plane. The situation is illustrated in Fig. 1, where the two sub-arcs define Region 1 and Region 2.

To integrate the motion, the velocity is approximated as constant in each region. Assuming for the moment that the average velocity in each region is known, then the altitude and flight path angle histories in each region are given by:

$$\gamma(t) = k(t-t_o) + \gamma_o, \qquad k > 0 \tag{17-a}$$

$$h(t) = V_1\{k(t-t_o)^2/2 + \gamma_o(t-t_o)\} + h_o, \qquad t_1 \geq t \geq t_o \tag{17-b}$$

in Region 1, and

$$\gamma(t) = -C(t-t_1) + \gamma_1, \qquad C = \bar{\mu}/V_2\bar{r}^2 - V_2/\bar{r} > 0 \tag{18-a}$$

$$h(t) = V_2\{-C(t-t_1)^2/2 + \gamma_1(t-t_1)\} + h_1, \qquad t_f \geq t \geq t_1 \tag{18-b}$$

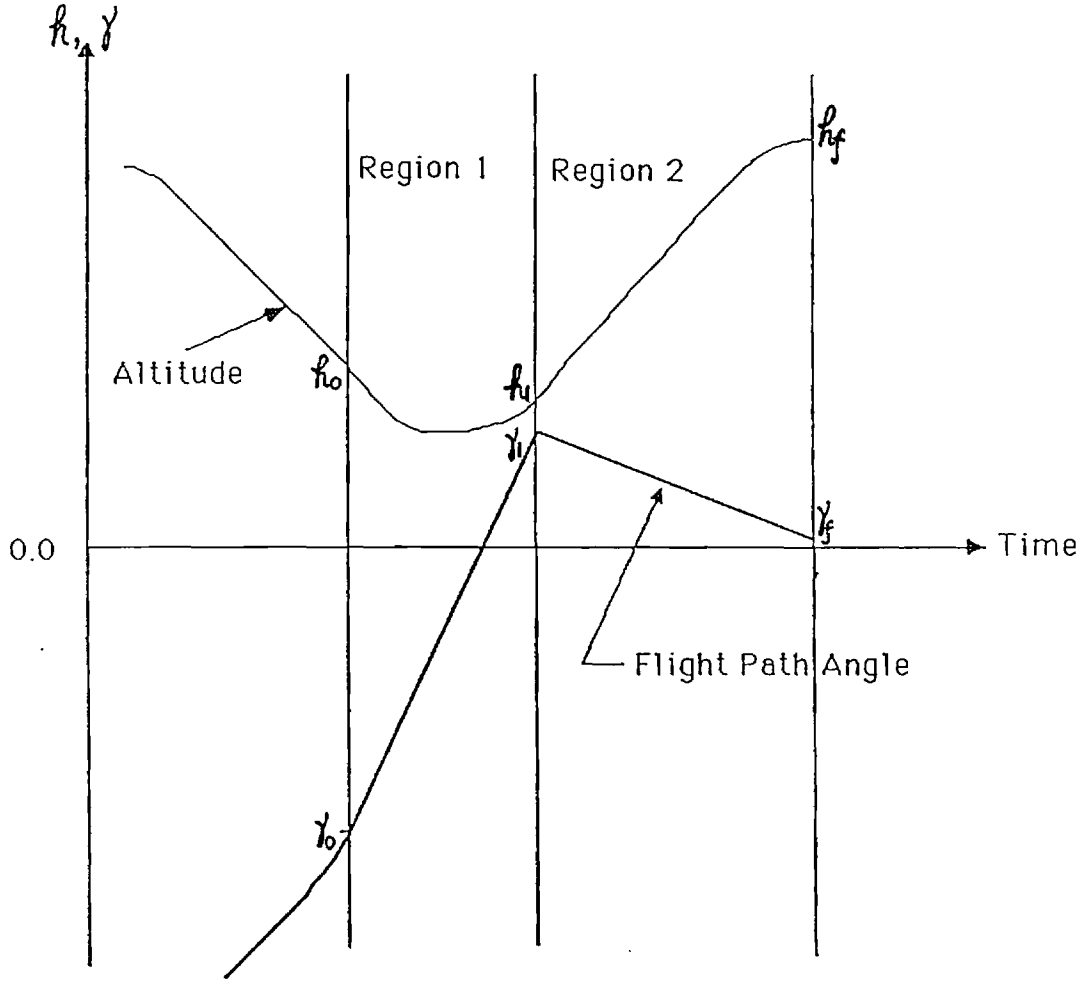

Figure 1. Two sub-arcs in the climbing phase

in Region 2. Time t_o represents current time, and t_1 is the time at the boundary of Regions 1 and 2. Requiring continuity at $t = t_1$, results in the following expression for γ_1 in terms of initial and final conditions:

$$\gamma_1 = \text{sqrt}\{-a/b\} \tag{19}$$

where

$$a = h_o - h_f - V_1\gamma_o^2/2k_1 - V_2\gamma_f^2/2C < 0 \tag{20}$$

$$b = (V_1/k + V_2/C)/2 > 0 \tag{21}$$

The time spent in both regions is then easily determined from (17-a) and (18-a)

$$\tau_1 = (\gamma_1 - \gamma_o)/k, \qquad \tau_2 = (\gamma_1 - \gamma_f)/C \tag{22}$$

and the altitude at $t = t_1$ at the boundary can be directly computed from (17-b).

$$h_1 = V_1\{k\tau_1^2 + \gamma_o\tau_1\} + h_o \tag{23}$$

During the TBL, it is common to encounter the condition that $\tau_1 < 0$, in (22). This implies that there is no Region 1 and γ_f cannot be attained. If this should occur, we set $\tau_1 = 0$, $\gamma_1 = \gamma_o$, $h_1 = h_o$, and compute τ_2 from (18-b). Likewise, early in the trajectory it is common to encounter the condition $\tau_2 < 0$, implying that there is no Region 2 and that γ_f cannot be attained. In this case, we set $\tau_2 = 0$, $h_1 = h_f$, and compute τ_1 from (17-b).

The heading change in Regions 1 and 2 can be obtained by integrating (4) for the altitude profiles in (17-b) and (18-b). Replacing V by its average value in each region, and using the approximations $\lambda \simeq 1$, $\mu \simeq \pi/2$

$$\dot{\psi} = k_{\psi 1} \exp\{-(h-h_o)/\beta\}, \qquad k_{\psi 1} = C_L^* \rho_o S V_1/2m \tag{24}$$

in Region 1 and

$$\dot{\psi} = k_{\psi 2} \exp\{-(h-h_1)/\beta\}, \qquad k_{\psi 2} = C_L^* \rho_1 S V_2/2m \tag{25}$$

where $\rho_i = \rho(h_i)$, and β is the scale height for an exponential atmosphere. The integrations were performed using a symbolic manipulation program, which yielded:

$$\Delta\psi_i = 2 \operatorname{sqrt}\{\pi/A\} \exp\{B^2/4A\} \operatorname{erf}\{(2At+B)/2\operatorname{sqrt}\{A\}\Big|_0^{\tau_i} \tag{26}$$

where for Region 1

$$A = V_1 k/2\beta > 0, \qquad B = V_1 \gamma_o/\beta \tag{27-a}$$

and for Region 2

$$A = -V_2 C/2\beta < 0, \qquad B = V_2 \gamma_1/\beta > 0 \tag{27-b}$$

The erf function is computed using a truncated power series expansion of the form

$$\operatorname{erf}\{x\} = 2 \exp\{-x^2\} \sum_{k=o}^{m} 2^k \, x^{2k+1}/(2k+1)!! \tag{28}$$

where $n!! \equiv 1 \cdot 3 \cdot 5 \cdots n$. It is interesting to note that despite the fact that A in Region 2 is negative, the expression in (26) will yield a real value due to the fact that the summation in (28) involves only odd powers of x.

The prediction of heading change depends on the values used for the average velocities in Regions 1 and 2. The actual velocity at the start and end of each region can be related to the heading change in each region using (15). Thus, the average velocities are related to the corresponding heading changes by:

$$V_1 = V_o[1 + \operatorname{sqrt}\{\exp(K^* \Delta\psi_1)\}]/2 \tag{29-a}$$

$$V_2 = V_o\left[\text{sqrt}\{\exp(K^*\Delta\psi_1)\} + \text{sqrt}\{\exp[K^*(\Delta\psi_1+\Delta\psi_2)]\}\right]/2 \qquad (29\text{-b})$$

Hence, it was necessary to iterate the solution for $\Delta\Psi_i$ to convergence, updating the estimate for the average velocities using (29). It was found that the procedure converged in less than five iterations, even for poor initial guesses for the average velocity. Since the calculation is updated throughout the trajectory, the starting guess is the value from the previous update, and it is very close to the converged value to start with, except possibly at the beginning.

The above calculations are initially used to decide when to switch to the TBL. This is defined to be the time where the heading to go is first less than or equal to the estimated heading change $(\Delta\psi_1+\Delta\psi_2)$. Following the switch to the terminal boundary, the same algorithm is used to provide closed-loop guidance.

In the initial pull-up maneuver, when the estimated time duration in Region 1 (τ_1) is greater than zero, the vertical component of the normalized lift coefficient (L_2) required to produce a constant flight path angle rate is

$$L_2 = 2mk/C_L^*S\rho V - M\cos\gamma \qquad (30)$$

If $\tau_1 = 0$, then we are in Region 2. In this region we set $L_2 = 0$, and regulate the heading change using L_1:

$$L_1 = L_1^* + k_\psi\,[\Delta\psi - \Delta\psi_2] \qquad (31)$$

where $\Delta\psi = \psi_f - \psi$, $\Delta\psi_2$ is the estimated heading change in Region 2, and L_1^* is defined in (11). The objective is to achieve $\Delta\psi = 0$, when $h = h_f$.

To use the above guidance law, it is necessary to define the parameters k, k_ψ, and γ_f. To provide continuous guidance and reasonable TBL flight times, γ_f should be chosen on the order of one degree. The parameter $k > 0$

was chosen as a simple multiple (on the order of 3) of C to insure a reasonable pull-up while maintaining $L_2 \ll 1$. The guidance gain k_ψ in (31) was chosen as 100 to provide sufficient regulation with excessively large values of L_1.

SECTION 3
NUMERICAL RESULTS

This section evaluates the performance of the predictor/corrector guidance algorithm described in Section 2, and compares the results to the optimal solutions in [5], which were computed using a numerical optimization code. A simple exponential atmospheric model, fitted to match the standard atmosphere at 100,000 and 200,000 feet, was used to obtain our results, while the results in [5] used a more exact standard atmosphere. In addition, the aerodynamic parameters were treated as constant in our simulation, while [5] used tabulated values. However, we feel that the differences in the modeling are small, and will not have a significant impact on the comparisons.

Figure 2 illustrates the effect that the choice of k in (17-a) has on the resulting guided profiles, for a 40° plane change trajectory with $k_\psi = 1/\tau = 100$. As the value of k increases, initiation of the TBL is delayed slightly, due to the increase in the flight path angle rate during the initial pull-up maneuver. Figures 3 and 4 give the corresponding time histories for the control components L_1 and L_2. Note that the peak amplitude in L_2 is relatively independent of k. The apparent variation in L_1 that takes place in Region 2 is not directly related to k, but is largely a result of the control update rate, which was chosen as once per second of trajectory time. Thus, the variation in L_1 can be greatly reduced by using a variable update rate in the vicinity where Region 2 begins.

Figure 5 shows the guided trajectories for orbit plane changes of 10°, 20°, 30°, and 40°, for k = 3. Figure 6 gives the corresponding angle-of-attack profiles. The peak angle of attack occurs at the end of the pull-up maneuver in Region 1, and is approximately 24° for all the maneuvers. The angle of attack corresponding to maximum L/D, which the optimal solution uses

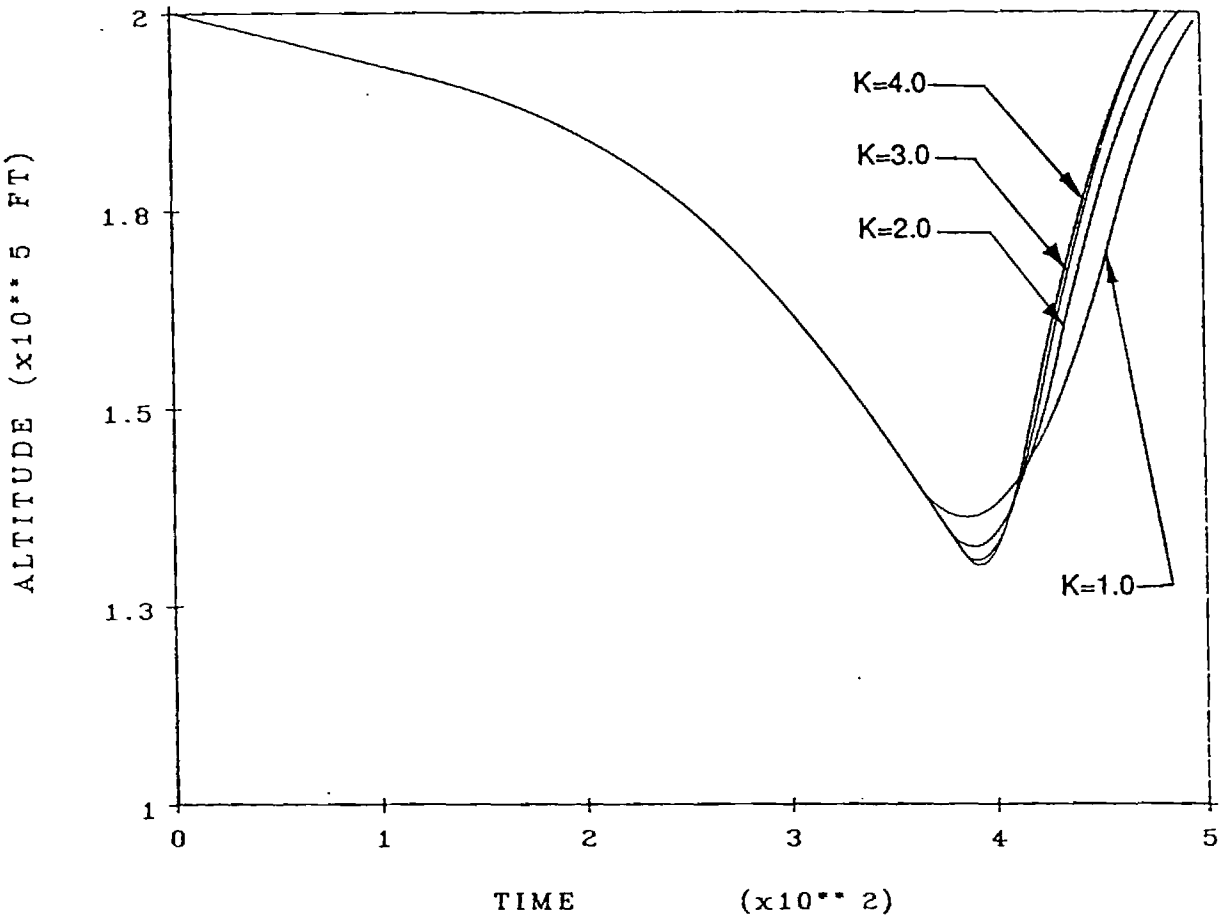

Figure 2. Guided Altitude Profiles for Values of τ = 0.01, K=1.0, 2.0, 3.0, 4.0 for 40^0 Orbital Plane Change.

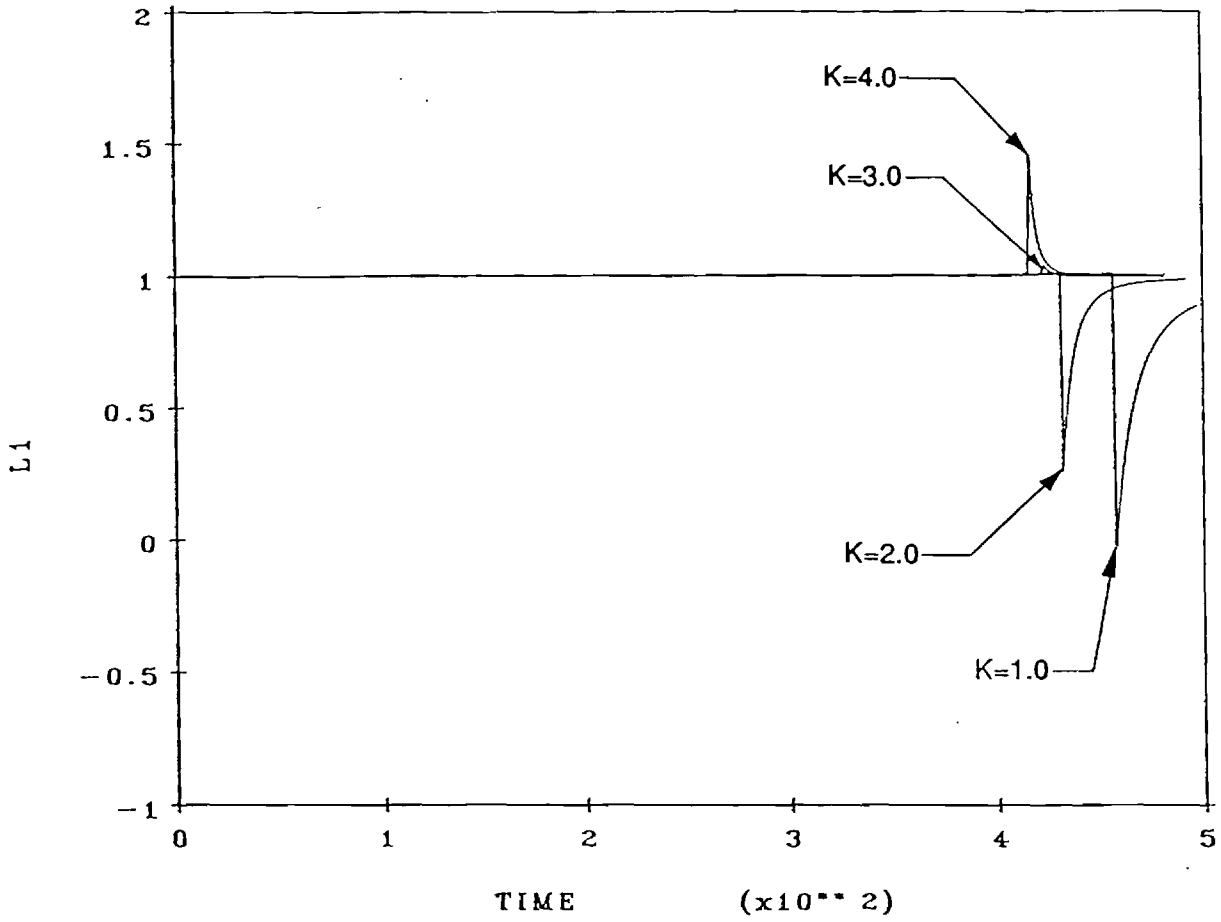

Figure 3. Time Histories of The Horizontal Component of The Normalized Lift Force for Values of τ=0.01, K=1.0, 2.0, 3.0, 4.0 for 40° Orbital Plane Change.

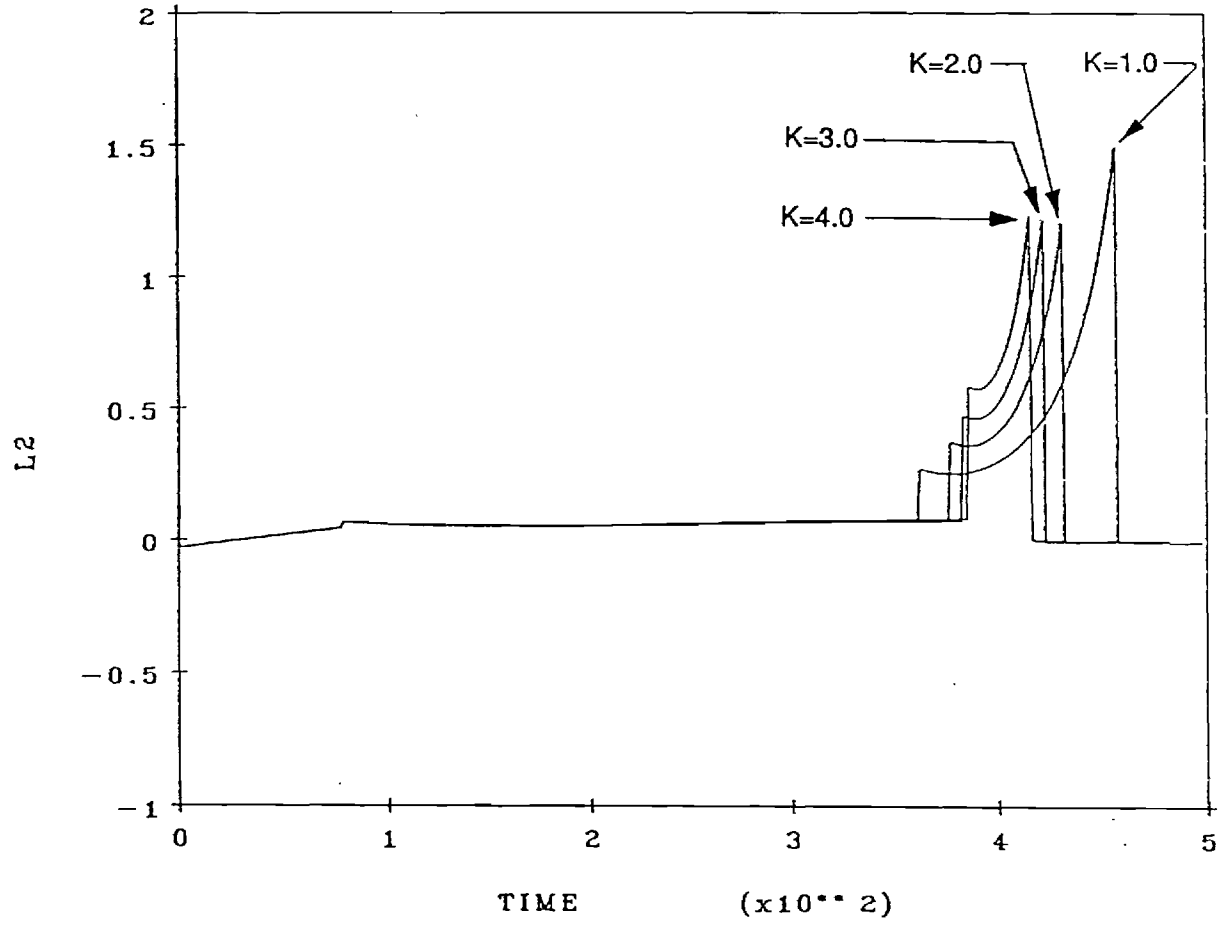

Figure 4. Time Histories of The Vertical Component of The Normalized Lift Force for Values of τ=0.01, K=1.0, 2.0, 3.0, 4.0 for 40° Orbital Plane Change.

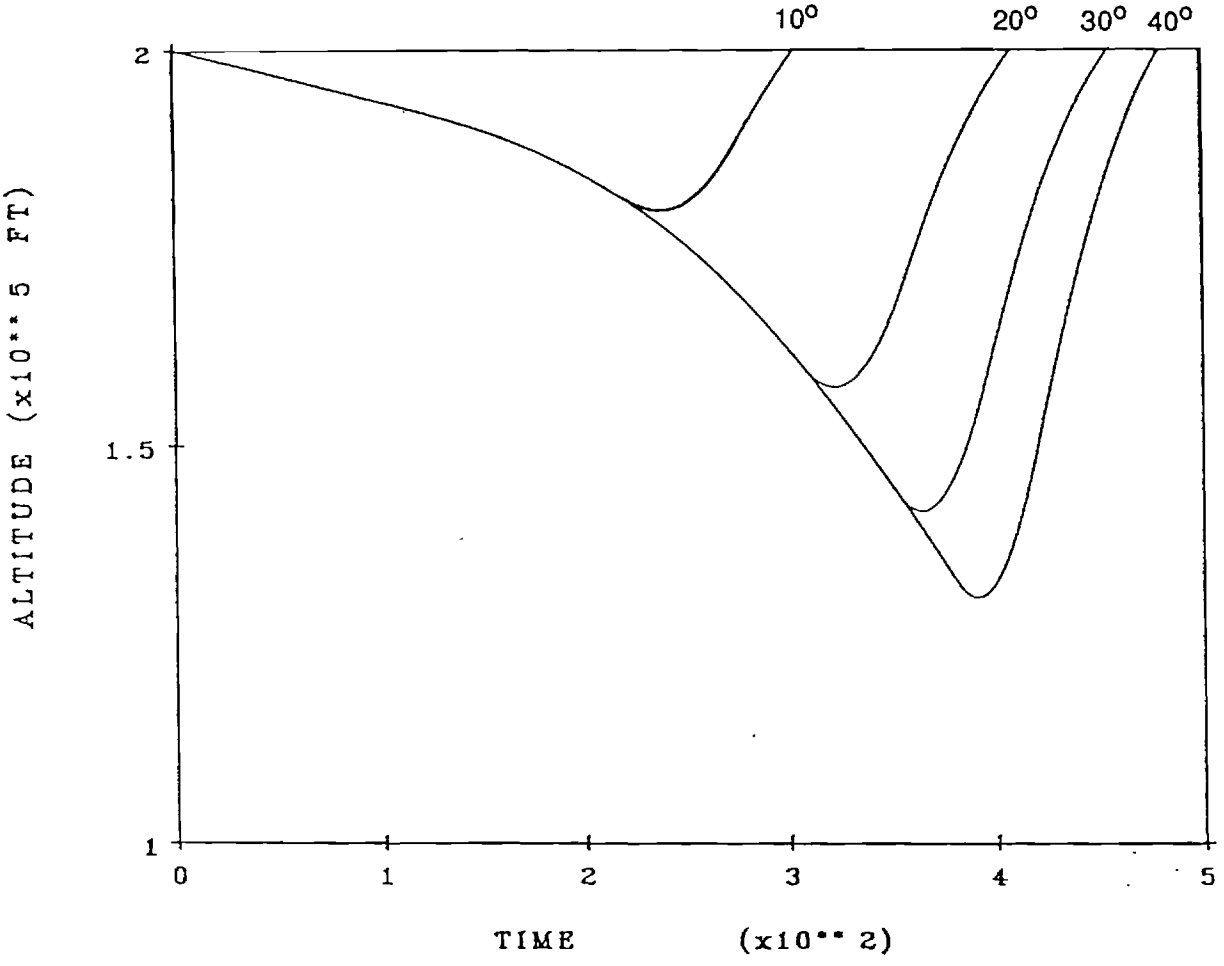

Figure 5. Guided Optimal Trajectories With 10°, 20°, 30°, 40° Orbital PLane Change.

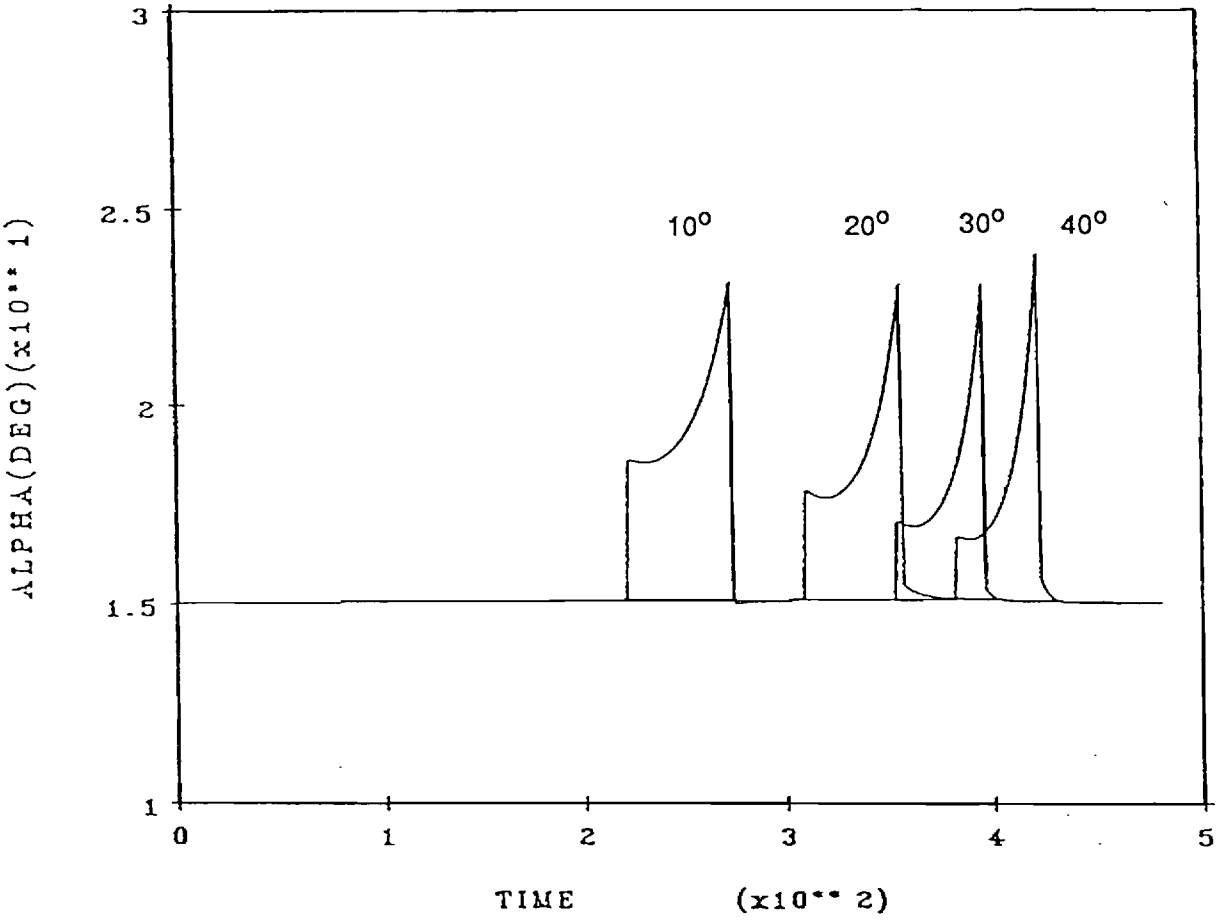

Figure 6. Guided Angle of Attack Time Histories With 10°, 20°, 30°, 40° Orbital PLane Change..

throughout, is approximately 15°. The increase in α in the guided solution results from the increase in L_2 required to maintain constant flight path angle rate in Region 1, which in turn is due to the loss in energy that takes place during this portion of the maneuver. It would be possible to further reduce the peak if some other assumption is used for flight path angle rate in this region; however, this may increase the complexity in predicting the future motion of the vehicle. In any case, these results represent a significant improvement over the angle-of-attack profile reported in [6], where the maximum is approximately 30°, and occurs at the end of the maneuver. An important aspect in comparing these results is that the major corrections here occur around the middle of the trajectory, while the corrections in [6] increase as the end condition is reached. This will give rise to important differences when effects such as atmospheric uncertainty are included, since it is difficult to make significant changes to the trajectory near the end of the maneuver.

The near optimality of the guided trajectories of Figure 5 are examined in Table 1 on the basis of fuel fraction. Note that the S.P. guided solutions are very close to equaling the performance of the optimal solutions, and represent a significant improvement over an exoatmospheric single impulse maneuver.

Table 1

Comparison of Fuel Fractions Between The Pure Propulsive Maneuver and The Aeroassisted Guided Solution

PLANE CHANGE	OPTIMAL SOLUTION	S.P. GUIDED SOLUTION	SINGLE IMPULSE
10	.19	.201	.36
20	.32	.333	.59
30	.41	.434	.73
40	.49	.515	.83

SECTION 4
FUTURE RESEARCH

During the next reporting period, we plan to generate numerically optimized trajectories using a multiple shooting algorithm. This will provide a better basis for comparison, which will remove the uncertainty that presently exists due to small differences in aerodynamic and atmospheric modeling between our results and that reported in [6]. We also plan to refine the predictor/corrector guidance law so as to minimize the peak angle of attack. Other issues, such as enforcing heating rate and heating load constraints will also be addressed.

Following this activity, we plan to initiate research on the application of singular perturbation methods to the hypersonic aerocruise problem. Reference [7] will serve as an excellent starting point, since it essentially solves the cruise portion, which amounts to the reduced solution in a singular perturbation formulation. The optimal arcs, to and from the cruise arc, were not analyzed in [7]. The dynamics associated with this problem, and the issues related to singular perturbation analysis, will be totally different from that encountered thus far, due to the presence of thrusting that can take place along the entire trajectory.

REFERENCES

1. Calise, A.J., Bae, G., "Singular Perturbation Analysis of AOTV Related Trajectory Optimization Problems," Progress Report for the Period 14 April - 30 Oct., Nov. 1986.

2. Calise, A.J., Bae, G., "Singular Perturbation Analysis of AOTV Related Trajectory Optimization Problems," Progress Report for the Period 1 Sept. - 30 July, July 1986.

3. Calise, A.J., "Singular Perturbation Analysis of the Atmospheric Orbital Plane Change Problem," To appear in J. of Astro. Sci., Jan.-March 1988.

4. Calise, A.J., Bae, G., "Optimal Heading Change with Minimum Energy Loss for a Hypersonic Gliding Vehicle," AIAA Atmospheric Flight Mechanics Conf., Aug. 1987.

5. Hull, D.G., Giltner, J.M., Speyer, J.L., Mapar, J., "Minimum Energy-Loss Guidance for Aeroassisted Orbital Plane Change," J. of Guidance, Control, and Dynamics, Vol. 8, No. 4, Jul.-Aug. 1985.

6. Hull, D.G., McClendon, J.R., Speyer, J.L., "Improved Aero-Assisted Plane Change Using Successive Approximation," AIAA Atmospheric Flight Mechanics Conf., Williamsburg, VA, Aug. 1986.

7. Mease, K.D., Lee, J., Vinh, N.X., "Orbital Changes During Hypersonic Aero-Cruise," AIAA Atmospheric Flight Mechanics Conf., Aug. 1987.

SINGULAR PERTURBATION ANALYSIS OF AOTV-RELATED TRAJECTORY OPTIMIZATION PROBLEMS

PROGRESS REPORT

1 December - 31 August, 1988

September 1988

Research Supported by NASA - Langley Research Center

NASA Grant No. NAG-1-660

Principal Investigator: Dr. Anthony J. Calise

Research Assistant: Mr. Gyoung Bae

NASA Grant Monitor: Dr. Daniel Moerder

Georgia Institute of Technology
School of Aerospace Engineering
Atlanta, GA 30332-0150

TABLE OF CONTENTS

LIST OF FIGURES

LIST OF TABLES

SECTION 1
SUMMARY OF RESEARCH ACCOMPLISHMENTS

Research to date has concentrated on the problem of aeroassisted orbital plane change. The results reported earlier [1,2] indicate the usefulness of singular perturbation theory in developing analytic guidance solutions. However, a difficult terminal boundary layer (TBL) analysis is required to satisfy the terminal constraint on altitude. All of these results have also appeared in the open literature [3,4]. Unfortunately, we have not been able to explicity solve the TBL problem in closed form, since it requires a forward integration of the equations of motions to invoke the terminal constraint. In [5] a suboptimal control solution for the vertical component of lift, which is based on a predictive/corrective type guidance law, was proposed. This guidance law provides a highly accurate method of controlling terminal heading and altitude with nearly minimum energy loss. The horizontal component of lift is based on the earlier results reported in [2,4]. Unfortunately, this law resulted in peak angles of attack around 24^{o}, which is significantly higher that the angle of attack for maximum L/D, which is around 15^{o}. In any case, these results represent a significant improvement over the angle-of-attack profile reported in [6], where the maximum is approximately 30^{o}, and occurs at the end of the maneuver. An important aspect in comparing these results is that major corrections should occur early in the trajectory, while major corrections near the end are difficult to achieve in the presence of atmospheric uncertainty at high altitudes.

Research during this period has concentrated on a detailed comparison of three guidance algorithms that result from analyzing the initial boundary layer (reentry phase) dynamics, and on improving the predictive/corrective guidance algorithm (terminal phase) to avoid high angle of attack during the pull-up maneuver. This was accomplished by constraining the vehicle to fly at maximum L/D, and using only bank angle for terminal guidance. In addition, optimal solutions were generated for the first time using a multiple shooting algorithm [7] for comparison purposes.

Section 2 summarizes the results on the reentry phase analysis. Of particular interest here is that energy is included as a state variable for the first time in the reduced problem. Our earlier work treated Energy as constant in the dynamics, and energy loss was accounted for only in the performance index. Section 3 presents the rational for the new terminal

guidance law, which is used to both initiate the terminal maneuver and to define the bank angle control. Numerical results that demonstrate the performance of the reentry phase guidance and of the total guidance algorithm are contained in Section 4. Included in this section are comparisons to numerically computed optimal trajectories using the multiple shooting code. Future research activities are summarized in Section 5.

SECTION 2
OPTIMAL REENTRY GUIDANCE

As reported in [1,4], the reduced solution defines the optimal altitude profile for maneuvering as a function of vehicle energy, which is defined by the following function minimization

$$h_o = \arg\min_h \{V^2(1+M^2)^{1/2}\} \mid E = \text{current energy} \tag{1}$$

where

$$E = V^2/2 - \nu/r < 0 \tag{2}$$

$$M(h,V) = (2m/C_L^* S)[1-\nu/V^2 r]/\rho r \tag{3}$$

In these equations V is velocity, r is the radius from the earth's center, ρ is air density, m is vehicle mass, S is the aerodynamic reference area, and C_L^* is the lift coefficient at maximum L/D. The corresponding optimal horizontal and vertical lift components are defined in a separate boundary analysis, where it is shown that:

$$L_1^* = \lambda^* \sin \mu^* = (V_0/V)^2(1+M_o)^{1/2}/\cos \gamma \tag{4}$$

$$L_2^* = \lambda^* \cos \mu^* = -(C_L^*/C_D^* V^2)\lambda\gamma \tag{5}$$

where C_D^* is the drag coefficient at maximum L/D, γ is the flight path angle, λ is the normalized lift coefficient (C_L/C_L^*) and μ is the bank angle.

Note that (4) is valid throughout, and represents a closed form guidance law. The difficulty lies in the fact that λ_γ in (5) is unknown. One approach is to use the reduced solution for λ_γ given by

$$\lambda_\gamma{}^o = C_D{}^* V_o{}^2 M_o / C_L{}^* \tag{6}$$

Use of (6) in (5) yields

$$L_2{}^* = (V_o/V)^2 M_o \tag{7}$$

This we denote as the SP1 solution. In [4] it is shown that λ_γ can also be estimated during the initial boundary layer using a linearized analysis of the boundary layer necessary conditions. This provides a correction term of the form

$$\lambda_\gamma = \lambda_\gamma{}^o + \delta\lambda_\gamma(\delta h, \gamma, E), \qquad \delta h = h - h_o \tag{8}$$

Use of (8) in (5) results in a SP2 solution. Both of these solutions have treated energy as constant in the dynamics, with energy loss accounted for only in the performance index.

In [8], a third formulation is presented in which energy dynamics are treated along with heading rate dynamics in the reduced solution. This introduces a second costate in the reduced problem. However, an approximate integration of λ_E was obtained for $\lambda \simeq 1$, $\mu \simeq \pi/2$, $\gamma \simeq 0$, which resulted in

$$\lambda_E \simeq - \exp\{-2C_D{}^*(\psi_f - \psi)/C_L{}^*\} \tag{9}$$

where ψ_f is the specified final heading (which approximates the inclination change for the orbit plane change problem). It is shown in [8] that the SP1 solution remains the same when E is modeled in the dynamics. The SP2 solution on the other hand is affected, which results in a new SP3 solution.

SECTION 3
A GUIDANCE ALGORITHM FOR THE EXIT PHASE

The above guidance algorithm does not satisfy the terminal constraint (exit condition) on h, which was lost in the reduced formulation. Enforcing this constraint results in a terminal boundary layer problem, whose necessary conditions are identical in form to those for the initial boundary layer. However, the solution asymptotically approaches the reduced solution backwards in time, starting from the terminal constraint on altitude. In addition, the change in ψ during the terminal maneuver must be accounted for to insure that both terminal constraints on h and ψ are met simultaneously. This requires an analytical integration of the state and costates. To circumvent this problem, a predictor/corrector guidance law was developed based on the known properties of the optimal solution: $\lambda^* \simeq 1.0$, $\mu^* \simeq \pi/2$.

To simplify the problem of integrating the forward motion, it is assumed that the nominal exit maneuver consists of two regions. In the first, a constant (negative) bank angle perturbation is used to increase the flight path angle. This is followed by a second region in which γ is influenced only by gravity. A bank angle correction is computed throughout the maneuver based on the predicted heading error at the final altitude. Constraints are enforced to insure continuity at the junction of the two regions, and satisfaction of the terminal constraint on altitude.

During terminal guidance we maintain $\lambda = 1.0$, and modulate the bank angle according to the following equations:

$$\mu = \mu_0 - \delta\mu_0 + \delta\mu \tag{10}$$

where in Region 1:

$$\mu_0 = \cos^{-1}(-M), \qquad \delta\mu_0 = \text{const.} > 0 \tag{11}$$

and in Region 2:

$$\mu_0 = 90^o, \qquad \delta\mu_0 = 0 \tag{12}$$

Note that μ_0 in Region 1 is the bank angle needed to cancel the gravitation

and centrifugal acceleration force terms. The nominal trajectory ($\delta\mu = 0$) can be analytically predicted, using the approximations:

$$\cos\mu \approx -M + \delta\mu_o \sin\mu_o, \qquad \sin\gamma \approx \gamma \tag{13}$$

the details of which are omitted for brevity. The predicted heading change ($\Delta\psi_p$) for the exit maneuver is calculated at each integration step along the trajectory, and is used to both initiate the maneuver (when $\Delta\psi_p = \psi_{go}$), and to track the terminal contraint using a simple proportional control law,

$$\delta\mu = k(\psi_{go} - \Delta\psi_p) \tag{14}$$

Region 2 guidance is initiated when the present altitude satisfies the continuity contraint at the junction of the two regions. The above calculations are initially used to decide when to switch to the TBL. This is defined to be the time where the heading to go is first less than or equal to the predicted heading change. Following the switch to the terminal boundary the same algorithm is used to provide closed loop guidance.

SECTION 4
NUMERICAL RESULTS

4.1 Reentry Guidance Performance

A numerical study was performed to evaluate the performance of the three reentry guidance laws discussed in Section 2. The parameter values were chosen to approximate the vehical studied in [6]. The initial conditions were also chosen to match the 40^o heading change maneuver in [6], where the sensible atmosphere was defined to begin at an altitude of 200,000 ft. The corresponding entry velocity and flight path angles are $V(0) = 25{,}926$ ft/s and $\gamma(0) = -.265^o$. A simple exponential atmospheric model was defined using standard atmospheric data for air density at altitudes of 10^5 and 2×10^5 feet. All of the comparisons are for a 40^o heading change.

Figure 1 compares the reduced solution altitude profile obtained from (1) with the SP1 and SP3 guided solution profiles, which on this scale are identical. A similar comparison is given for the SP2 guided solution in Fig. 2. Note that the reduced solution provides a reasonable altitude profile except at high energies near the initial time. However, this region of the solution is of little interest since the air density is negligably small. In any case, it is not physically possible to follow this profile (recall that h is used as a control variable in the reduced solution). Thus it was decided to maintain $\lambda = 1$ and $\lambda\cos\mu = -M$ until $h_0(E)$ falls below the current altitude. In order to evaluate the optimality of these solutions, an optimal solution was numerically computed using a multiple shooting algorithm [7]. In this case, the complete four state model (ψ,E,h,γ) was used to define the dynamics. The SP1 guided solution was used as an initial guess for the state time histories, and the reduced costate solutions were used as an initial guess for the costate time histories. The solution converged to a relative precision of 10^{-12} in 8 iterations. The value of the Hamilitonian was constant and essentially zero considering the relative precision accuracy required for convergence. This served as an independent check on the accuracy of the solution.

Figure 3 compares the optimal altitude profile with the profiles that result from the three guided solutions. Note that the optimal solution dips slightly more into the atmosphere near the end, and consequently results in slightly decreased flight time. The corresponding control time histories and heading profiles are compared in Fig's. 4-6. Note that in Fig. 4, the optimal bank angle at the final time is 90^o, which follows from (5) and the fact that $\lambda_\gamma(t_f) = 0$. In the context of singular perturbation theory, this gives rise to a terminal boundary layer which must be solved backwards in time. Since this was ignored in our analysis, the guided solutions approach the condition in (6) instead. This expalins the departure in the altitude profiles of Fig. 3. It is apparent that this effect is a minor one, and the dip in the optimal profile may not be desirable in any case (particularly for the orbit plane change problem).

It may be somewhat surprizing at this point that the SP1 and SP3 solutions are nearly identical. However, recall that the SP1 solution is not sensitive to the approximation that E is modeled as constant in the dynamics. That is it remains the same even if E dynamics are included in the reduced problem. The SP3 solution on the other hand corrects the SP2 solution for this modeling approximation, and results in essentially the

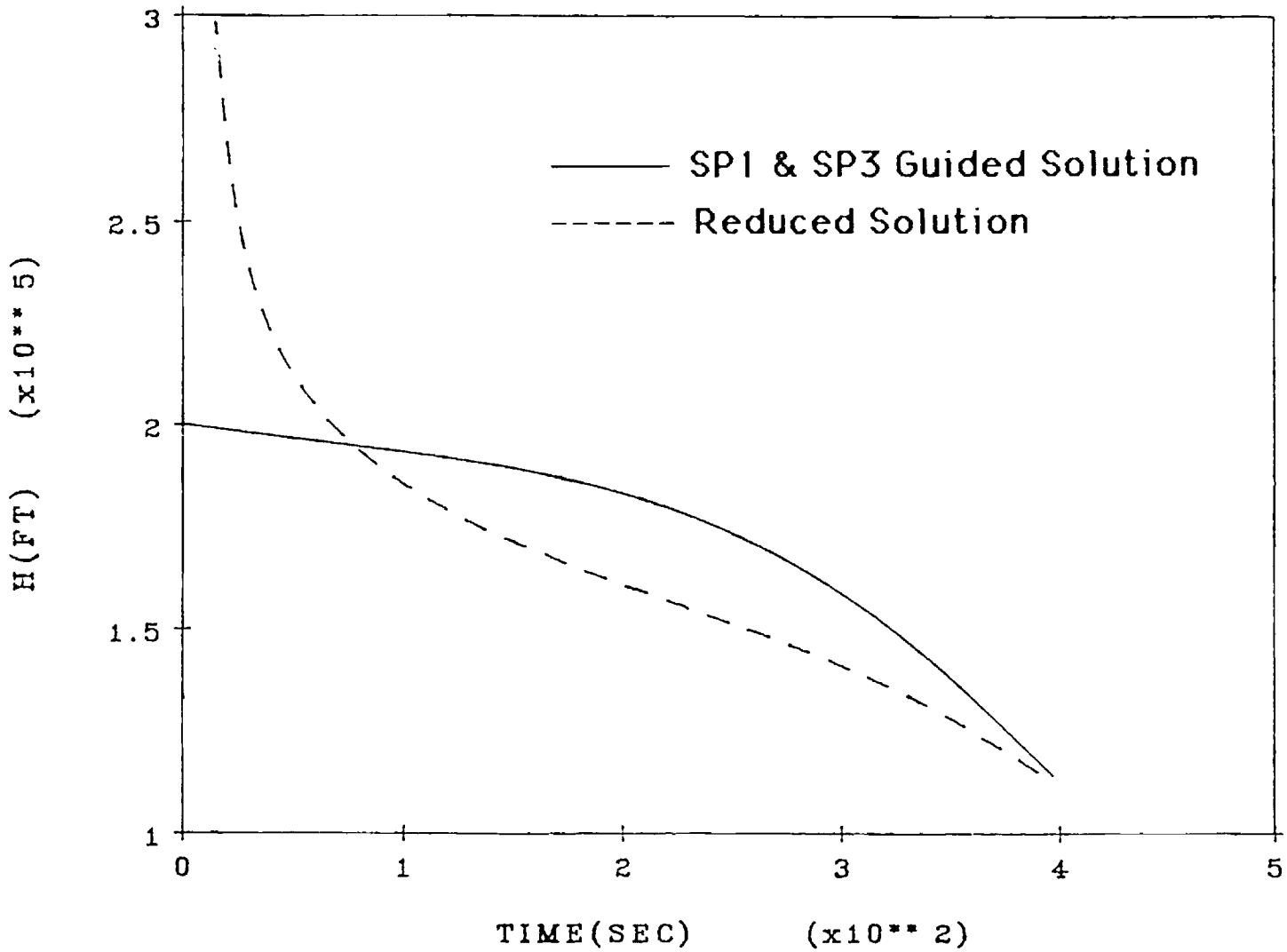

Figure 1. Comparison of the SP1 and SP3 guided altitude profiles with the reduced solution

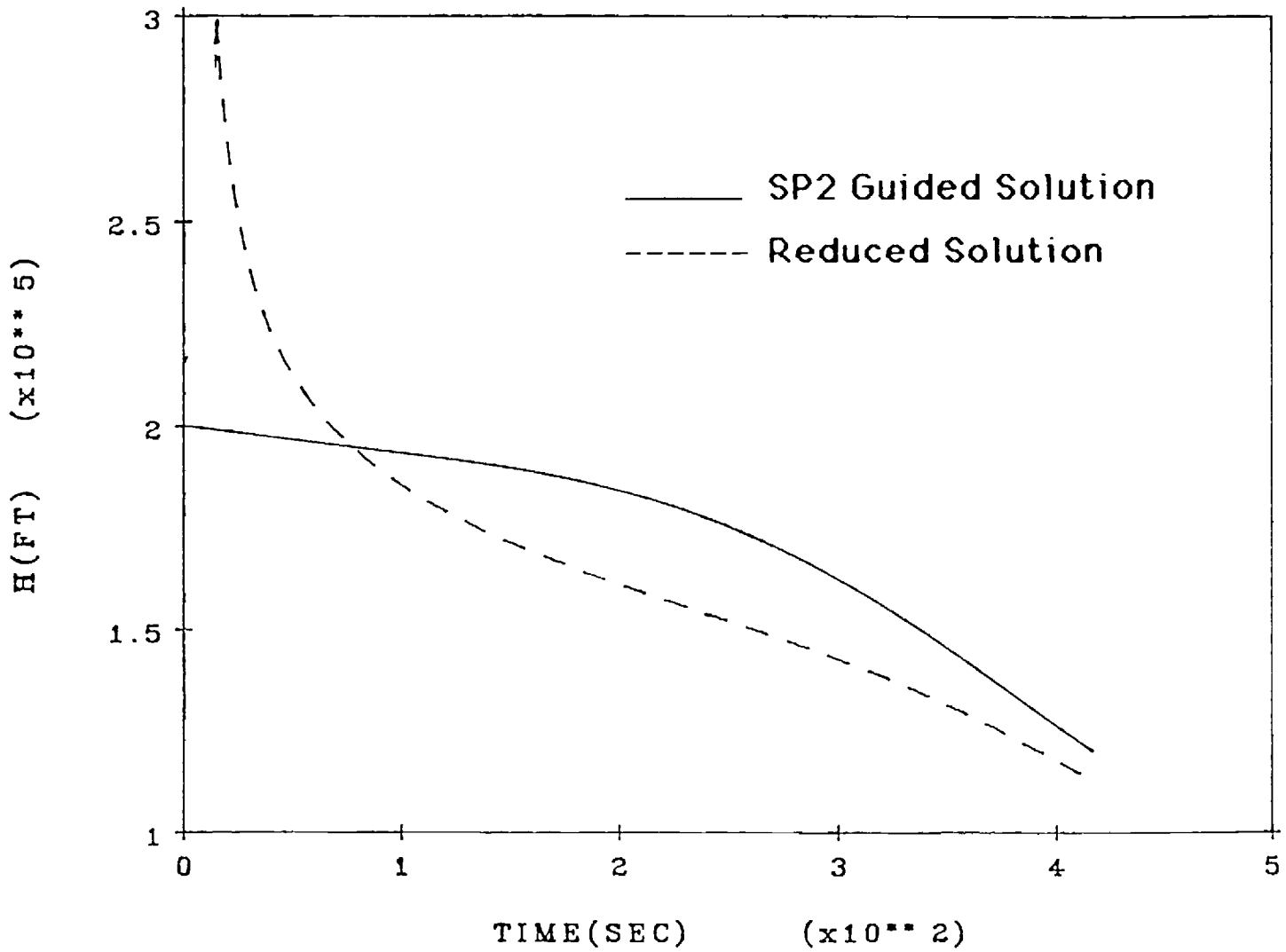

Figure 2. Comparison of the SP2 guided altitude profile with the reduced solution

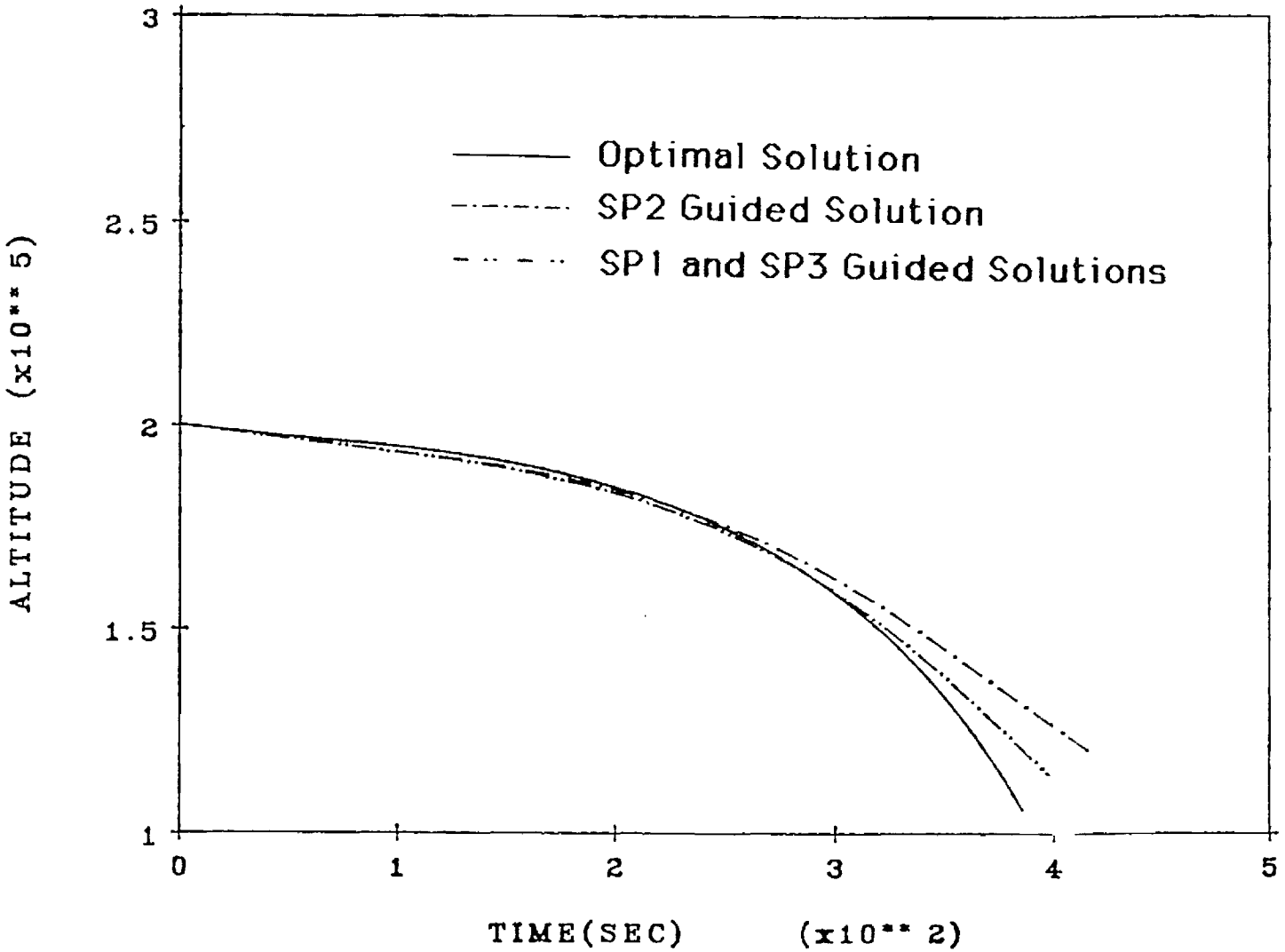

Figure 3. Comparison of the guided altitude profiles with the true optimal solution

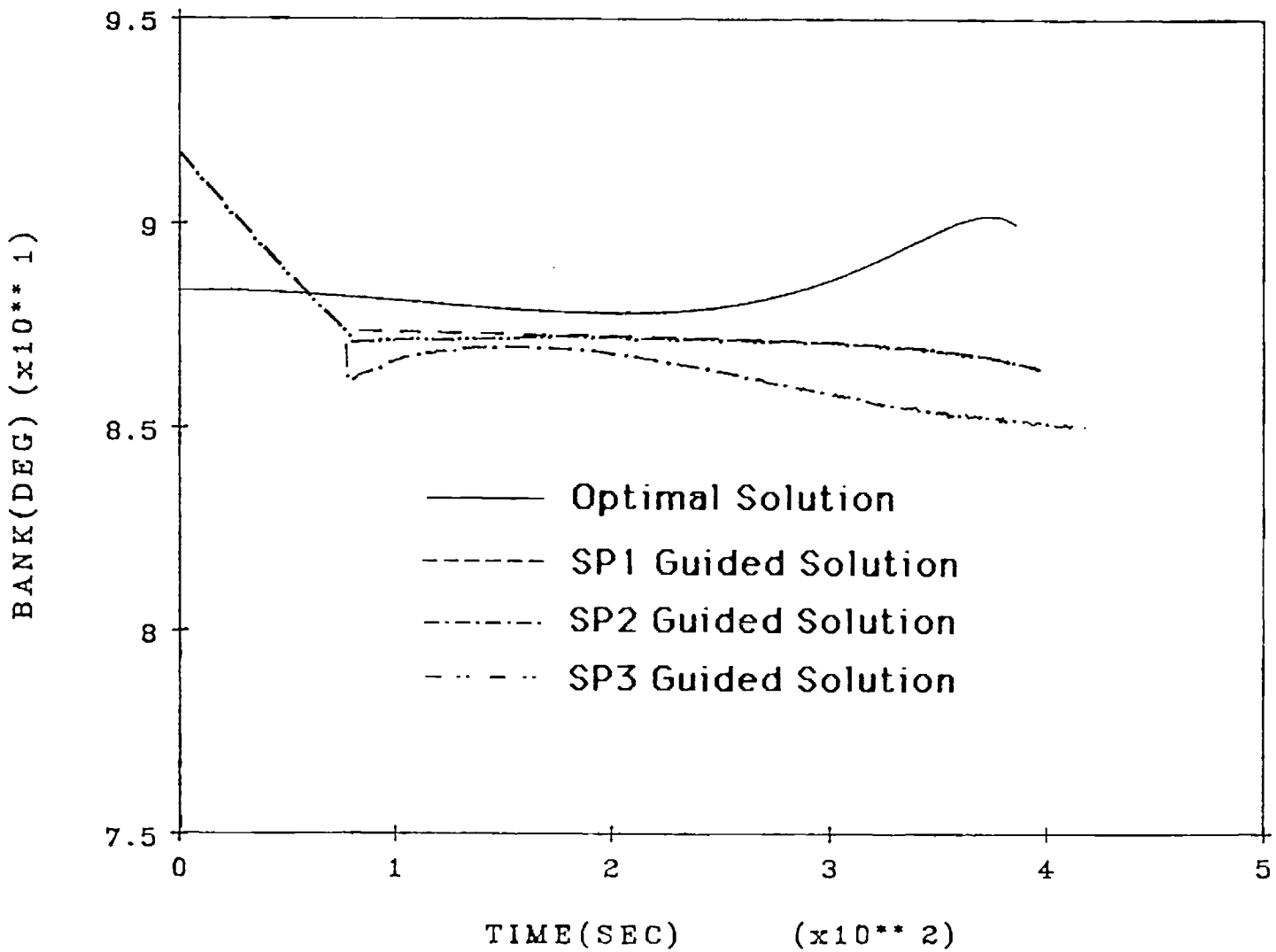

Figure 4. Bank angle profiles

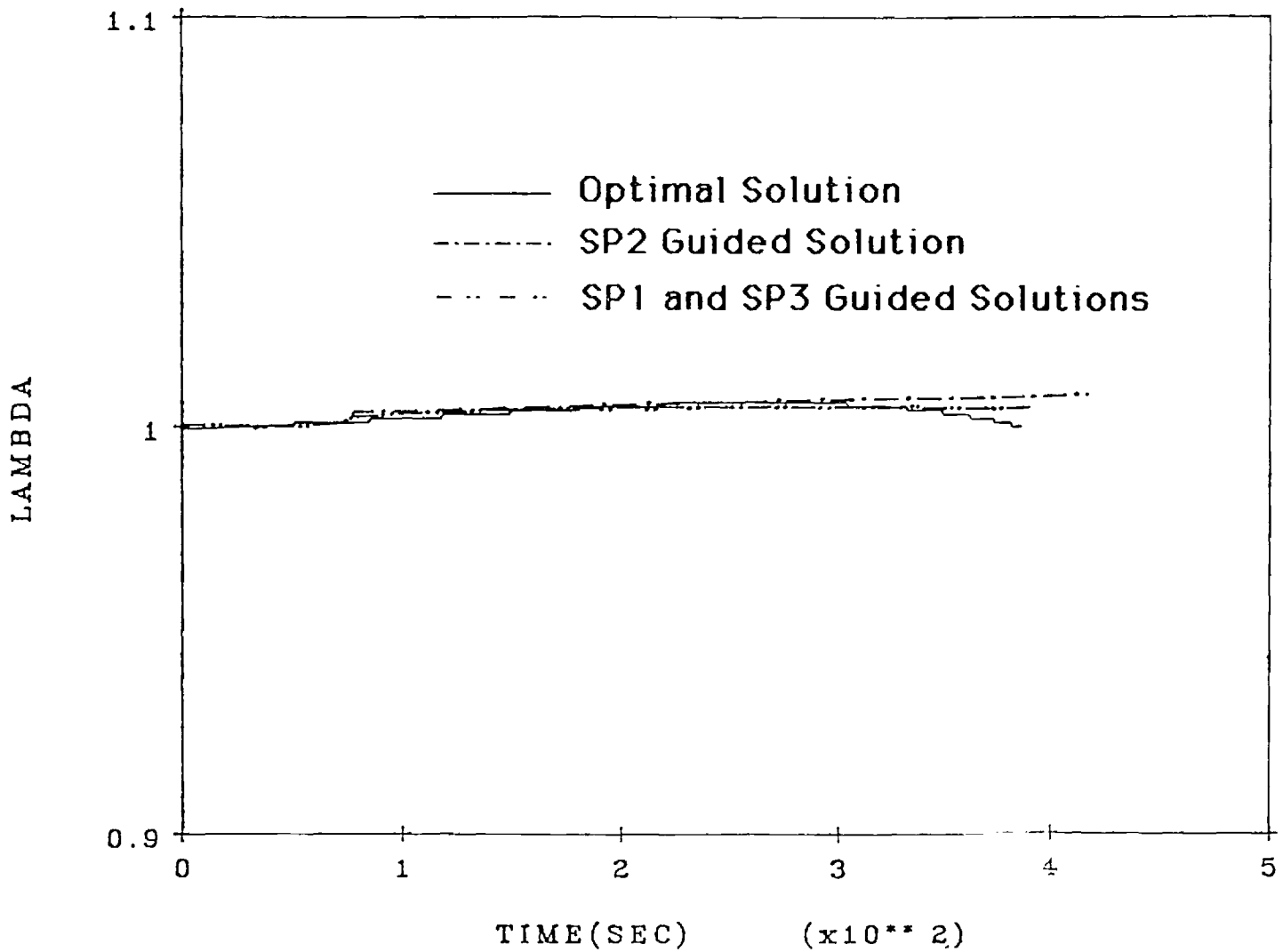

Figure 5. Normalized lift coefficient profiles

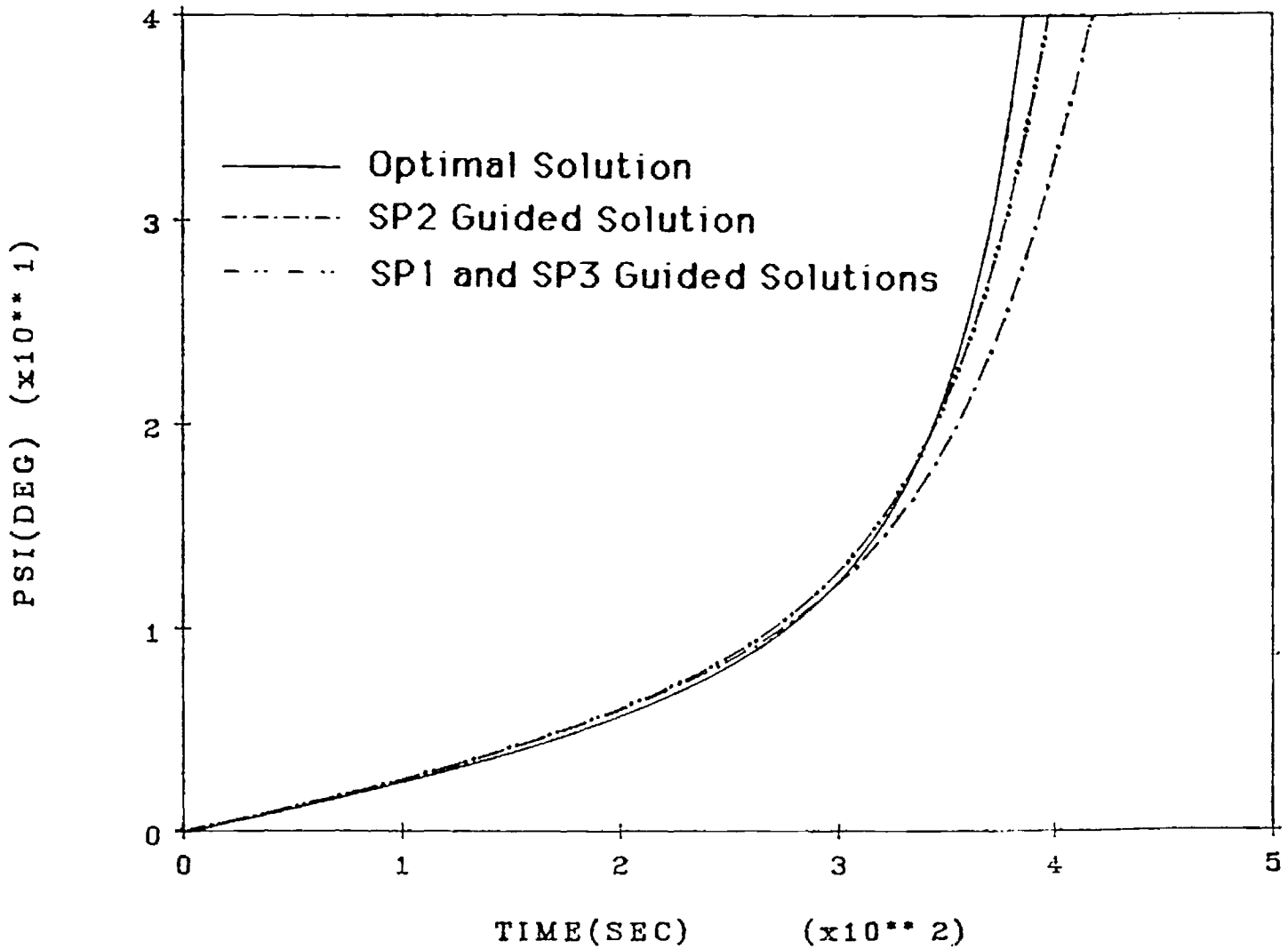

Figure 6. Heading profiles

same solution as the SP1 solution. This fact also justifies the use of the same solution as the SP1 solution. This fact also justifies the use of the approximation $\lambda_\gamma = \lambda_\gamma{}^o$ in the SP1 solution. Table 1 compares the energy loss for all the solutions, and shows that the three guided solutions produce essentially optimal performance.

4.2 Orbit Plane Change Guidance Performance

Since the SP1 solution is the simplest to implement, it was used in evaluating the terminal guidance algorithm of Section 3 for the orbit plane change problem. Fig's 7 and 8 illustrate the guided altitude profiles and the corresponding bank angle profiles obtained for heading changes up to 40^o, in increments of 10^o. The λ profiles are very close to 1.0 throughout for all the maneuvers, and are not illustrated. These results were generated for $\delta\mu_o = 25^o$, k = 50; however, it was found that the general character of the solutions did not change as these guidance parameters were varied. Note from Fig. 8 that, following the initial perturbation, bank angle continues to decrease in Region 1. This is due to the variation in M that takes place as the altitude departs from the reduced solution profile. After completing Region 1, the bank angle remains very close to 90^o, or in other words $\delta\mu$ in (14) is very close to zero, indicating the accuracy of the prediction algorithm.

In order to evaluate the optimality of the guidance algorithm, optimal solutions were obtained numerically using the multiple shooting algorithm. Fig's. 9 and 10 illustrate the optimal altitude and bank angle profiles. The most remarkable characteristic in these solutions is that the final time is nearly independent of the final heading. Also, the maximum bank angle variation is 30^o. The corresponding λ profiles are shown in Fig. 11, which verifies that the optimal solution lies close to $\lambda = 1$.

Dispite the fact that the optimal profiles have a decidedly different character, the guided solution performance is not far from optimal. Table 2 illustrates the near optimality by comparing the energy loss of the guided solutions with that of the optimal solutions.

Table 1
Comparison of Energy Loss (ft^2/s^2) for the
Reentry Guidance Algorithm

Guidance	t_f(s)	$E_f \times 10^8$	$\Delta E \times 10^8$
Optimal	358.6	-4.813	1.510
SP1	397.0	-4.813	1.510
SP2	415.8	-4.814	1.511
SP3	398.0	-4.813	1.510

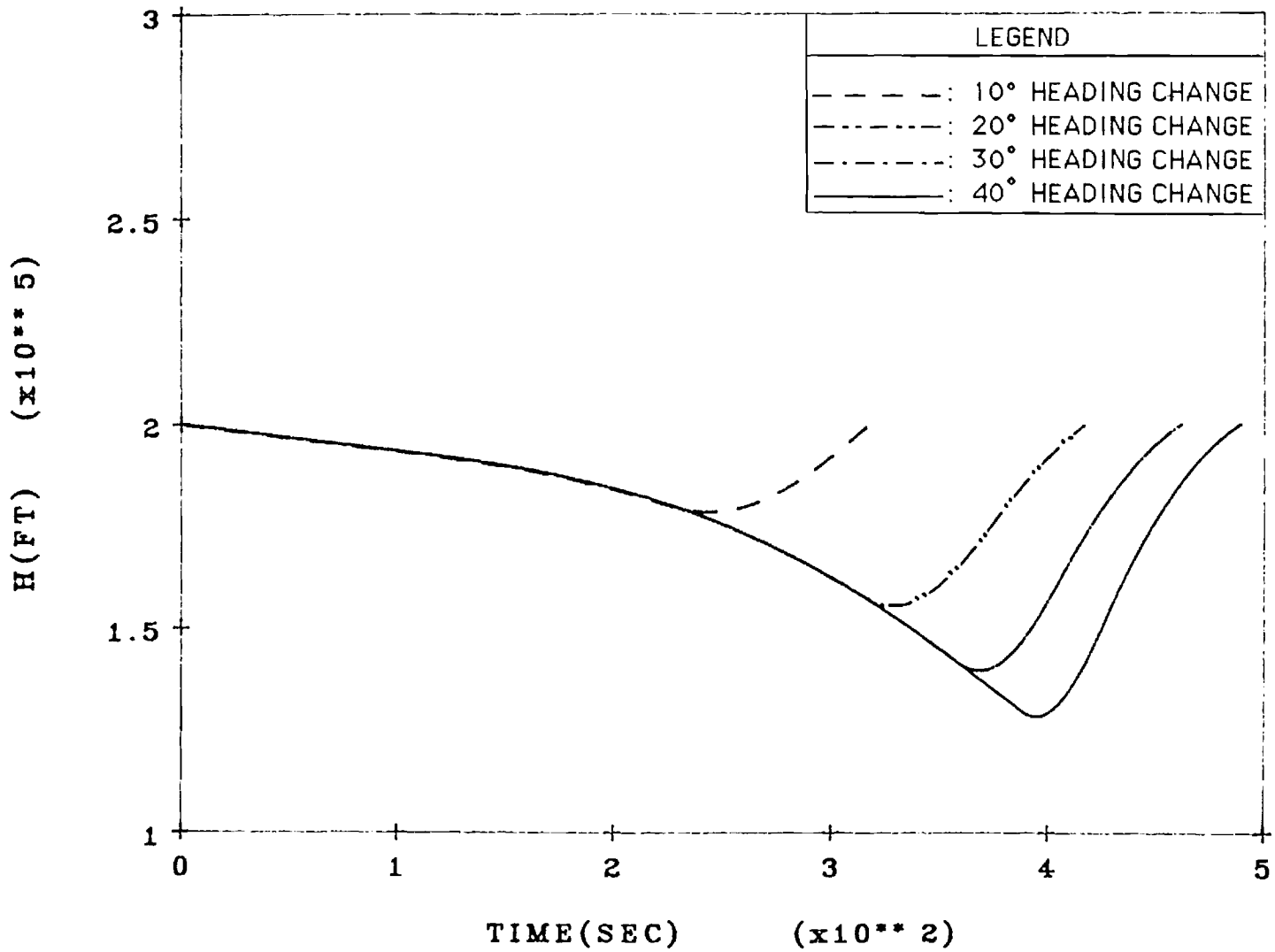

Fig. 7 Guided solution altitude profiles.

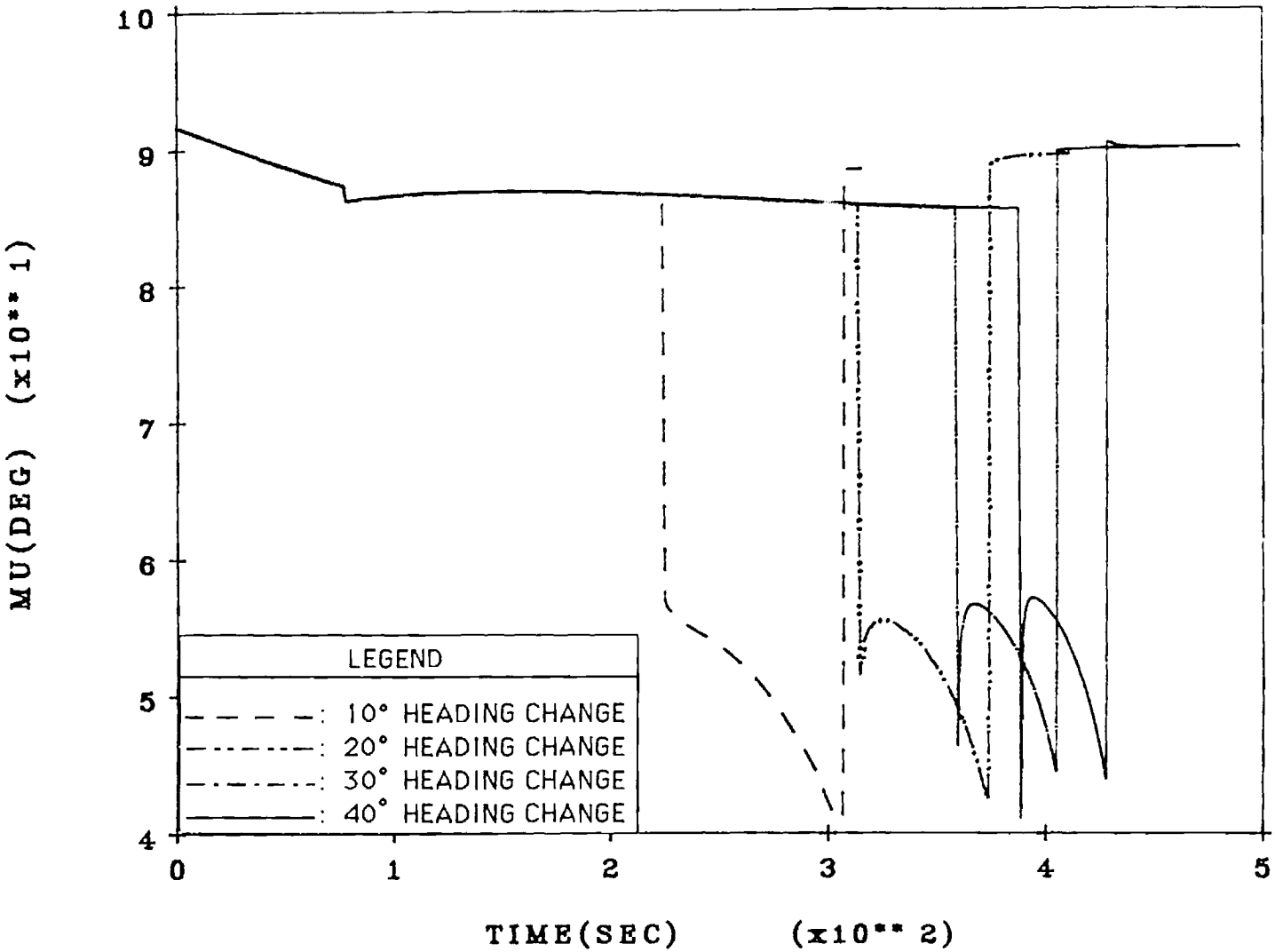

Fig. 8 Guided solution bank angle profiles.

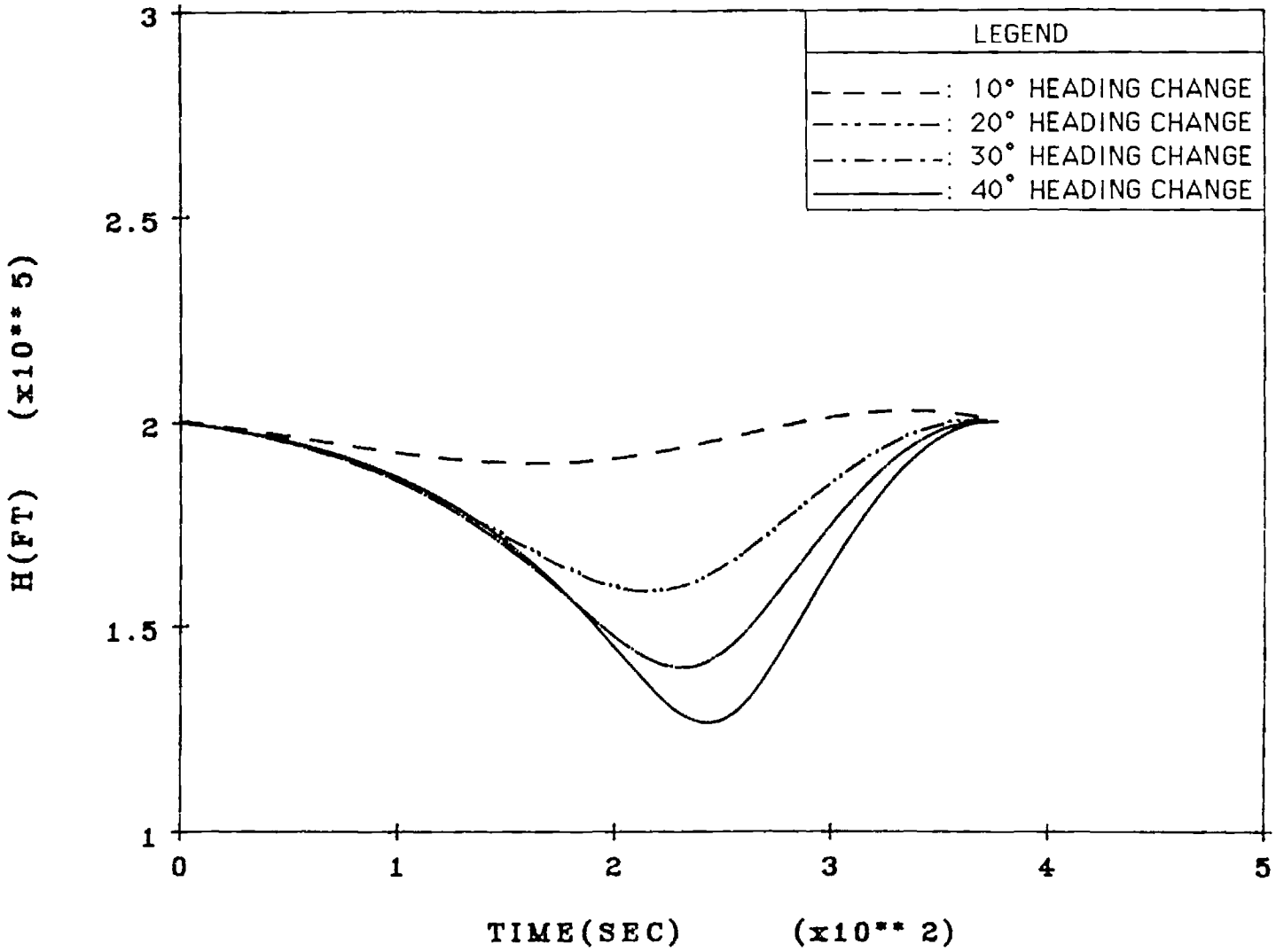

Fig. 9 Optimal solution altitude profiles.

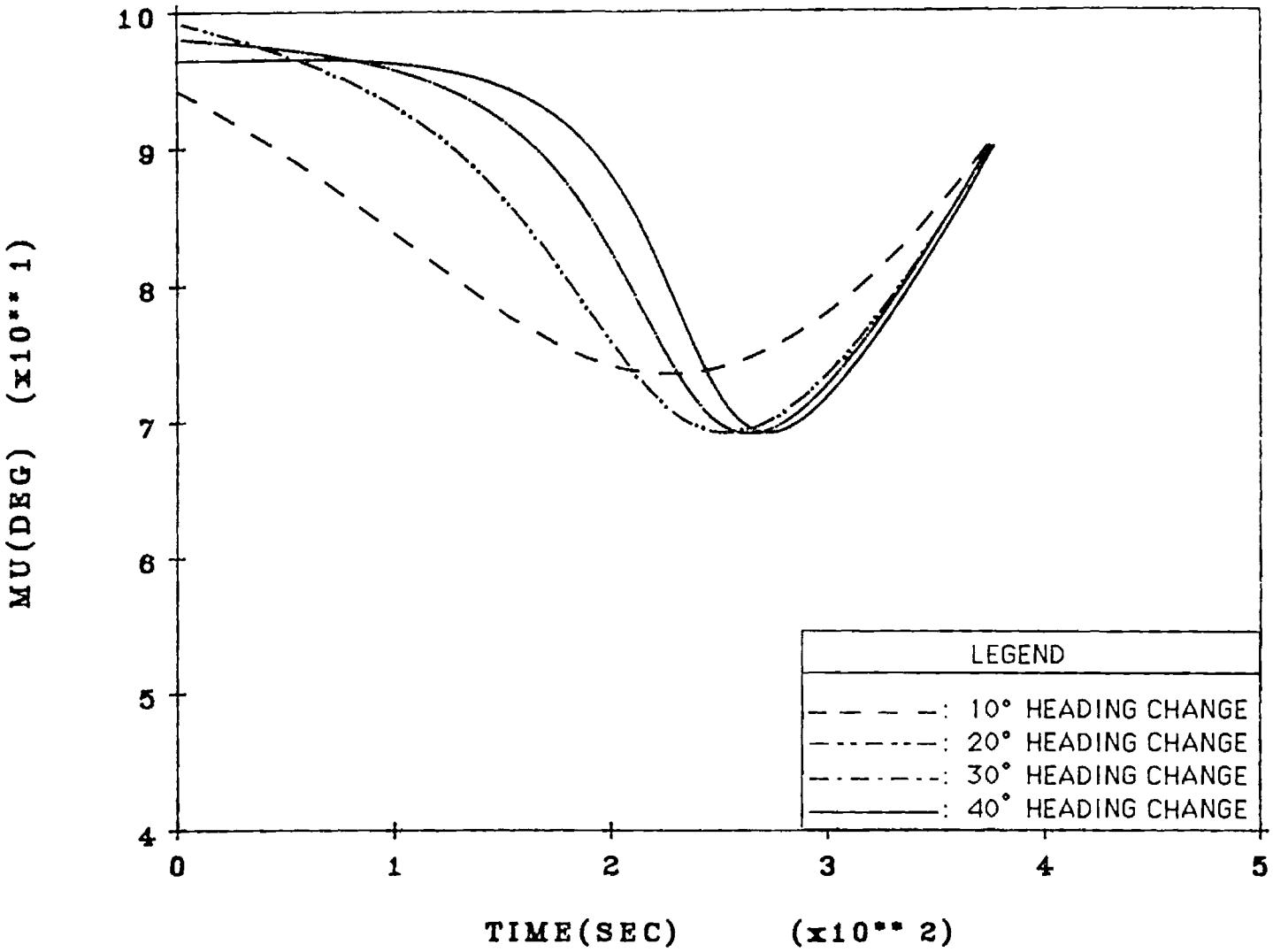

Fig. 10 Optimal solution bank angle profiles.

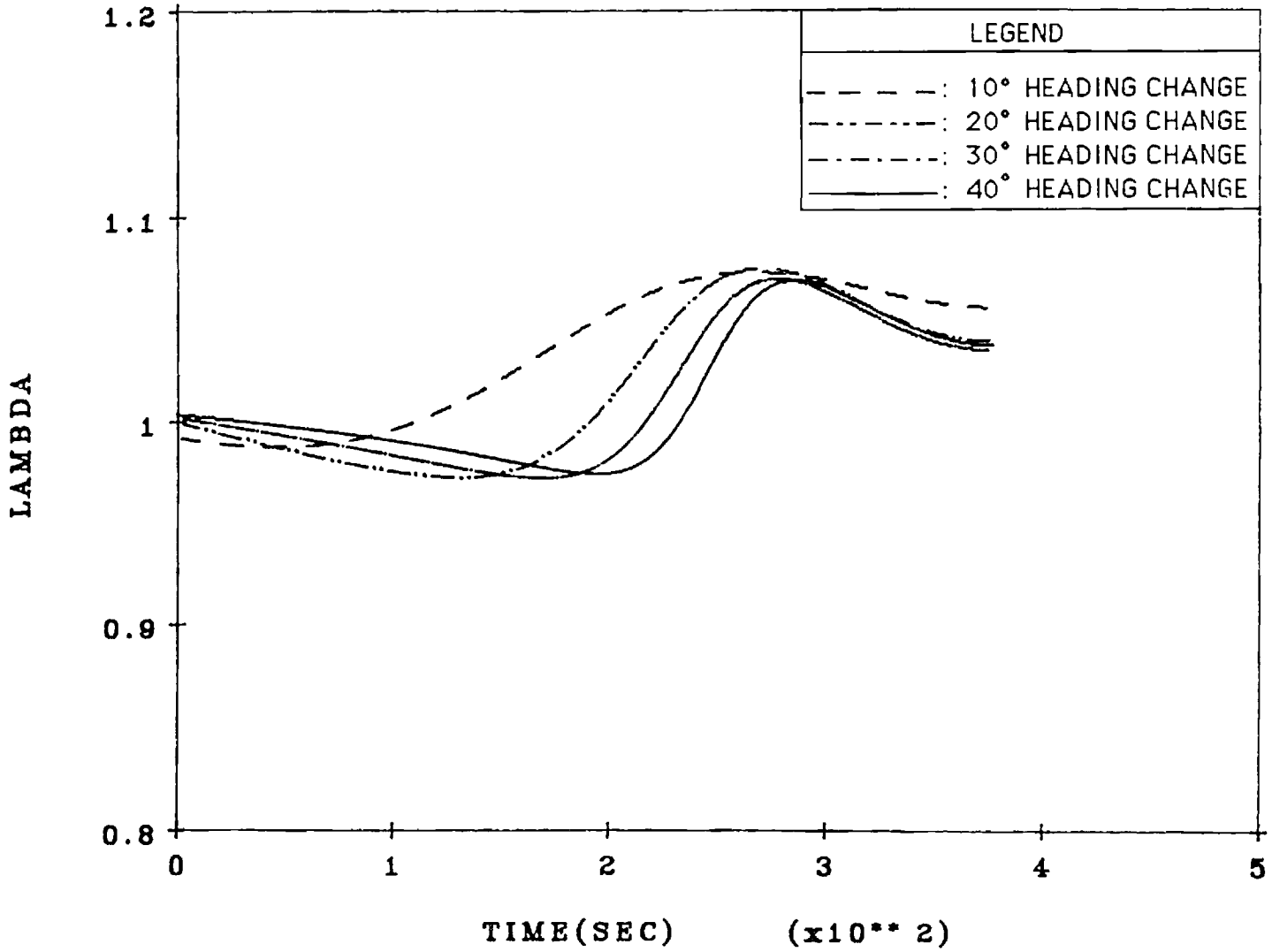

Fig. 11 Optimal solution normalized lift coefficient profiles.

Table 2
Comparison of Energy Loss (ft^2/s^2) for the
Orbit Plane Change Guidance Algorithm

Heading Change	Optimal Solution $x10^7$	Guided Solution $x10^7$	% Error
10^o	4.7129	4.9707	5.47
20^o	8.8585	9.1094	2.83
30^o	12.379	12.632	2.04
40^o	15.399	15.659	1.69

SECTION 5
FUTURE RESEARCH

During the next reporting period we plan to examine the influence of a heating rate constraint on the optimal gliding AOTV maneuver. It is anticipated that this constraint will significantly reduce the maximum inclination change achievable. Also, the analysis will be considerably complicated by the fact that it will no longer be possible to ignore cross range and down range dynamics. This will increase the problem order to six. Thus, we will innitially concentrate on obtaining numerically optimized solutions, which to date have not been carried out in an accurate fashion. Once heating rate constraints are enforced, it will be possible to carry out a meaningful comparison to aero-cruise maneuvers. Reference [9] will serve as an excellent starting point, since it essentially solves the cruise portion, which amounts to the reduced solution in a singular perturbation formulation. The optimal arcs to and from the cruise arc were not analyzed in [9]. The dynamics associated with this problem, and the issues related to singular perturbation analysis, will be totally different from that encounted thus far due to the presence of thrusting that can take place along the entire trajectory.

REFERENCES

1. Calise, A.J., Bae, G., "Singular Perturbation Analysis of AOTV Related Trajectory Optimization Problems," Progress Report for the Period 14 April - 30 Oct., Nov. 1986.

2. Calise, A.J., Bae, G., "Singular Perturbation Analysis of AOTV Related Trajectory Optimization Problems," Progress Report for the Period 1 Sept. - 30 July, July 1987.

3. Calise, A.J., "Singular Perturbation Analysis of the Atmospheric Orbital Plane Change Problem," J. of Astro. Sciences, Vol. 36, Nos. 1/2 Jan. - June, 1988.

4. Calise, A.J., Bae, G., "Optimal Heading Change with Minimum Energy Loss for a Hypersonic Gliding Vehicle," AIAA Atmospheric Flight Mechanics Conf., Aug. 1987.

5. Calise, A.J., Bae, G., " Singular Perturbation Analysis of AOTV Related Trajectory Optimization Problems," Progress Report for the Period 1 Aug. - 30 Nov., Dec. 1987.

6. Hull, D.G., McClendon, J.R., Speyer, J.L., "Improved Aero-Assisted Plane Change Using Successive Approximation," AIAA Atmospheric Flight Mechanics Conf., Williamsburg, VA, Aug. 1986.

7. Burlish, R., "The Multiple Shooting Method for Numerical Solution of Nonlinear Boundary Value Problems and Optimal Control Problems," (in German), Carl-Cranz-Gesellchaft, Techn., Rep., Heidelberg, 1971.

8. Calise, A.J., Bae, G., "Optimal Heading Change with Minimum Energy Loss for a Hypersonic Gliding Vehicle," Amer. Cont. Conf., Atlanta, GA, June 15-17, 1988. (Submitted to AIAA J. Guid., Cont. & Dynamics)

9. Mease, K.D., Lee, J.Y., Vinh, N.X., "Orbital Changes During Hypersonic Aerocruise," J. of Astro. Sciences, Vol. 36, Nos. 1/2, Jan.-June 1988.

SINGULAR PERTURBATION ANALYSIS OF AOTV-RELATED TRAJECTORY OPTIMIZATION PROBLEMS

PROGRESS REPORT

1 September - 31 January, 1989

January 1989

Research Supported by NASA - Langley Research Center

NASA Grant No. NAG - 1 - 660

Principal Investigator: Dr. Anthony J. Calise

Research Assistant: Mr. Gyoung Hyun Bae

NASA Grant Monitor: Dr. Daniel D. Moerder

Georgia Institute of Technology
School of Aerospace Engineering
Atlanta, GA 30332-0150

TABLE OF CONTENTS

LIST OF FIGURES

LIST OF TABLES

SECTION 1
SUMMARY OF RESEARCH ACCOMPLISHMENTS

During this period research has concentrated on examining the influence of a heating rate constraint on the optimal gliding AOTV maneuver. This optimization problem has not been addressed in any of the studies to date. The most closely related study appears in [1], which constrains the problem to including a thrusting phase within the atmosphere. Aerocruise (constant altitude and velocity) performance at high altitude has been studied in [2]. Both of these studies indicate that the optimal solution involves flight at angles of attack much larger than that for maximum L/D. In fact, for flight at high altitude (250,000-300,000 ft) most of the maneuver (approximately 65%) is propulsive. This raises the question of why aerodynamic maneuvering should be considered in the first place as an alternative to purely exoatmospheric maneuvering. Thus, our effort is directed at quantifying the minimum energy loss for a purely aerodynamic maneuver in the presence of a heating rate constraint.

To date, we have found that for large heating rate limits, the optimal trajectory results in a so-called "touch point" solution. Lower heating rate limits will produce a constrained arc solution. The touch point solutions indicate that the optimal angle of attack profiles remains near maximum L/D, and that the increase in energy loss is minimal. Unfortunately, we have not yet been able to obtain converged solutions for the constrained arc problem. We are employing the multiple shooting code used in our earlier reports.

Section 2 of this report discusses the modeling of aerodynamic heating rate, and the problem formulation. The numerical results obtained to date are also presented. Section 3 summarizes research activity. A presentation of all the equations needed to define the necessary conditions is given in a technical Appendix.

SECTION 2
OPTIMAL ORBIT PLANE CHANGE WITH CONSTRAINED AEROGLIDE

A constrained AOTV aeroglide problem is considered in this section. A first order state variable inequality constraint is imposed on the full order AOTV system equations using a simple aerodynamic heating rate equation. First, the atmospheric trajectory is constrained to a touch point problem and a range of maximum allowable aerodynamic heating rates is considered. The approximate range of the aerodynamic heating rate limit which yields a touch point extremal solution is determined. Next, the constrained arc problem was attempted for lower values of the heating rate limit. However, the absolute error of the numerical iteration for a small change in a parametric value (maximum allowable aerodynamic heating rate or Lagrangian multiplier associated with costate jump condition) was too sensitive and convergence was not obtained . Unfortunately, both the unconstrained aeroglide control solutions and the touch point solutions severely violate the practical maximum allowable aerodynamic heating rate constraint. Hence, the nature of the optimal profiles for a practical range of heating rate limit remains an open research issue.

2.1. Estimation of Aerodynamic Heating Rate

Many equations have been developed to predict the convective aerodynamic heating rate of a hypersonic reentry vehicle (Table 1). The equation adopted in this study is as follows[3]:

$$\dot{Q} = 17600 \sqrt{\frac{\rho}{\rho_S}} \left(\frac{V}{V_S}\right)^{3.15} \text{(BTU/sec/ft}^2\text{)} \qquad (1)$$

where ρ is the air density at the current altitude, V is the current velocity, ρ_s is the sea-level air density, and V_s is the circular orbital velocity at sea-level. The above aerodynamic heating rate equation has frequently been used in such tasks as parametric studies, conceptual vehicle design, and trajectory optimization. In [4,5], it is assumed that the space vehicle can withstand a 3000^0 R (2540^0 F) temperature behind the nose. This temperature sets the limit of the convective aerodynamic heating rate of the hypersonic vehicle during atmospheric flight. Currently, this aerodynamic heating rate (38 Watt/cm^2) is the maximum allowable heat flux. An inequality constraint function is defined as

$$S = 17600 \sqrt{\frac{\rho}{\rho_S}} \left(\frac{V}{V_S}\right)^{3.15} - \dot{Q}_{max} \leq 0 \qquad (2)$$

Table 2 shows the maximum allowable heat flux and temperature limit for current heat resistant materials and for future materials under development.

2.2. Multiple Shooting Formulation

Imposing (2) results in a first order state variable inequality constraint. Such a constraint can result in a significant change in cross range angle $\phi(t_f)$. Thus it is no longer appropriate to employ the approximation $\psi(t_f) \simeq i(t_f)$, and it becomes necessary to include the ϕ dynamics in the equations of motion. The down range angle (θ), however, remains an ignorable coordinate. Thus, we have the following equations of motion:

$$d\phi/dt = V \cos\gamma \sin\psi / r \qquad (3)$$

$$dr/dt = V \sin\gamma \qquad (4)$$

$$dV/dt = -(C_D^* S / 4m) \rho V^2 (1 + \lambda^2) - (\nu/r^2) \sin\gamma \qquad (5)$$

$$d\gamma/dt = (C_L^* S / 2m) \rho V (\lambda \cos\mu + M \cos\gamma) \qquad (6)$$

$$d\psi/dt = (C_L^* S / 2m) \rho V \lambda \sin\mu / \cos\gamma - V \cos\gamma \cos\psi \tan\phi / r \qquad (7)$$

Table 1
Summary of Convective Heating Rate Equations

No	Mon/Yr	Auther	Journal	Aerodynamic Heating rate equations
1	Mar/1959	Loh	ARS J.	For small Flight path angle
				* Time rate and max time rate of local stagnaton
				region heat input per unit area.
				$\frac{dH_S}{dt} = 6.8\times10^{-6}\sqrt{\frac{2mg}{C_D A\,(L/D)\sigma}}$
				$\sqrt{1-\frac{V^2}{g\,r_0}}\;V^2$
				$\left(\frac{dH_S}{dt}\right)_{max} = \frac{2}{3\sqrt{3}}\,6.8\times10^{-6}\left(\frac{2mg}{C_D A(L/D)\sigma}\right)^{1/2}(gr_0)$
				* Time rate and max time rate of average heat input
				per unit area
				$\frac{dH_{av}}{dt} = \frac{C_F' mgV}{2(L/D)C_D A}\left(1-\frac{V^2}{gr_0}\right)$
				$\left(\frac{dH_{av}}{dt}\right)_{max} = \frac{C_F' mg}{3\sqrt{3}\,(L/D)A}\sqrt{gr_0}$

2	Feb/1960	Loh	ARS J.	For large flight path angle * Time rate and max time rate of local stagnation
				region heat input per unit area
				$\frac{dH_S}{dt} = C_{12}\{(C_{10} - C_{11}\cos\theta)[C_{13}F(\theta)+$
				$C_{14}e^{C_1(\theta_F - \theta)}]^3\}$
				$\frac{dH_S}{dt}_{max} = C_{12}(C_{10}-C_{11}\cos\theta_3)^{1/2}\ e^{-3/2C_1(\theta_3 - \theta_F)}$
				* Time rate and max time rate of average heat per
				unit area
				$\frac{dH_{av}}{dt} = (C_8-C_9\cos\theta)[C_{13}F_1(\theta)+C_{14}e^{C_1(\theta_F-\theta)}]^{3/2}$
				$\frac{dH_{av}}{dt}_{max} = (C_8 - C_9\cos\theta_2)\ e^{-3/2C_1(\Theta_2-\theta_F)}$
3	Oct/1960	Loh	J. A/Sp	$\frac{dH_S}{dt} = K'\sqrt{\frac{\rho}{\sigma}}\ V^3$
			&Science	
4	Jan/1961	London	"	$\frac{dq_{S\text{-}max}}{dt} = \frac{C}{\sqrt{R_S}}\left(\frac{\beta R w}{3C_D A\rho_0 V_S^2}\right)^{1/2}\left(\frac{V_E}{V_S}\right)^3$

				$\sqrt{\sin\theta_B}\ e^{[-3(\theta_E-\theta_B)]/(L\cos\gamma/D)}$
				where θ = flight path angle, γ = bank angle
5	May/1965	Caudra	J. S/crft	* At the spherical nose of the vehicle, laminar
				stagnation point convective heating rate
				$\frac{dq_L}{dt} = (\frac{2x10^{-8}}{\sqrt{R}})\sqrt{\rho}\ V^3$
				* General expression for the heating
				$(1+\frac{1}{\varepsilon(L/D)})\frac{dq_L}{dt} = 13.1(\frac{2w}{C_L SR})^{1/2}\eta\{(Q\eta)^2+$
				$(1-\eta)^2\}^{1/4}$
				ε=burning surface slope, $\eta=(V/V_C)^2$
				V_C=circular orbital velocity, $Q=(1-\eta)\tan\beta/\eta$
				β=bank angle, R=vehicle nose radius
				w=vehicle weight
6	May/1967	Johann	J.S/crft	* stagnation point heating rate
		Lau	V4, N5	$\frac{dq_S}{dt} = 17600\sqrt{\frac{\sigma}{R_N}}(\frac{V}{26000})^{3.15}(\frac{h_S-h_W}{h_S-130})$
				$\sigma = \rho/\rho_s$, R_N = nose radius, $h_S = 130+20(V/1000)^2$

				$h_W = C_{PW}\, T_W$ = wall enthalpy
				* Local heating rate on a simple flat plate at angle of
				attack (α_0 = vehicle nose angle)
				$\frac{dq_L}{dt} = 0.0312(\alpha+\alpha_0)^{2/3}(V/1000)^3[(h_S-h_W)/h_S]/\sqrt{L}$
7	Feb/1977	Brauer	NASA	$\frac{dq}{dt} = K\,(17600/\sqrt{R_N})\sqrt{\rho/\rho_S}\ (\frac{V}{V_C})^{3.15}$
			CR2770	
8	Oct/1983	Miele	ACTA	* peak heat rate
			Astront.	$\frac{dq}{dt} = \sqrt{\rho}\ V^{3.08}$
9	Jan/1984	Rheder	AIAA	* Maximum reference convective stagnation point
			Aerosp.	heat rate to a 1-ft-radius sphere (BTU/ft^2/sec)
			Scienc.	$\frac{dq_{max}}{dt} = 41.97(\frac{W}{C_D A})^{0.485}\eta^{-.556}$
10	Jun/1984	Scott	"	* Max reference sphere heat flux
				$\frac{dq_{max}}{dt}\sqrt{R_N} = 7.3(\frac{m}{C_D A})^{0.467}(L/D)^{-.242}$
				m=kilogram (Watt/cm^2)(m)$^{1/2}$

				* Heat flux calculated by engineering correction
				formula
				$\frac{dq}{dt}\sqrt{R_N} = 18300\sqrt{\rho}\ (V/10000)^{3.05}$
				$\rho = 0.8\rho_{ref}$ (1962) $\qquad$ $(Watt/cm^2)(m)^{1/2}$
11	Jun/1986	Tauber	AIAA	Thermophysics &Heat Transfer Conference
				$\frac{dq}{dt} = C(2NK)^N(\frac{V_S}{\sqrt{M}})^M(M-2N)^{M/(2-N)}$
				$C = 1.83x10^{-8}(r_n)^{-1/2}(1-q_w)$
				$K = \frac{2}{R_0}\frac{m}{C_L A}$

Table 2
High Temperature materials

Items / Materials / Unit	Limit Temperature				$\dot{Q}_{max}$	Thermal Control
	F^0	R^0	K^0	C^0	Watt/cm^2	
Hastelloy	2240.6	2700.	1500.	1227.	20.	None
Hastelloy	2780.6	3240.6	1800.	1527.	45.	active cooling
Silicon Carbide	3140.6	3600.	2000.	1727.	65.	None
Hafnium Carbide	4040.6	4500.	2500.	2227.	200.	None

with the boundary conditions,

$$\phi(t_0) = 0 \tag{8}$$

$$h(t_0) = h_0 \qquad h(t_f) = h_0 \tag{9}$$

$$V(t_0) = V_0 \qquad V(t_f) = \text{free} \tag{10}$$

$$(t_0) = 0 \qquad (t_f) = \text{free} \tag{11}$$

$$(t_0) = 0 \tag{12}$$

In addition, final inclination is specified. Thus $\phi(t_f)$ and $\psi(t_f)$ are constrained by

$$\cos\{\phi(t_f)\}\cos\{\psi(t_f)\} = \cos\{i_f\} \tag{13}$$

The performance index of this problem is the same as that used in our earlier reports [7,8].

$$J = -\int_{t_0}^{t_f} \dot{E}\, dt \tag{14}$$

A detailed presentation of the necessary conditions is given in the Appendix. In formulating the multiple shooting problem, time was normalized so that total time interval runs from 0 to 1.0. Final time was taken as an auxiliary state variable. The three Lagrangian multipliers (ν_1, ν_2, σ) associated respectively with the constraint on terminal altitude, the constraint on terminal orbit inclination angle, and the costate jump condition were also taken as auxiliary state variables. Therefore the dimension of the constrained aeroglide problem was increased to 14, which is composed of five system states, five adjoint states, and four auxiliary states. This was later reduced to 13 by treating σ as an input parameter, instead of $(dQ/dt)_{max}$. The unconstrained problem was first solved for $h_0=h_f$=365,000 ft. Then taking the converged solution of the unconstrained problem as the initial guess for the states at each time-node, the atmospheric trajectory was constrained by gradually reducing maximum allowable aerodynamic heat rate. The next section summarizes the results for the touch point formulation of the necessary conditions.

2.3. Numerical Results for The Touch Point Formulation

The same vehicle characteristic data in [6,7] was used in this study. The initial and terminal data are as follows.

$\theta(t_0) = 0$ $\phi(t_0) = 0$ $h(t_0) = 365{,}000$ ft $V(t_0) = 25{,}745.704$ ft/sec

$\gamma(t_0) = 0.55^0$ $\psi(t_0) = 0$ $h(t_f) = 365{,}000$ ft $i(t_f) = 18^0$

The initial h, V, and γ correspond to the same deorbit impulse employed in [7,8]. The number of time-grid points is 28, which were more densely arranged near the bottom portion of the trajectory. A simple exponential air-density model was used taking the same reference altitudes used in [6,7]. The required relative precision of solution was set to 10^{-6}. The relative deviation for numerical differentiation was set to 10^{-7}.

Figures (1-3) show the time histories of h, V, γ for the unconstrained case and for the touch point case corresponding to $\dot{Q}_{max} = 600$ BTU/sec/ft^2. As the aerodynamic heating rate limit is decreased, the minimum altitude and flight time increase. Figure 4 shows the profiles of normalized lift coefficient. In the case of a touch point solution, the results show a slight jump in normalized lift coefficient. However, this is likely due to numerical inaccuracy in satisfying the jump conditions at the touch point. The bank angle time history (Figure 5) is continuous. Figure 6 shows that the terminal constraint on the final inclination angle is satisfied. Figures (7 and 8) show the time histories of the h and V costate variables. Note the jump that occurs at the touch point. All the other costates are continuous. Figure 9 shows the aerodynamic heating rate profiles. The aerodynamic heating rate was decreased to approximately 600 BTU/sec/ft^2 in the touch point solution. Energy loss is shown in Figure 10. Note that the additional energy loss due to the constraint is negligible. The value of Hamiltonian was checked throughout the trajectory, and it was verified that Hamiltonian was constant and near zero.

In the case of the unconstrained 18^0 orbit inclination change maneuver, the resulting maximum aerodynamic heating rate is 729.3156 BTU/sec/ft^2. The lowest value of $(dQ/dt)_{max}$ for the touch point problem was found by gradually decreasing maximum allowable aeroheating rate until the program failed to converge. The approximate range of the constraint value for touch point problem was found to be

$$599.387 \leq \dot{Q}_{max} \leq 729.3156 \quad \text{BTU/sec/ft}^2 \qquad (15)$$

In decreasing allowable aeroheating rate, final flight time was increased from 1017.5 sec for the unconstrained case to 1077.0 sec for the lowest touch point case. The minimum altitude also increased from 137,431 ft for the unconstrained case to 146,372 ft for the touch point case. Unfortunately, this solution still violates the practical range of upper limits for $(dQ/dt)_{max}$. Though the constrained arc formulation was attempted to obtain solutions for lower values of $(dQ/dt)_{max}$, the multiple shooting code did not converge to an extremal solution, except for a slight decrease in $(dQ/dt)_{max}$ which resulted in a constrained arc of approximately 10 seconds duration.

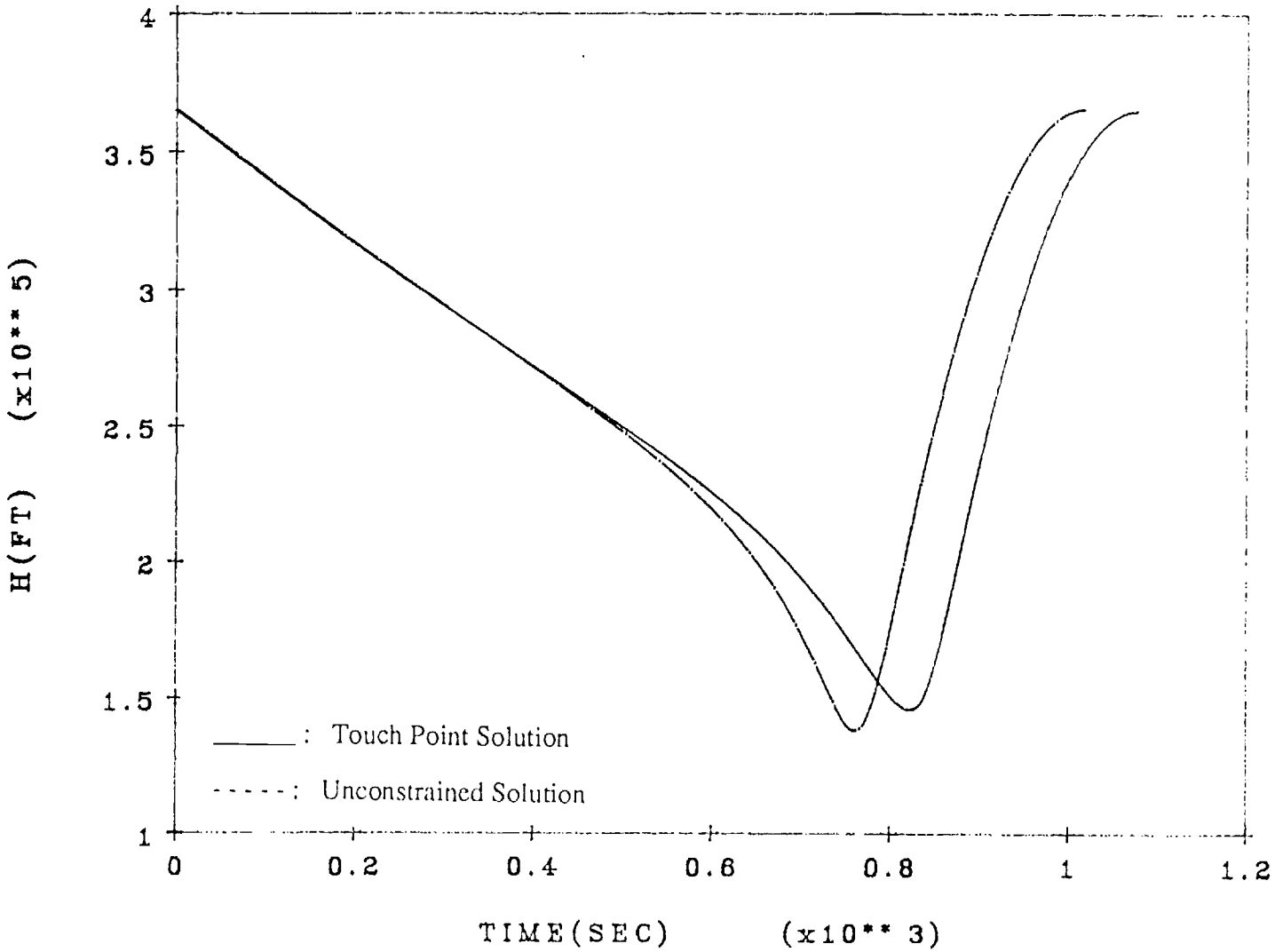

Figure 1 Altitude profiles of the unconstrained and touch point solutions.

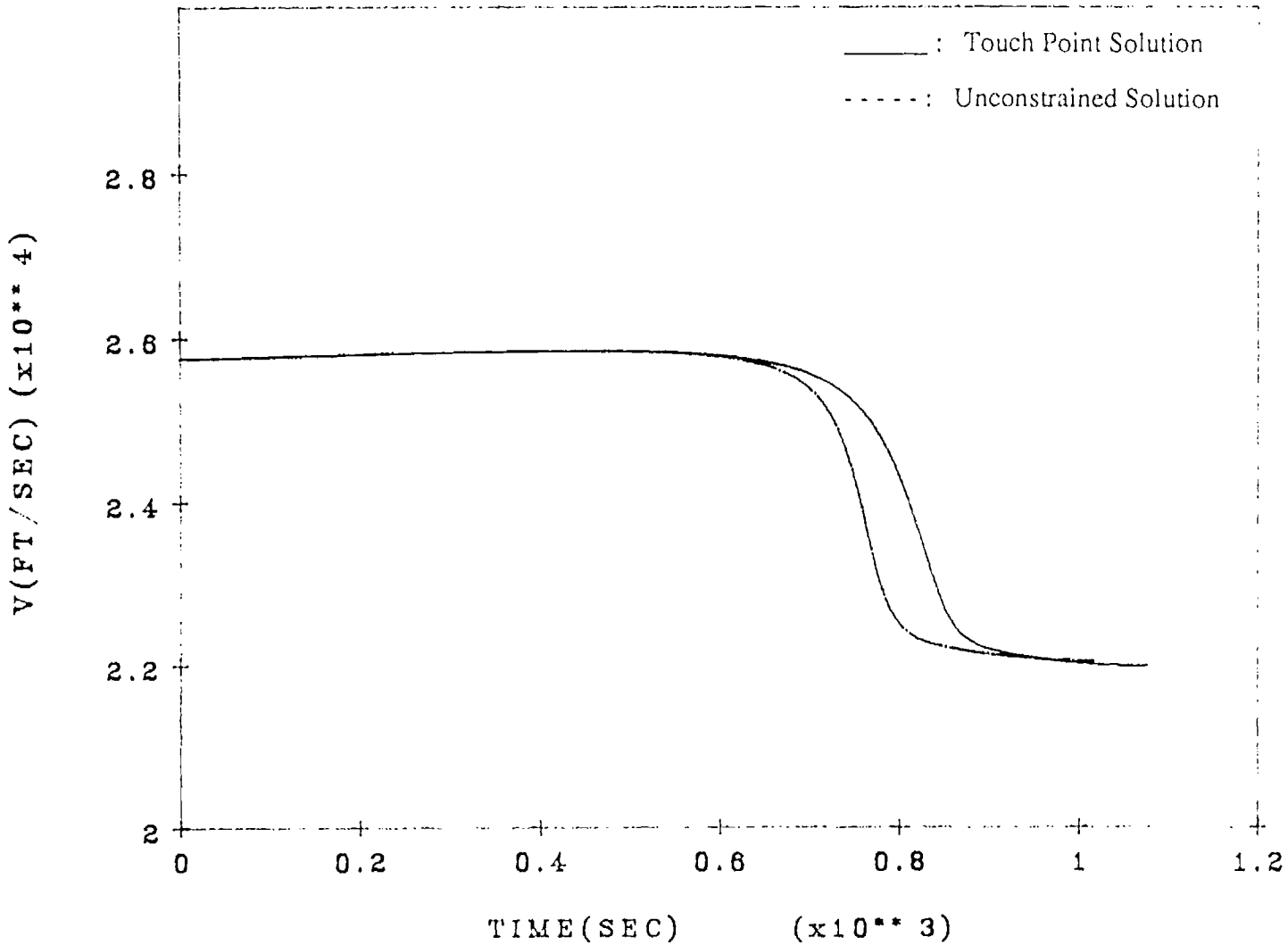

Figure 2 Velocity profiles of the unconstrained and touch point solutions.

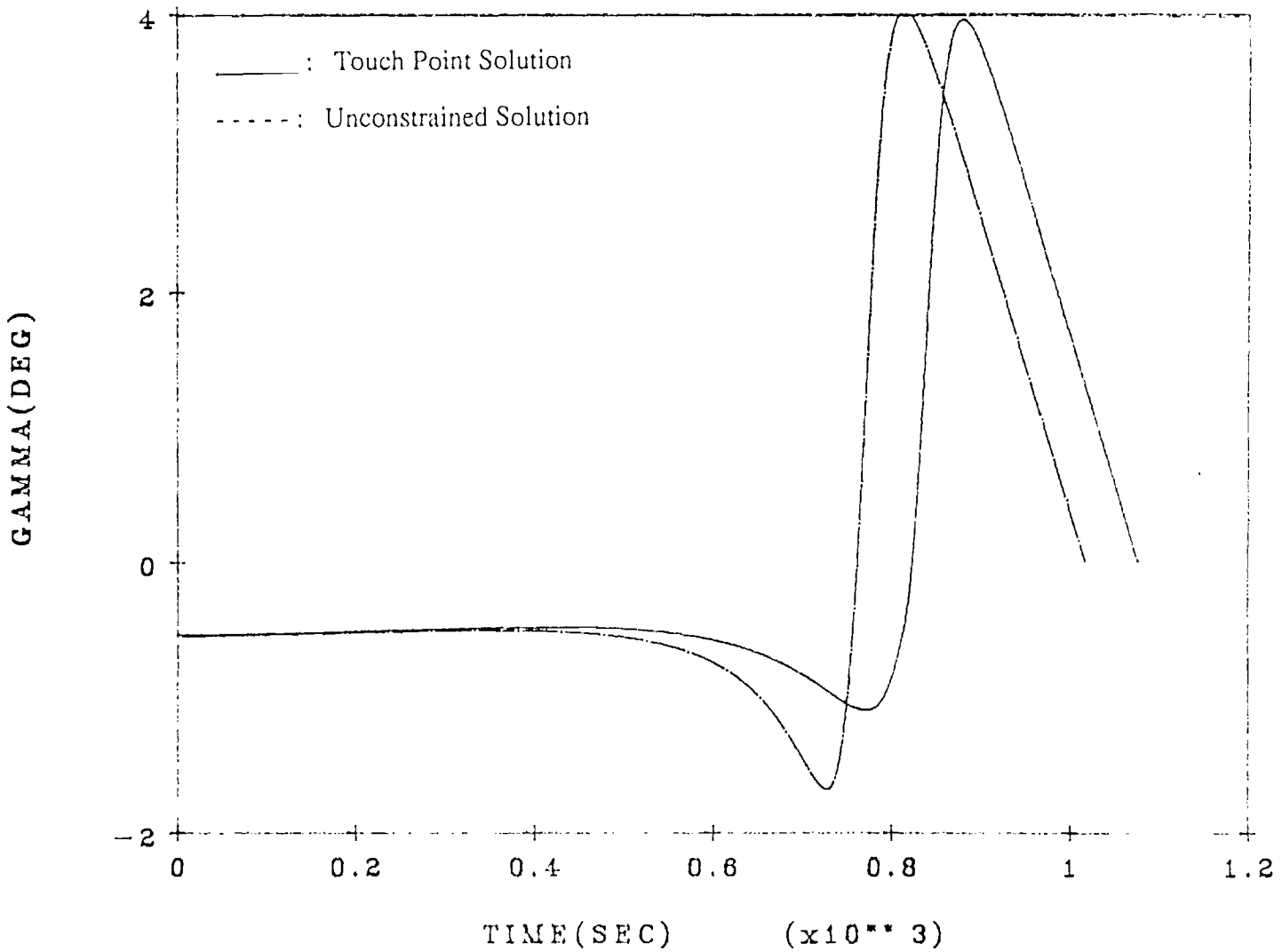

Figure 3 Flight path angle profiles of the unconstrained and touch point solutions.

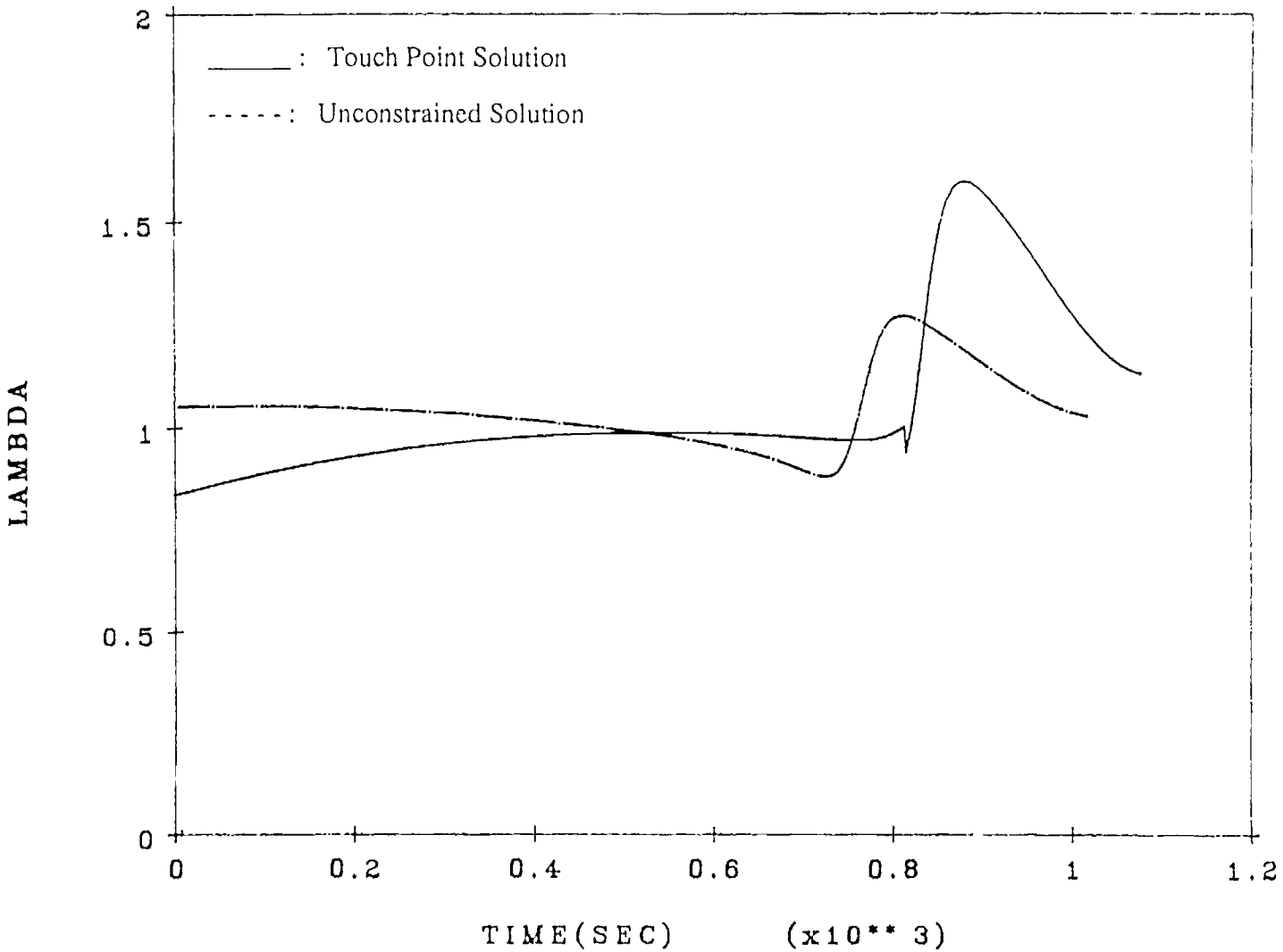

Figure 4 Normalized lift coefficient profiles of the unconstrained and touch point solutions.

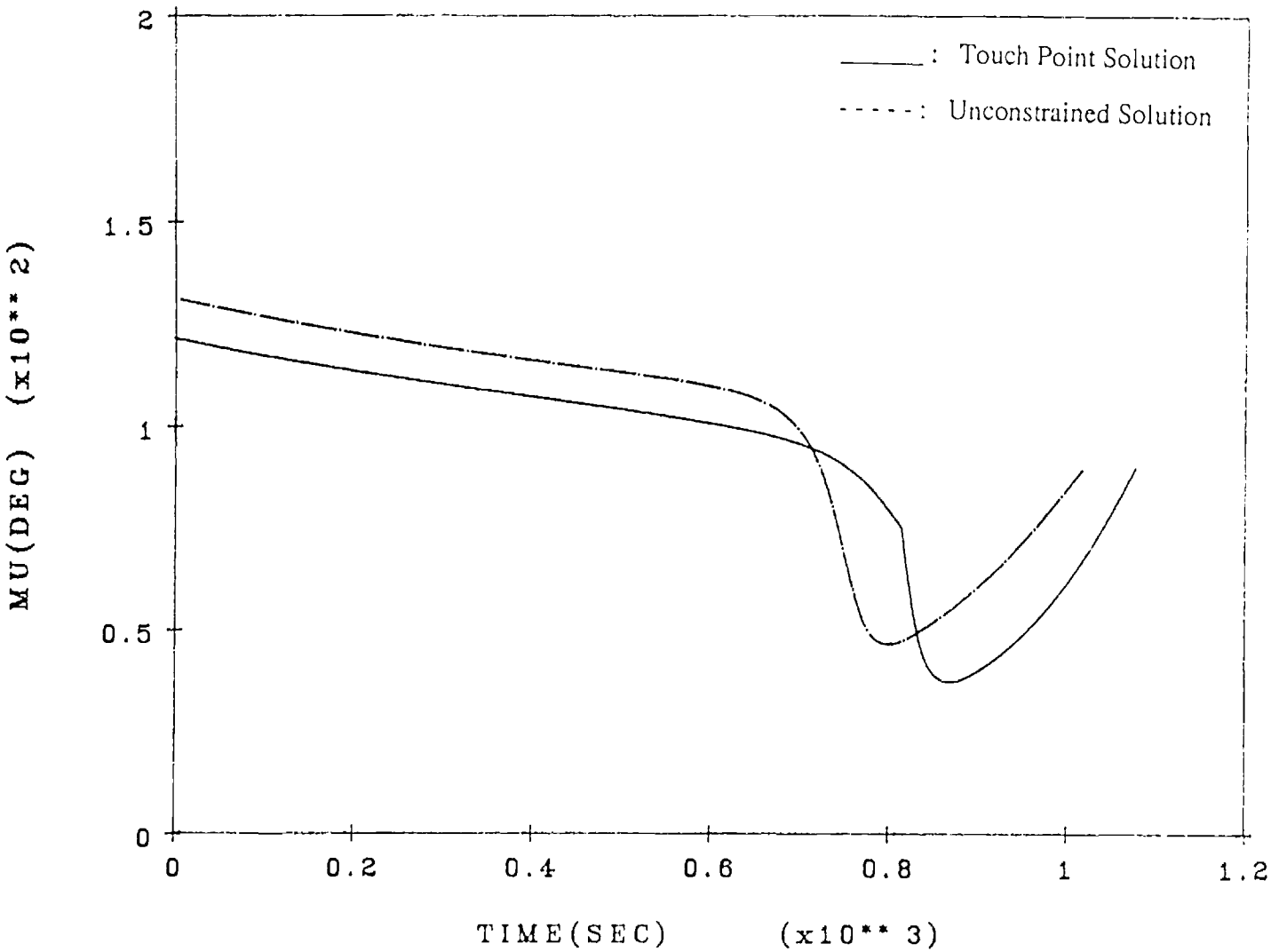

Figure 5 Bank angle profiles of the unconstrained and touch point solutions.

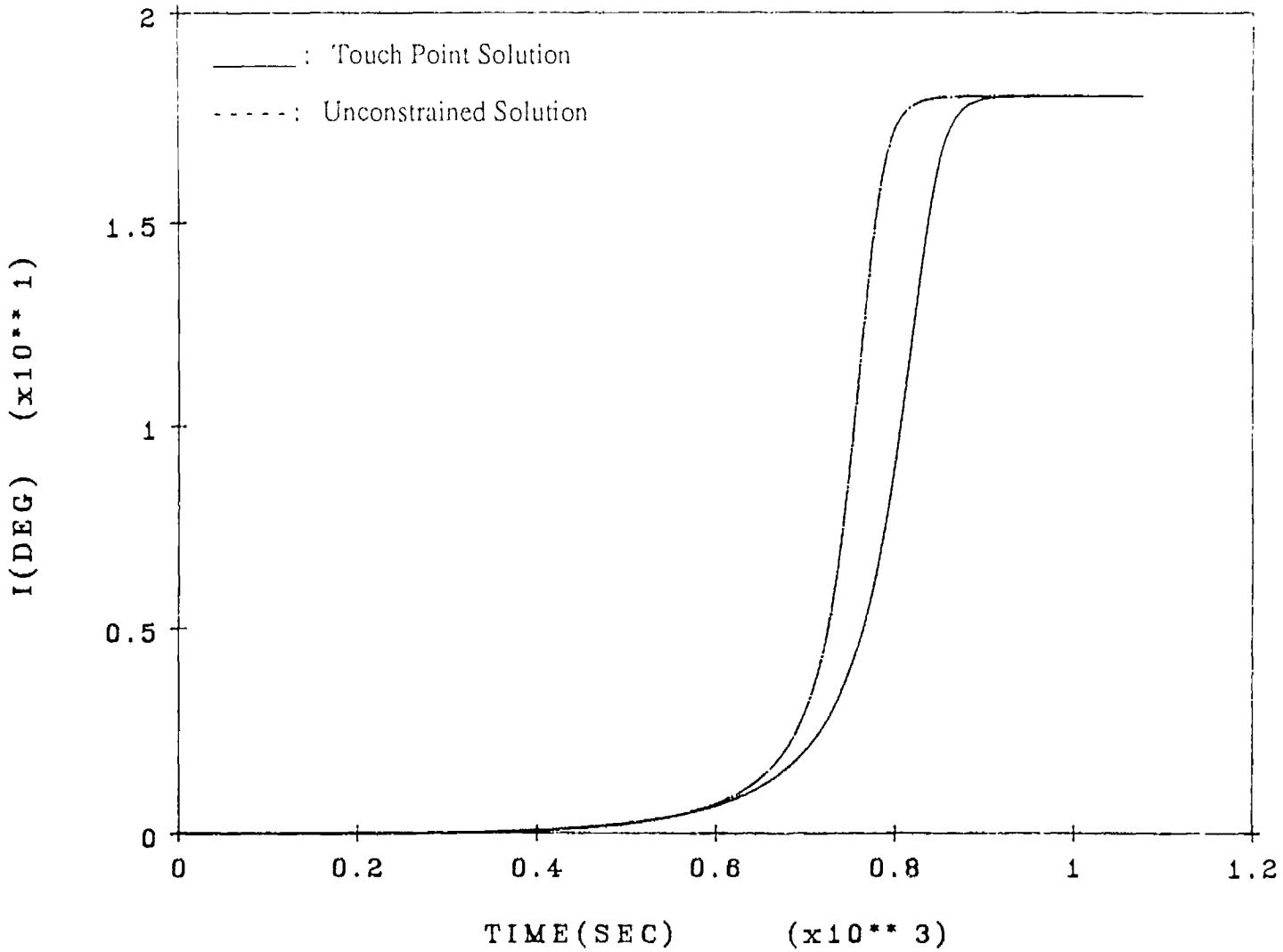

Figure 6 Orbit inclination angle profiles of the unconstrained and touch point solutions.

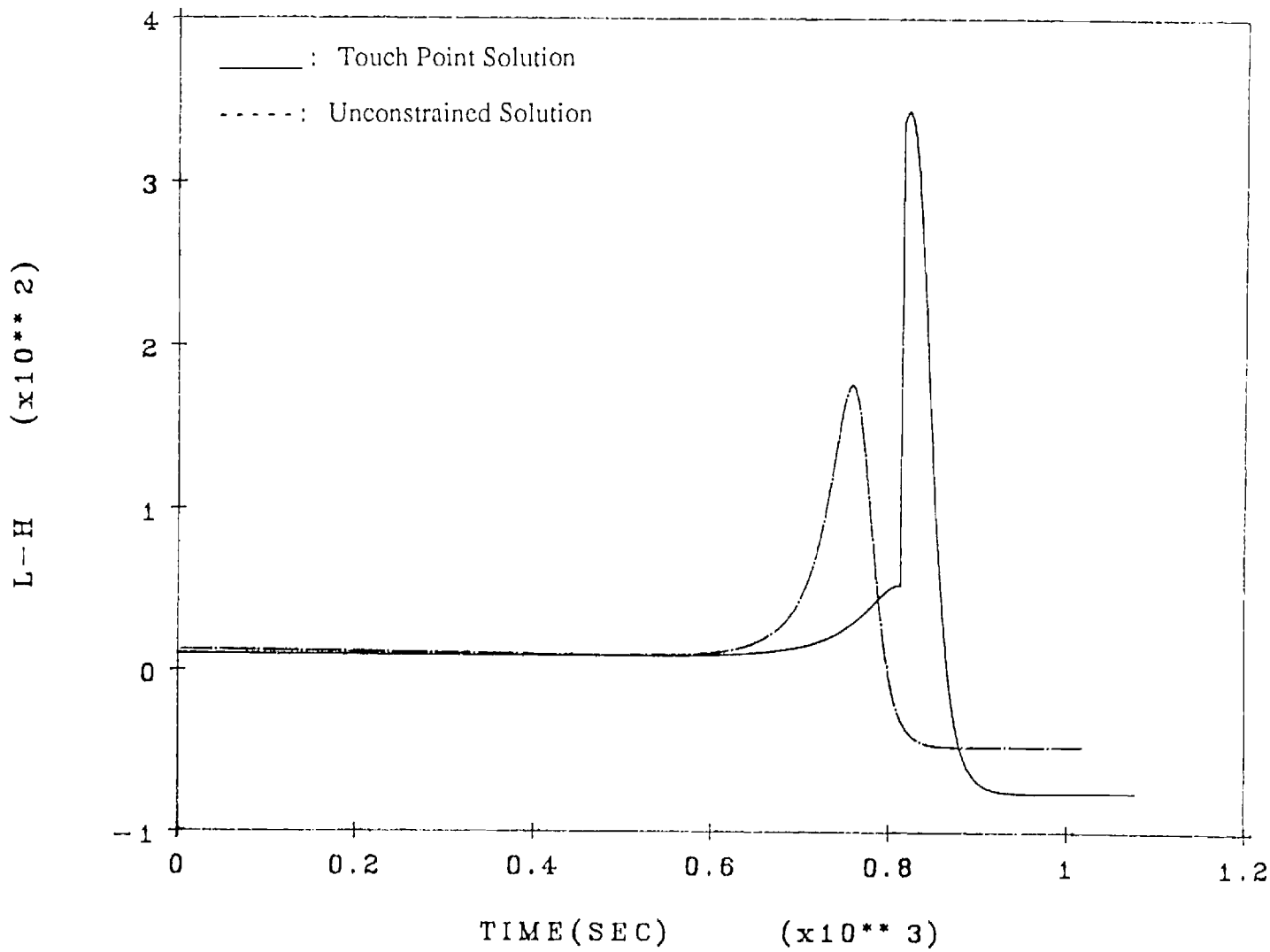

Figure 7 Time histories of the costate associated with altitude.

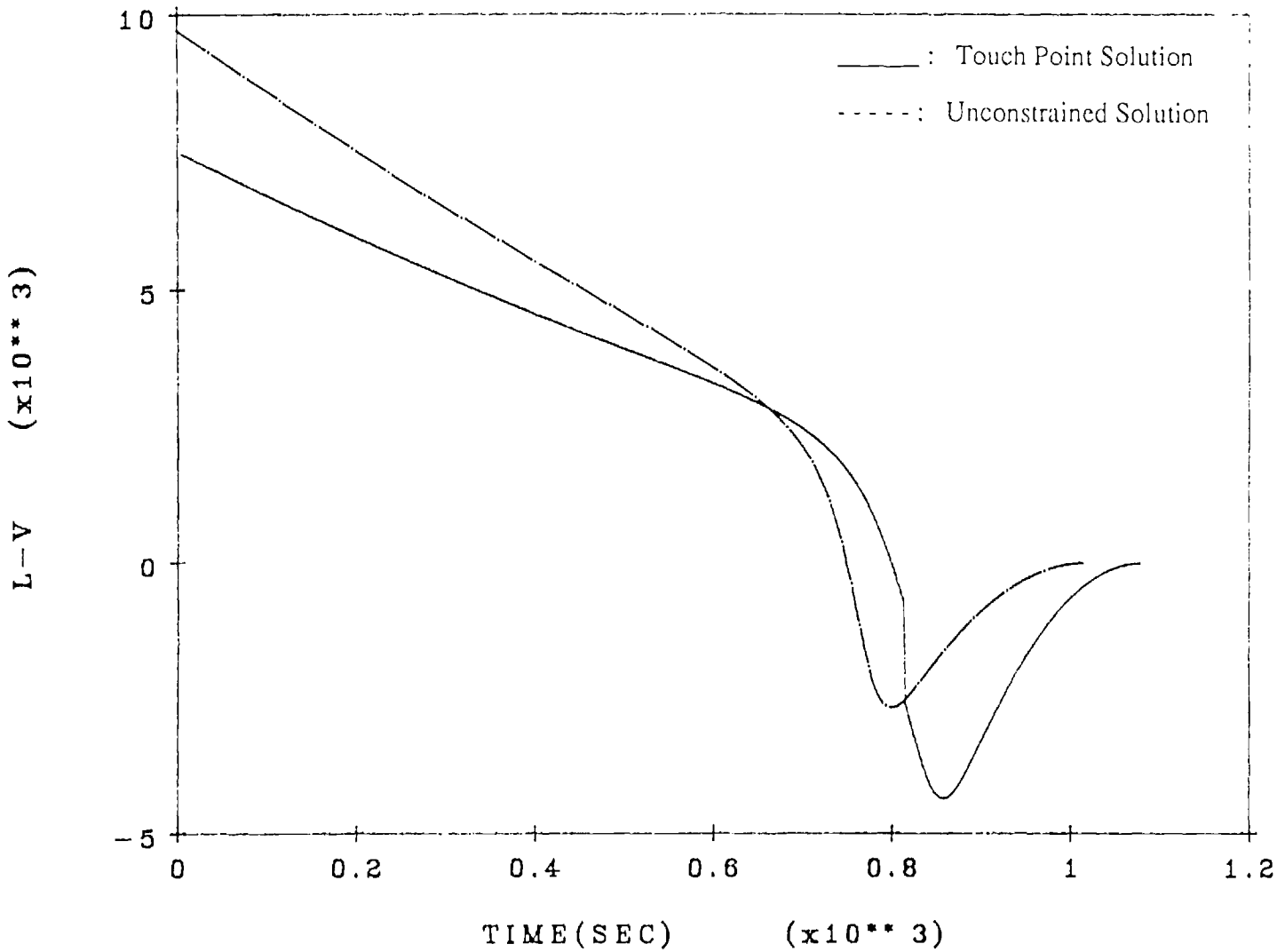

Figure 8 Time histories of the costate associated with velocity.

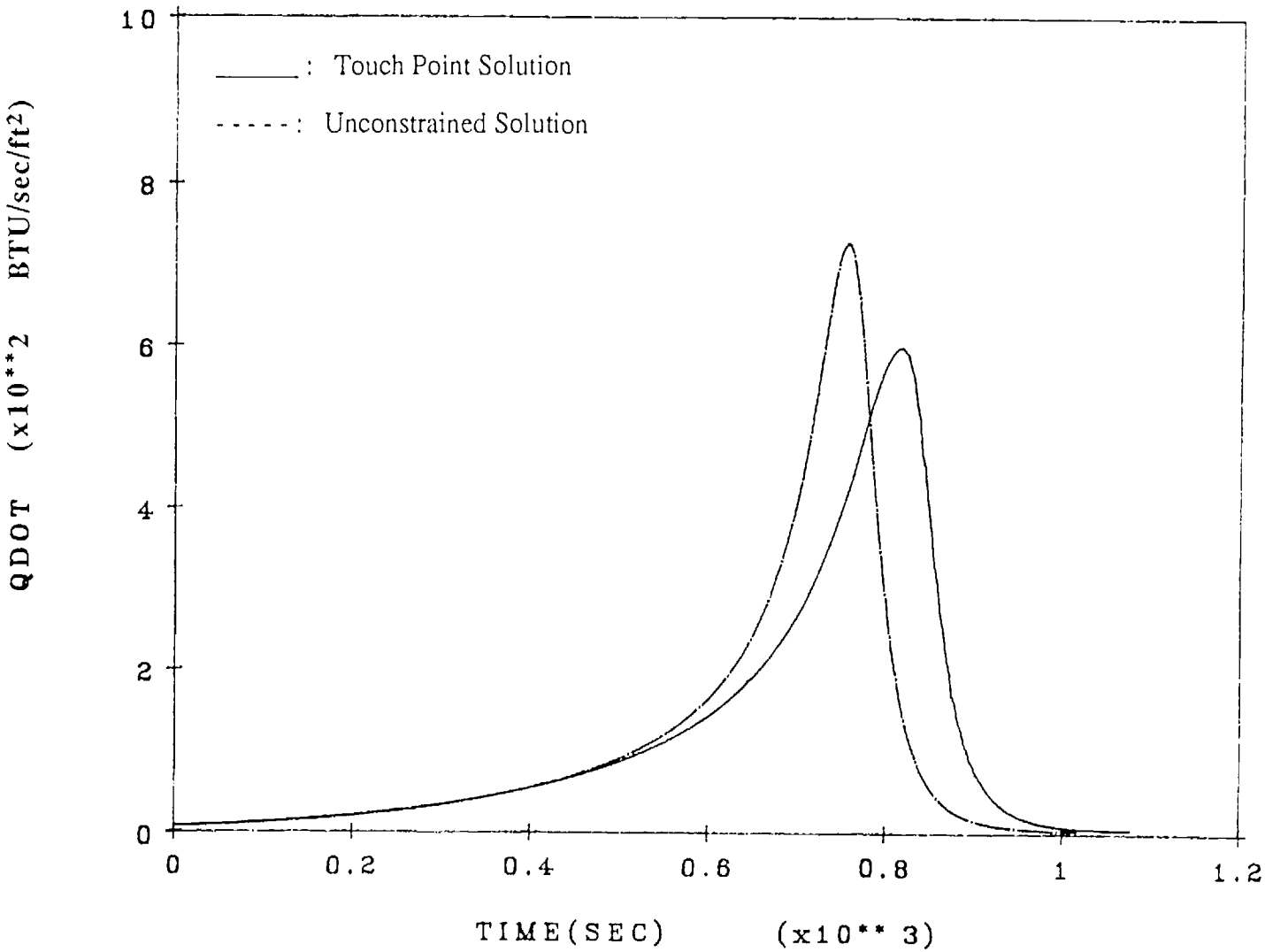

Figure 9 Aerodynamic heating rate profiles.

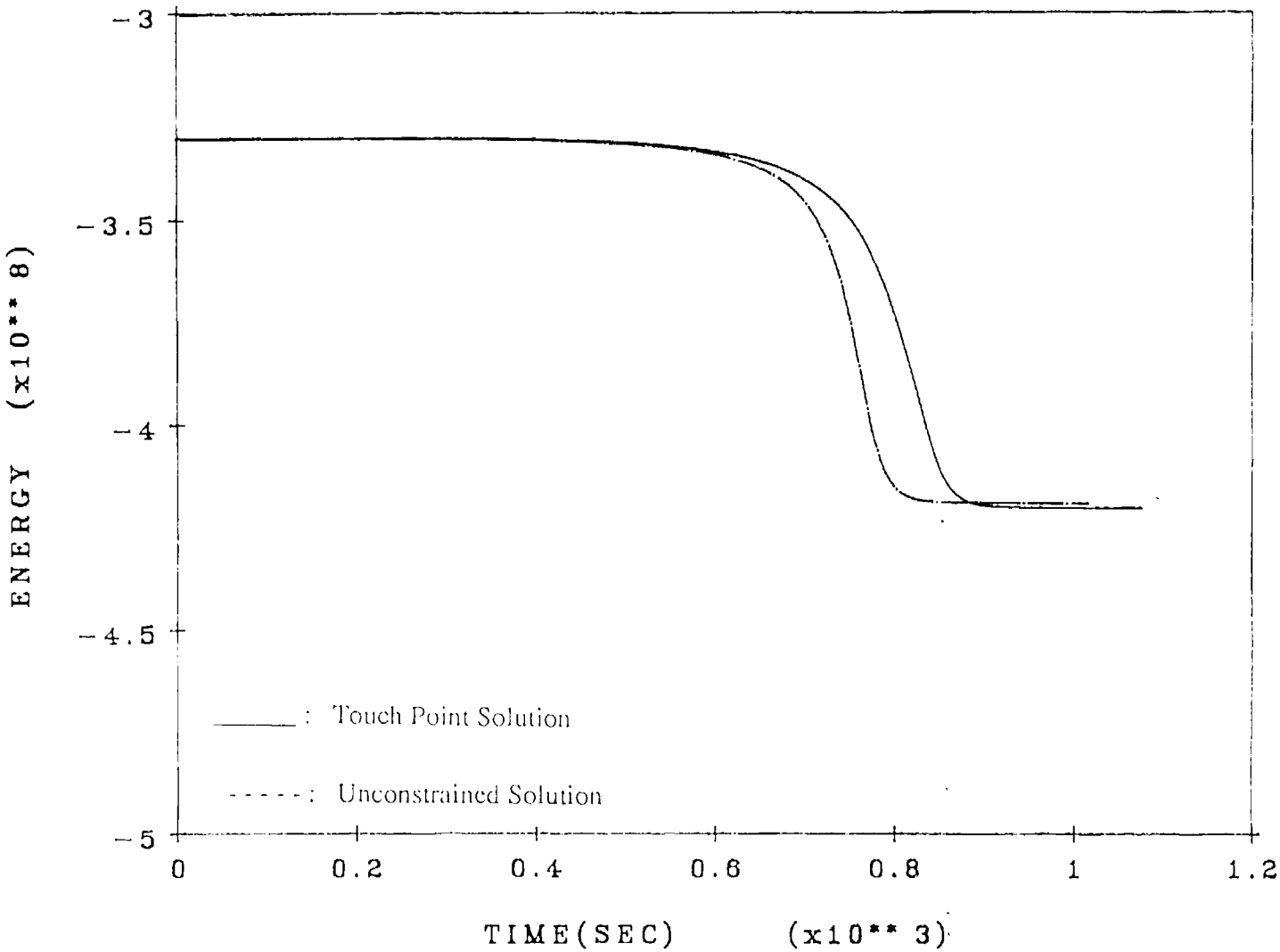

Figure 10 Energy profiles.

SECTION 3
FUTURE RESEARCH

During the next reporting period we will concentrate on completing this numerical study, by constructing the constrained arc solutions for lower values of the aerodynamic heating rate limit. We will also study the effect of a constraint on heating load, and a comparison with the results on heating rate limit. One of the main objectives of this part of the research is to identify the nature of the resulting optimal solutions, and to extend the analytical results based on reduced order models to obtain feedback solution approximations.

$$- \lambda_{\dot{s}} \{ \frac{V}{2\beta} + \frac{3.15\,\nu}{Vr^2} \} \cos\gamma$$

$$\dot{\lambda}_{\psi} = - \lambda_{\phi} \{ \frac{V \cos\gamma \cos\psi}{r} \} - \lambda_{\psi} \{ \frac{V \cos\gamma \tan\phi \sin\psi}{r} \} \qquad \text{(A-8)}$$

where β is the scale height. Boundary conditions for the adjoint dynamic equations are as follows:

$$\lambda_{\phi}(t_f) = - \nu_2 \cos\psi(t_f) \sin\phi(t_f) \qquad \lambda_h(t_f) = \nu_1$$

$$\lambda_V(t_f) = \lambda_{\gamma}(t_f) = 0 \qquad \lambda_{\psi}(t_f) = - \nu_2 \sin\psi(t_f) \cos\phi(t_f) \qquad \text{(A-9)}$$

By partial differentiating Hamiltonian with respect to the controls, and setting the result to zero, we obtain:

$$\lambda = \frac{C_L^* \{ \lambda_{\gamma} \cos\mu + \lambda_{\psi} \sin\mu/\cos\gamma \}}{C_D^* V \{ \lambda_V - V - \lambda_{\dot{s}} (\frac{3.15}{V}) \}} \qquad \text{(A-10)}$$

$$\mu = \tan^{-1} (\frac{\lambda_{\psi}}{\lambda_{\gamma} \cos\gamma}) \qquad \text{(A-11)}$$

When the trajectory is on the constraint, λ is determined from (A-1) as

$$\lambda_C = \sqrt{- \{ \frac{(\frac{V}{6.3\,\beta} + \frac{\nu}{Vr^2}) \sin\gamma}{C_2 \rho V} + 1 \}} \qquad \text{(A-12)}$$

From (A-10), the expression for $\lambda_{\dot{s}}$ becomes

$$\lambda_{\dot{S}} = \frac{-V(\frac{N}{\lambda_C} - \lambda_V + V)}{3.15} \qquad \text{(A-13)}$$

where

$$N = \frac{C_L^* \{ \lambda_\gamma \cos\mu + \lambda_\psi \sin\mu / \cos\gamma \}}{C_D^* V} \qquad \text{(A-14)}$$

Off the constraint arc, $\lambda_{\dot{S}} = 0$ and (A-10) is used to compute λ.

Constrained Arc Problem

In the case of a state constrained problem, we have a set of interior boundary conditions to be satisfied at the start of the constrained arc. Since in this case the control appears in the first derivative of the constraint, the only interior point constraint is

$$N\{X(t_1)\} = 17600 \sqrt{\frac{\rho}{\rho_s}} (\frac{V}{V_C})^{3.15} - \dot{Q}_{max} = 0 \qquad \text{(A-15)}$$

where t_1 is the time at the start of the constrained arc.

At the start of the unconstrained and the constrained arc, the following jump conditions apply

$$\lambda_X^T(t_1^-) = \lambda_X^T(t_1^+) + \sigma^T \frac{\partial N}{\partial X(t_1)}$$

$$\frac{\partial N}{\partial X} = [\frac{\partial N}{\partial \phi} \quad \frac{\partial N}{\partial h} \quad \frac{\partial N}{\partial V} \quad \frac{\partial N}{\partial \gamma} \quad \frac{\partial N}{\partial \psi}]$$

$$\frac{\partial N}{\partial \phi} = \frac{\partial N}{\partial \gamma} = \frac{\partial N}{\partial \psi} = 0$$

$$\frac{\partial N}{\partial h} = -\frac{17600}{2\beta} \sqrt{\frac{\rho}{\rho_S}} (\frac{V}{V_C})^{3.15}$$

$$\frac{\partial N}{\partial V} = 17600 \left(\frac{3.15}{V_C}\right) \sqrt{\frac{\rho}{\rho_S}} \left(\frac{V}{V_C}\right)^{2.15} \tag{A-16}$$

Therefore, the costates λ_ϕ, λ_γ, λ_ψ associated with the three angles are continuous, and

$$\lambda_h(t_1^+) = \lambda_h(t_1^-) + \sigma\left(\frac{8800}{\beta}\right) \sqrt{\frac{\rho}{\rho_S}} \left(\frac{V}{V_C}\right)^{3.15} \tag{A-17}$$

$$\lambda_V(t_1^+) = \lambda_V(t_1^-) - \sigma\left(\frac{55440}{V_C}\right) \sqrt{\frac{\rho}{\rho_S}} \left(\frac{V}{V_C}\right)^{2.15} \tag{A-18}$$

Because time is implicit in this problem, the Hamiltonian at time t_1, and t_2 should be continuous.

$$H(t_1^-) = H(t_1^+) \qquad H(t_2^-) = H(t_2^+) \tag{A-19}$$

where t_2 is the time at the end of the constrained arc.

Touch Point Problem

In the touch point problem, we drop the constraint in (A-1). In this case, λ_s is not needed (or set to zero), and the control in (A-10) is used for the entire trajectory. We also drop the second condition in (A-19). The remaining jump conditions, and the continuity condition on H at time t_1 (the touch point time) are all enforced.

REFERENCES

1 Lee,J.Y., Hull, D.G., : "Maximum orbit plane Change with Heat-Transfer-rate constraints," AIAA J. of Guidance and Control (to appear).

2. Mease,K.D., Lee, J., Vinh,N.X. : "Orbital Changes During Hypersonic Aerocruise," AIAA Atmospheric Flight Mechanics, Aug., 1987

3. Brauer G.L., Cornick D.E., and Stevenson R. : "Capabilities and Applications of the Program to optimize simulated Trajectories (POST)" NASA CR-2770, National Aeronautics and Space Administration, Washington,D.C., Feb. 1977

4. Ikawa, h., and Rudiger, T.F. : "Synergetic Maneuvering of Winged Spacecraft for Orbital Plane Change," AIAA Paper 82-0361, AIAA 20th Aerospace Sciences Meeting, Jan. 11-14, 1982, Orlando, Fla

5. Cervisi,R.T. : "Analytic Solution for a Cruise Plane Change Maneuver," J. of Spacecraft and Rockets, Vol.22, No. 2, Mar.-Apr., 1985, pp. 134-140

6. Calise,A.J., Bae,G.H. : "Singular Perturbation Analysis of AOTV Related Trajecory Optimization Problems," Progress Report for the Period 1 Aug.-30 Nov., 1988, Dec. 1988.

7. Calise,A.J., Bae,G.H. : "Singular Perturbation Analysis of AOTV Related Trajecory Optimization Problems," Progress Report for the Period 1 Dec.-31 Aug., 1988, Sept. 1988.

SINGULAR PERTURBATION ANALYSIS OF AOTV-RELATED TRAJECTORY OPTIMIZATION PROBLEMS

PROGRESS REPORT

1 February - 30 April, 1989

May 1989

Research Supported by NASA - Langley Research Center

NASA Grant No. NAG-1-660

Principal Investigator: Dr. Anthony J. Calise

Research Assistant: Mr. Nahum Melamed

NASA Grant Monitor: Dr. Daniel Moerder

Georgia Institute of Technology
School of Aerospace Engineering
Atlanta, GA 30332-0150

SUMMARY OF RESEARCH ACCOMPLISHMENTS

During this period we have concentrated on refining the numerical study of optimal gliding AOTV maneuvers subject to a heating rate constraint. As reported in our last progress report, for large heating rate limits, the optimal trajectory results in a touch point solution. For lower heating rate limits a constrained arc solution emerges. However, we have encountered numerical problems for this constrained arc case. There are two possible causes for this problem. One difficulty may be due to the fact that we have to date been working with equations in dimensional form. A second possibility is that we may be encountering a conjugate point. This would give rise to multiple solutions which satisfy the first order necessary conditions. To eliminate the first possibility we are currently working with a new set of equations in non-dimensional form. Unfortunately, we have not been able to work out all the bugs in this formulation. If a conjugate point emerges then we will have to use a direct method such as a gradient based algorithm which can be used to find the true optimal solution. At the same time we have been looking at alternative formulations which may avoid the problem altogether.

FUTURE RESEARCH

During the next reporting period we will concentrate on completing this numerical study, by constructing constrained arc solutions for lower values of the aerodynamic heating rate limit. This may necessitate use a numerical method other than the multiple shooting code which we have used to date. It would also be of theoretical interest to demonstrate that a conjugate point exists for this class of problem. We will also study the effect of a constraint on heating load, and compare with the results on heating rate limit. One of the main objectives of this part of the research is to identify the nature of the resulting optimal solutions, and to extend the analytical results based on reduced order models to obtain feedback solution approximations.

SINGULAR PERTURBATION ANALYSIS OF AOTV-RELATED TRAJECTORY OPTIMIZATION PROBLEMS - FINAL REPORT

January, 1990

Research Supported by
NASA Langley Research Center
Grant No. NAG-1-660

Principal Investigator: Dr. Anthony J. Calise
Research Assistant: Dr. Gyoung H. Bae
NASA Grant Monitors: Dr. Christopher Gracey
Dr. Daniel D. Moerder

Georgia Institute of Technology
School of Aerospace Engineering
Atlanta, GA 30332

SINGULAR PERTURBATION ANALYSIS OF AOTV-RELATED TRAJECTORY OPTIMIZATION PROBLEMS

Anthony J. Calise
Georgia Institute of Technology
School of Aerospace Engineering
Atlanta, GA 30332

SUMMARY

This research has addressed the problem of real time guidance and optimal control of Aeroassisted Orbit Transfer Vehicles (AOTV's), using singular perturbation theory as an underlying method of analysis. Trajectories have been optimized with the objective of minimum energy expenditure in the atmospheric phase of the maneuver. Two major problem areas were addressed: optimal reentry, and synergetic plane change with aeroglide. For the reentry problem, several reduced order models were analyzed with the objective of optimal changes in heading with minimum energy loss. It has been demonstrated that a further model order reduction to a single state model is possible through the application of singular perturbation theory . The optimal solution for the reduced problem defines an optimal altitude profile dependent on the current energy level of the vehicle. A separate boundary layer analysis is used to account for altitude and flight path angle dynamics, and to obtain lift and bank angle control solutions. By considering alternative approximations to solve the boundary layer problem, three guidance laws were derived, each having an analytic feedback form. The guidance laws were evaluated using a Maneuvering Reentry Research Vehicle model and all three were found to be near optimal.

For the problem of synergetic plane change with aeroglide, a difficult terminal boundary layer control problem arrises which to date has been found to be analytically intractable. Thus a predictive/corrective solution was developed to satisfy the terminal constraints on altitude and flight path angle. A composite guidance solution was obtained by combining the optimal reentry solution with the predictive/corrective guidance method. Numerical comparisons with the corresponding optimal trajectory solutions show that the resulting performance is very close to optimal.

An attempt was made to obtain numerically optimized trajectories for the case where heating rate is constrained. A first order state variable inequality constraint was imposed on the full order AOTV point mass equations of motion, using a simple aerodynamic heating rate model. For high heating rate limits (just below the peak heating rate for the unconstrained case), the resulting solution appears to satisfy the first order necessary conditions for a "touch point" problem, where the constraint is met at a single point. Lower heating rate limits likely result in a constrained arc, of finite duration. Unfortunately, numerically converged optimal trajectories for this range of solutions could not be obtained using the multiple shooting method employed in this research.

TABLE OF CONTENTS

LIST OF FIGURES

LIST OF TABLES

SECTION 1
INTRODUCTION

Energy state approximations combined with singular perturbation theory have proven useful in aircraft trajectory optimization, both in obtaining algebraic control solutions and in satisfying trajectory and control constraints [1-4]. However, the underlying flat earth and constant gravitational field assumptions in aircraft modeling do not apply to hypersonic vehicles. Moreover, the use of singular perturbation theory requires an inherent time scale separation in the problem formulation for successful application. The intent of this research effort has been to explore the usefulness of singular perturbation analysis in the development of real time guidance algorithms for problems related to AOTV maneuvers.

The problem of optimal atmospheric heading change with minimum energy loss has application to maneuvering reentry vehicle guidance and to aeroassisted orbit transfer vehicle (AOTV) guidance. The problem of aeroassisted orbit plane change requires the use of three impulses - one to deorbit, one to reorbit and one to recircularize at the new orbit. The orbit plane change is effected entirely in the atmosphere through the use of lift and bank angle control. Circular orbit plane changes in which the initial and final orbital altitudes are equal were studied in [5-9]. These studies considered various problem formulations with the underlying approximation that an expression related to the sum of the centrifugal and gravitational forces (Loh's term) is constant or piecewise constant over the atmospheric maneuver. Furthermore, in the absence of heating constraints, the optimal trajectories are of short duration, and the inclination change is closely approximated by the heading change. For this situation, the dynamics can be reduced to fourth order, and minimization of fuel consumption is closely approximated by minimizing the energy loss in the atmospheric portion of the trajectory [6]. As a point of reference, the optimal AOTV maneuver requires approximately 50% of the fuel needed for the single impulse pure propulsive maneuver in the case of a 40 degree low Earth orbit plane change. In [10], a regular perturbation method is used to remove the approximations related to Loh's term in the earlier work and demonstrates a significant improvement over the solutions in [5-9]. However, this approach requires a quadrature at

each update of the control solution and the approach can not be readily extended to include the effect of heating constraints.

Examples of numerical optimization studies related to orbit plane change can be found in [11-13]. In particular, [12-13] examine the effect of a heating rate constraint with thrusting in the atmosphere. Since the duration of the AOTV maneuver is much greater when a heating rate constraint is enforced, it is necessary to consider a more complete set of dynamics which includes the cross range angle. Ref. [12] treats the problem of optimal aerocruise (flight at constant altitude and velocity), and does not consider the transitions to and from the cruise condition. In [13], a more general problem is treated with a constant thrust segment inserted during the atmospheric phase. Thus, in our work we decided to place emphasis on optimal aeroglide (no thrusting in the atmosphere) subject to a heating rate constraint. A more complete account of related work in noncoplanar transfer, including other competing transfer modes, can be found in [14].

Section 2 of this report presents the problem formulation and issues related to model order reduction. Section 3 treats the problem of optimal heading change with minimum energy loss in the context of singular perturbation analysis. Section 4 addresses the AOTV synergetic plane change problem by introducing a predictive/corrective solution to satisfy the terminal constraints on altitude and flight path angle. Section 5 summarizes the results for a numerical study of the effects of a heating rate constraint on the AOTV synergetic plane change problem. Section 6 summarizes the results and recommendations for further research along this line.

SECTION 2
PROBLEM FORMULATION

2.1 Equations of Motion

The equations of motion for gliding flight about a sperical nonrotating Earth are given by:

$$d\theta/dt = V\cos\gamma\cos\psi/r\cos\phi: \quad r = r_s+h \tag{1}$$

$$d\phi/dt = V\cos\gamma\sin\psi/r \tag{2}$$

$$dh/dt = V\sin\gamma \tag{3}$$

$$dV/dt = -D/m - g\sin\gamma: \quad g = \nu/r^2 \tag{4}$$

$$Vd\gamma/dt = L\cos\mu/m + (V^2/r-g)\cos\gamma \tag{5}$$

$$Vd\psi/dt = L\sin\mu/m\cos\gamma - (V^2/r)\cos\gamma\cos\psi\tan\phi \tag{6}$$

where θ is the longitude, ϕ is the latitude, h is the altitude, r_s is the Earth's radius, V is the velocity, γ is the flight path angle, ψ is the heading angle, D is the drag force, ν is the Earth's gravitational constant, and m is the vehicle mass. The control variables are the lift force (L) and bank angle (μ).

The orbit inclination angle is given by the relation

$$\cos i = \cos\phi\cos\psi \tag{7}$$

The plane change is the angle between the normals to the initial and final orbital planes. The actual inclination (i) is defined relative to the equatorial plane. Many studies on optimal plane change have taken the equatorial plane as the initial plane, in which case the plane change equals the final inclination angle (i_f). However, it has been shown in [12] that, under the assumption of spherical symmetry, maximizing the inclination is equivalent to maximizing the plane change angle provided that the deorbit burn is properly timed so that the plane change occurs at the proper location. This depends only on the location of the ascending node for the final orbit plane.

Thus, there is no loss in generality in assuming that the initial plane is the equitorial plane, and that the inclination change is the final inclination angle. A second consequence of this fact is that θ becomes an ignorable coordinate in most AOTV optimization problems since it does not appear in the right hand side of the equations of motion, and it does not enter the boundary conditions or the performance index for optimal control problem formulations of practical interest.

For short duration maneuvers, the cross range angle can be treated as being negligibly small in (1),(6) and (7). In this case the inclination change is approximated by the heading change, and ϕ also becomes an ignorable coordinate. Thus it is possible to reduce the equations of motion to a four state model, which for the purposes of this study are expressed in the following form:

$$dh/dt = V\sin\gamma \tag{8}$$

$$dE/dt = -C_D^* S(1+\lambda^2)\rho V^3/4m \tag{9}$$

$$d\gamma/dt = (C_L^* \rho SV/2m)(\lambda\cos\mu+M\cos\gamma) \tag{10}$$

$$d\psi/dt = C_L^* \lambda\rho SV\sin\mu/2mV\cos\gamma \tag{11}$$

where

$$C_D = C_{Do} + KC_L^2 \tag{12}$$

$$M(h,V) = (2m/C_L^* S)[1-\nu/V^2 r]/\rho r, \qquad r = r_s+h \tag{13}$$

In these equations the superscript * denotes the maximum lift-to drag values:

$$C_L^* = (C_{Do}/K)^{1/2} \qquad C_D^* = 2C_{Do} \tag{14}$$

and λ is the normalized lift coefficient

$$\lambda = C_L/C_L^* \tag{15}$$

Here we have employed E as a state variable in place of velocity (V), where

$$E = V^2/2 - \nu/r \qquad (16)$$

In [6] velocity is used as a state variable, and the gravity component was ignored in the velocity rate equation. One advantage to using E as a state variable is that (9) is independent of γ. In (16), the reference point for zero potential energy is taken at $r = \infty$. This transformation implies that wherever V appears in the equations, it is replaced by $[2(E+\nu/r)]^{1/2}$. The control variables are λ and the bank angle (μ). Under the hypothesis that the cross range angle is small, ψ closely approximates the change in orbit inclination.

A further reduction to a third order model is justifiable if the objective is minimize the energy loss in the atmospheric phase of the maneuver. In this case one can treat energy as constant in the dynamics, and account for the energy loss in the performance index using the following integral form

$$J = \int_o^{t_f} C_D S(1+\lambda^2)\rho V^3/4m \, dt \qquad (17)$$

Thus, E can also be regarded as an ignorable coordinate in this case. This will result in a reasonable approximation if the energy loss is small compared to the total vehicle energy. This approximation is greatly improved if the control solution is periodically updated to account for the present vehicle energy during the maneuver, which would be the case if a feedback (analytic) optimal control solution form was obtainable.

2.2 Singular Perturbation Formulation

The main approximation introduced here is that altitude and flight path angle dynamics can be regarded as fast compared to heading dynamics. In the context of singular perturbation theory, this implies a further order reduction to a single state model, with altitude as the control variable. To motivate this viewpoint, it is desirable to identify a small parameter which

appears as a multiplying factor on the left side of the altitude and flight path angle equations of motion. Currently, there is no systematic procedure for putting the equations of motion in this standard form. However, it is generally agreed that the equations of motion should always be non-dimensionalized as an initial step. The following transformations are introduced here to justify the formulation adopted in this study.

Define the following non-dimensional variables:

$$\psi_1 = \psi/\psi_f \qquad t_1 = (C_L^* S\rho_o V_c/2m\psi_f)t \tag{18}$$

$$V_1 = V/V_c \qquad \rho_1 = \rho/\rho_o \tag{19}$$

$$h_1 = h/h_o \qquad r_1 = r/r_o \tag{20}$$

where h_o is the entry altitude, ρ_o is the air density at $h = h_o$, $V_c = [\nu/r_o]^{1/2}$ is the circular velocity at h_o, and ψ_f is the final heading (final inclination for small changes in ϕ). Also assume that for the altitudes of interest that $r = r_s$. Then (9), (11-12) become:

$$d\psi_1/dt_1 = \rho_1 V_1 \lambda \sin\mu/\cos\gamma \tag{21}$$

$$\varepsilon dh_1/dt_1 = V_1 \sin\gamma \tag{22}$$

$$\varepsilon d\gamma_1/dt_1 = C_L S\rho V_c V_1 \lambda \cos\mu/2m + V_c V_1[1-1/V_1^2 r_s]\cos\gamma/r_s \tag{23}$$

where $\varepsilon = C_L^* S\ \rho_o h_o/2m\psi_f$. Hence ε is a small parameter for sufficiently large heading changes, or if

$$C_L^* S\rho_1 h_o/2m << \psi_f \tag{24}$$

A typical calculation for a 40^o plane change and h_o = 200,000 ft gives ε = 0.0043 for a vehicle with a maximum L/D of 2.3.

The analysis in Section 3 of this report uses the original state variables and artificially introduces ε = 1.0 as a scaling parameter. It can

be shown that this formal procedure results in the same control solution as that obtained using the formulation in (21-23) in the non-dimensionalized variables.

2.3 Boundary Conditions

In [6], the sensible atmosphere is assumed to occur at h(0) = 200,000 ft. The starting velocity and flight path angle are derived using a deorbit impulse ΔV_1 from circular orbit at h_c = 100 nm, which is optimized for the atmospheric maneuver of interest. The initial heading angle is taken as zero. In the singular perturbation formulation, altitude appears as a control variable in the reduced problem. The optimal solution appears in the form

$$\overset{*}{h} = h_o(E) \tag{25}$$

For comparison purposes, in this paper the starting energy is chosen to match that of [8] for the case of a 40° heading change. From conservation of energy this results in the same deorbit impulse. The initial flight path angle is derived from conservation of angular momentum.

$$\gamma(o) = -\cos^{-1}[(r_c)(V_c-\Delta V_1)/(r_s+h(o)V(o))] \tag{26}$$

where r_c is the circular orbit radius and $V_c=(\nu/r_c)^{1/2}$ is the circular velocity. The vehicle begins the maneuver with a mass m_c and, as a result of the deorbit impulse, the mass for the atmospheric portion is given by

$$m = m_c \exp(-\Delta V_1/C) \tag{27}$$

The terminal condition is taken as:

$$\psi(t_f) = \psi_f > 0 \tag{28}$$

For the reentry problem there are no terminal constraints on altitude and flight path angle, thus their corresponding costate values are zero at the final time. For the noncoplanar orbit transfer problem, the final altitude is constrained to ensure exit from the atmosphere.

SECTION 3
HEADING CHANGE WITH MINIMUM ENERGY LOSS

The objective is to minimize the energy lost in maneuvering to a specified heading. Regarding energy as a slow variable, and altitude and flight path angle as fast variables, the following three state model was adopted for singular perturbation analysis:

$$d\psi/dt = C_L^* \rho SV\lambda \sin\mu/2m\cos\gamma \tag{29}$$

$$\varepsilon dh/dt = V\sin\gamma \tag{30}$$

$$\varepsilon\gamma/dt = C_L^* \rho SV(\lambda\cos\mu+M\cos\gamma)/2m \tag{31}$$

The objective is to minimize

$$J = -\int_o^{t_f} \dot{E}dt \tag{32}$$

where

$$\dot{E} = -C_D^*(1+\lambda^2)\rho SV^3/4m \tag{33}$$

Note that in the above formulation E is approximated as constant in the dynamics, but that changes in energy are accounted for in the performance index. This approximation will later be relaxed in the subsequent analysis. The perturbation parameter ε is introduced to signify the presence of fast dynamics, and is nominally equal 1.0. We seek a reduced and zero order boundary layer solution about $\varepsilon = 0$, in accordance with the procedures detailed in [2-4]. Regarding h and γ as fast states is characteristic of energy state analysis for fighter and transport aircraft. Therefore, we adopt the same framework in this analysis. Considering both h and γ in the same time scale results in a two point boundary value problem. A feedback guidance law is obtained by expansion of the necessary conditions to first order [15]. In this regard, it should be noted that there have been some studies that have also considered analysis of h and γ dynamics on separate time scales [16], which avoids linearization the boundary layer dynamics. Therefore, an additional set of guidance laws are possible beyond those presented here.

3.1 Singular Perturbation Analysis

Reduced Problem

Setting $\varepsilon = 0$ in (29-31) the necessary conditions for optimality become:

$$H_o = \lambda_\psi \dot{\psi} - \dot{E} = 0 \tag{34}$$

$$\gamma = 0, \qquad \lambda \cos\mu = -M \tag{35}$$

$$\mu_o, h_o = \arg \min_{h,\mu} \{\dot{\psi}/\dot{E}\} \tag{36}$$

It can be shown that this results in the following reduced solution:

$$\lambda_o = (1 + 2M_o^2)^{1/2} \tag{37}$$

$$\sin\mu_o = [(1 + M_o^2)/(1 + 2M_o^2)]^{1/2} \tag{38}$$

$$h_o = \arg \min_{h} \{V^2 (1 + M^2)^{1/2}\}\big|_{E = \text{const.}} \tag{39}$$

where M_o is the value of M for $h = h_o$. The quadrant for the bank angle in (38) is resolved based on the following inequalities:

$$0 < \mu_o < \pi/2 \text{ for } M_o < 0 \tag{40}$$

$$\pi/2 < \mu_o < \pi \text{ for } M_o > 0 \tag{41}$$

It can be seen from the above solution that M plays a crucial role in the solution process.

Since most of the energy is kinetic, V is weakly dependent on h for constant E. This can readily be seen from (16) where changes in h give rise to small changes in r. Thus, the minimization in (39) results in a value for M very close to zero. The interpretation is that the maneuver should be performed at an altitude where gravitational and centrifugal forces nearly

cancel one another. For M small, it can be seen from (37,38) that the maneuver is performed at near maximum L/D and at near 90° of bank angle. These results are in good agreement with the results in [6] for the AOTV problem. It will also been shown in Section 3.2 that the reduced solution altitude profile, $h_o(E)$, closely resembles the altitude profile of [6] for the case of large changes in inclination angle.

Boundary Layer Problem

Introducing the transformation $\tau = t/\varepsilon$ and again setting $\varepsilon = 0$, the necessary conditions in the boundary layer are:

$$H_{BL} = \lambda_\psi^o \dot{\psi} + \lambda_h V \sin\gamma + \lambda_\gamma \dot{\gamma} - \dot{E} = 0 \tag{42}$$

$$\partial H_{BL}/\partial L_1 = 0, \qquad \partial H_{BL}/\partial L_2 = 0 \tag{43}$$

where λ_ψ^o is determined in the reduced solution from (34)

$$\lambda_\psi^o = \dot{E}^o/\dot{\psi}^o = -C_D^* V_o^2 (1+M_o^2)^{1/2}/C_L^* \tag{44}$$

using the solutions for λ_o, μ_o and h_o. In (43), L_1 and L_2 represent the horizontal and vertical components of lift coefficient

$$L_1 = \lambda \sin\mu \qquad L_2 = \lambda \cos\mu \tag{45}$$

which are now used as control variables in place of λ and μ.

The first condition in (43) results in

$$L_1^* = (V_o/V)^2 (1 + M_o)^{1/2}/\cos\gamma \tag{46}$$

where M_o, V_o are the values of M and V corresponding to $h = h_o$ for the current value of E. This solution approaches the corresponding reduced solution as h approaches h_o.

The second condition in (43) yields

$$L_2^* = -(C_L^*/C_D^* V^2)\lambda_\gamma \tag{47}$$

which can also be shown to approach the reduced solution as h approaches h_o, where

$$\lambda_\gamma^o = C_D^* V_o^2 M_o/C_L^*, \quad \lambda_h^o = 0 \tag{48}$$

The reduced solution for λ_γ in (48) follows immediately from (31) and (47) with $L_2^* = -M_o$ ($\varepsilon\dot{\gamma} = 0$, in the reduced solution). The second condition in (48) is a consequence of the fact that h_o results from an unconstrained minimization of H^o. Note that λ_h^o satisfies the terminal boundary condition, but λ_γ^o does not. This point will be addressed in the numerical results section.

Unfortunately, evaluation of λ_γ needed in (47) requires the solution of a two-point boundary value problem. When close to the reduced solution it may be possible to use (48), which results in the following expression for flight path angle rate

$$d\gamma/dt = C_L^*\rho SV(M\cos\gamma^2 - V_o^2 M_o/V)/2m \tag{49}$$

For γ near zero and h near h_o, (49) simplifies to

$$d\gamma/dt = C_L^*\rho SV_o(M-M_o)/2m \tag{50}$$

Use of (46) and (47) with $\lambda_\gamma = \lambda_\gamma^o$ results in a guidance law in feedback form, which we denote as the "SP1" Solution.

Expansion of the Boundary Layer Problem [15]

A second feedback solution can be obtained by considering an expansion of the boundary layer necessary conditions of (42,43) together with the state and costate dynamics expressed in the stretched time scale $\tau = t/\varepsilon$:

$$dh/d\tau = V\sin\gamma, \qquad d\lambda_h/d\tau = -\partial H_{BL}/\partial h \tag{51}$$

$$d\gamma/d\tau = C^*_{L\rho} SV(L_2 + M\cos\gamma)/2m, \qquad d\lambda_\gamma/d\tau = -\partial H_{BL}/\partial\gamma \tag{52}$$

Substituting for L_1 and L_2 from (46,47), equations (51,52) are expanded about the reduced solutions equilibrium conditions:

$$\bar{h} = h_o(E), \qquad \bar{\gamma} = 0 \tag{53}$$

$$\bar{\lambda}_h = 0 \quad , \qquad \bar{\lambda}_\gamma = \lambda^o_\gamma \tag{54}$$

This results in the following linear perturbation equations:

$$\begin{bmatrix} \delta h' \\ \gamma' \\ \lambda'_h \\ \delta\lambda'_\gamma \end{bmatrix} = \begin{bmatrix} 0 & V_o & 0 & 0 \\ K_1 & 0 & 0 & K_2 \\ K_3 & 0 & 0 & -K_1 \\ 0 & K_4 & -V_o & 0 \end{bmatrix} \begin{bmatrix} \delta h \\ \gamma \\ \lambda \\ \delta\lambda_\gamma \end{bmatrix} \tag{55}$$

where

$$K_1 = [V^2r^2 - (\beta V^2 + \bar{\mu})r + 2\beta\bar{\mu}]/\beta V r^3$$

$$-2\bar{\mu}^2/V^3r^4 - C^*_L S\bar{\mu}M\rho/mVr^2 \tag{56}$$

$$K_2 = -C^*_L S\rho/2mC^*_D V \tag{57}$$

$$K_3 = -\partial^2 H_{BL}/\partial h^2 \leq 0 \tag{58}$$

$$K_4 = C^*_D S\rho V^3(1+2M^2)/2m \tag{59}$$

The expressions in (56-59) are evaluated at $h = h_o$, and β is the scale height in an exponential atmospheric model. The term in (58) is complicated to express analytically, but can easily be evaluated numerically taking into account the fact that both H_{BL} and $\partial H_{BL}/\partial h$ evaluated at $h = h_o$ is zero.

The eigenvalues of (55) are arranged symmetrically about the imaginary axis, and occur in complex conjugate pairs. In order to suppress the

instability in the boundary layer response, the state vector in (55) is expressed as

$$x = k_1\vec{a} + k_2\vec{b} \tag{60}$$

where $x^T = [\delta h, \gamma, \lambda_h, \delta\lambda_\gamma]$, and $\vec{a},\vec{b}$ are the real and imaginary parts of the eigenvectors associated with the stable eigenvalues. Knowing δh and γ, it is a simple exercise to solve for k_1, k_2, λ_h and $\delta\lambda\gamma$. Then L_2^* in (47) can be evaluated for

$$\lambda_\gamma = \bar{\lambda}_\gamma + \delta\lambda_\gamma \tag{61}$$

Equations (46,47) and (61) thus constitute a second feedback guidance law, which we term the "SP2" Solution.

Modeling Energy Rate Dynamics

If energy rate is modeled in the dynamics, the reduced model becomes a two-state problem, and the performance index is modified to minimize $-E(t_f)$. The Hamiltonian in this case is

$$H_o = \lambda_\psi\dot{\psi} + \lambda_E\dot{E} = 0, \qquad \lambda_E(t_f) = -1 \tag{62}$$

This gives rise to a two-point boundary value problem in the reduced solution. However, an approximate integration of λ_E is possible in this case, based on the known properties of the optimal solution. Using (62), it is easy to demonstrate that

$$d\lambda_E/dt = -\partial H_o/\partial E \stackrel{*}{=} \lambda_E C_D S\rho V^2(1+\lambda^2)/2m \tag{63}$$

Thus,

$$d\lambda_E/d\psi = (2C_D^*(1+\lambda^2)\cos\gamma/C_L^*\lambda\sin\mu)\lambda_E \simeq (2C_D^*/C_L^*)\lambda_E \tag{64}$$

where the approximations $\lambda \simeq 1$, $\mu \simeq \pi/2$, $\gamma \simeq 0$ have been employed. Integration of (64) results in

$$\lambda_E(\psi) \simeq -\exp\{-2C_D^*(\psi_f-\psi)/C_L^*\} \tag{65}$$

Comparing the Hamiltonian expressions in (34) and (62), it can be seen that modeling E as constant in the dynamics amounts to the approximation $\lambda_E = -1$. Equation (65) represents an improvement, but the approximation $\lambda_E = -1$ is apparently accurate for high L/D vehicles. So far as its effect on the reduced solution, (37-41) remain the same. The reduced costate solutions become:

$$\lambda_\psi^o = -\lambda_E C_D^* V_o^2 (1+M_o^2)^{1/2}/C_L^* \tag{66}$$

$$\lambda_h^o = 0, \qquad \lambda_\gamma^o = \lambda_E C_D^* V_o^2 M_o/C_L^* \tag{67}$$

Note that the ψ and γ costate solutions are now simply multiplied by λ_E. The boundary layer solution for L_1^* in (46) remains the same, but (47) becomes

$$L_2^* = -(C_L^*/C_D^* V^2)\lambda_\gamma/\lambda_E \tag{68}$$

Thus the SP1 control solution, which uses $\lambda_\gamma = \lambda_\gamma^o$ remains unchanged when E is modeled in the dynamics, since λ_E is canceled when λ_γ^o from (67) is substituted in (68). The SP2 solution, on the other hand, is affected in that several of the matrix elements in (55) are changed. In particular, K_2 and K_4 are divided by λ_E and H_{BL} used in the computation K_3 becomes

$$H_{BL} = \lambda_\psi \dot{\psi} + \lambda_h V \sin\gamma + \lambda_\gamma \dot{\gamma} + \lambda_E \dot{E} \tag{69}$$

We will refer to the control solution obtained with these modifications as the "SP3" Solution.

3.2 Numerical Results

A numerical study was performed to evaluate the performance of the three

guidance laws derived in the preceding section. The parameter values, chosen to approximate the vehicle studied in [5], are as follows:

$$C_{D_o} = .032, \quad S = 125.8 \text{ ft}^2, \quad K = 1.4, \quad m = 331.5 \text{ slugs}$$

The initial conditions were chosen to match the 40° heading change maneuver of [5], where the sensible atmosphere was defined to begin at an altitude of 200,000 ft. The corresponding entry velocity and flight path angles are $V(0) = 25{,}945$ ft/s and $\gamma(0) = -.148°$. A simple exponential atmospheric model was defined using the standard atmospheric data for air density at altitudes of 10^5 and $2\text{x}10^5$ feet. All of the comparisons are for a 40° heading change.

We first illustrate the validity of the singular perturbation formulation by comparison of the reduced solution altitude profile obtained from the use of (39), with the optimal solution for the 40° plane change problem. The optimal solution was calculated using a multiple shooting method described in [17]. Figure 1 illustrates this comparison. The optimal solution altitude profile satisfies a terminal constraint that $h(t_f) = h(0)$, needed for a typical AOTV orbit plane change. It can be seen that the reduced solution altitude profile closely follows the optimal altitude profile, with the exception of satisfying the initial and final values of altitude, which are lost in the reduced problem formulation (altitude is a control like variable). Clearly, the reduced solution can be used for the initial phase of an AOTV plane change maneuver, but a large terminal boundary layer correction is needed for the exit phase. This aspect will be addressed in Section 4 of this report.

We next consider the performance of the guided solutions for the reentry problem. Figure 2 compares the reduced solution altitude profile obtained from (39) with the SP1 and SP3 guided solution profiles, which on this scale are identical. A similar comparison is given for the SP2 guided solution in Fig. 3. Note that the reduced solution provides a reasonable altitude profile except at high energies near the initial time. However, this region of the solution is of little interest since the air density is negligibly small. In any case, it is not physically possible to follow this profile (recall that h is used as a control variable in the reduced solution). Thus, it was decided to maintain $\lambda = 1$ and $\lambda\cos\mu = -M$ ($\dot{\gamma}=0$) until $h_o(E)$ falls below the current altitude.

In order to evaluate the optimality of these solutions, an optimal solution was numerically computed using the four-state model in (8-11) to define the dynamics. The SP1 guided solution was used as an initial guess for the state time histories, and the reduced solutions in (44), (54), and (65) were used as an initial guess for the costate time histories. The solution converged to a relative precision of 10^{-12} in eight iterations. The value of the Hamiltonian was constant and essentially zero considering the relative precision accuracy required for convergence. This served as an independent check on the accuracy of the solution.

Figure 4 compares the optimal altitude profile with the profiles that result from the three guided solutions. Note that the optimal solution dips slightly more into the atmosphere near the end, and consequently results in slightly decreased flight time. The corresponding control time histories and heading profiles are compared in Figs. 5-7. Note that in Fig. 5, the optimal bank angle at the final time is 90°, which follows from (47) and the fact that $\lambda_\gamma(t_f) = 0$. In the context of singular perturbation theory, this gives rise to a terminal boundary layer which must be solved backwards in time. Since this was ignored in our analysis, the guided solutions approach the condition in (48) instead. This explains the departure in the altitude profiles of Fig. 4. It is apparent that this effect is a minor one. In any case, the dip in the optimal profile may not be desirable from a practical standpoint.

It may be somewhat surprising at this point that the SP1 and SP3 solutions are nearly identical. However, recall that the SP1 solution is not sensitive to the approximation that E is modeled as constant in the dynamics. The SP3 solution corrects the SP2 solution for this modeling approximation, and results in essentially the same solution as the SP1 solution. This fact also justifies the use of approximation $\lambda_\gamma = \lambda_\gamma^o$ in the SP1 solution. Table 1 compares the energy loss for all the solutions, and shows the three guided solutions produce essentially optimal performance. The energy loss for the SP1 and SP3 solutions is indistinguishable from the optimal solution to four significant places, while the energy loss for the SP2 solution is .06% greater.

SECTION 4
AEROASSISTED ORBIT TRANSFER

The preceeding section has demonstrated that singular perturbation theory can be used as an effective tool in model order reduction for the problem of hypervelocity heading change within the atmosphere with minimal energy loss. The extension to aeroassisted orbit transfer with inclination change requires that a contraint be imposed on the terminal altitude to insure that the vehicle exits the atmosphere when the heading change (which approximates the inclination change) is achieved. This introduces a difficult terminal boundary layer problem, which to date we have not been able to solve in closed form, since it requires an analytic integration of the boundary layer equations. In [5-9] this same problem arises, but in a different context. In these studies, the states and co-states associated with a four-state model are analytically integrated with the assumption that Loh's term, M(h,V), is constant or piecewise constant over the trajectory. While this is true for a large portion of the maneuver, M undergoes a large variation near the end. Consequently, the guidance algorithms resulting from these studies require large angles of attack near the end of the maneuver to compensate for this variation. This drawback was subsequently removed in [10], however, the resulting guidance algorithm requires that a complex quadrature be performed at each guidance interval. Moreover, this approach is not readily extended to the case where heating rate is constrained.

The essential problem in all these approaches lies in the fact that air density decreases exponentially as altitude increases, and corrections to satisfy terminal constraints must be accurately predicted while the vehicle is at lower altitudes.

In this section, the simplest guidance algorithm presented in Section 3 is used for the initial portion of the maneuver, and a predictor/corrector type algorithm is presented for the terminal maneuver. The predictor/corrector algorithm relies on bank angle control alone, and thus avoids the problem of large angle of attack. The form of the guidance algorithm was chosen to closely approximate the known properties of the optimal solution, while permitting an accurate integration of the equations of motion. The predictor/corrector algorithm provides the information needed

to both initiate the terminal maneuver, and to guide the vehicle in closed loop fashion. The availability of a closed loop guidance algorithm will be of paramount importance in future studies addressing the effect of atmospheric anomalies, and of course, for real time implementation. Comparisons are made to numerically optimized trajectories for a range of orbit plane angles to demonstrate the near optimality of the complete guidance algorithm.

4.1 Guidance During the Reentry Phase

Guidance during the reentry phase is based on the zero order reduced and boundary layer solution referred to as the SP1 solution in Section 3. This consists of first calculating the reduced solution in (39), and then calculating the horizontal and vertical components of the normalized lift vector using (46,47), with $\lambda_\gamma = \lambda_\gamma^o$ as given by (48).

4.2 Guidance During the Exit Phase

The reentry phase guidance algorithm does not satisfy the terminal constraint on h, which was lost in the reduced formulation. The terminal boundary layer necessary conditions are identical in form to those for the initial boundary layer. However, the solution asymptotically approaches the reduced solution backwards in time, starting from the terminal constraint on altitude. In addition, the change in ψ during the terminal maneuver must be accounted for to insure that both terminal constraints are met simultaneously. This requires an anlytical integration of the state and costates. To circumvent this problem, a predictor/corrector guidance law was developed based on the known properties of the optimal solution: $\lambda^* \simeq 1.0$, $\mu^* \simeq \pi/2$.

To simplify the problem of integrating the forward motion, it is assumed that the nominal exit maneuver consists of two regions. In the first, a constant (negative) bank angle perturbation is used to increase the flight path angle. This is followed by a second region in which γ is influenced only by gravity. A bank angle correction is computed throughout the maneuver

based on the predicted heading error at the final altitude. Constraints are enforced to insure continuity at the junction of the two regions, and satisfaction of the terminal constraint on altitude. The maneuver is depicted in Fig. 8.

During terminal guidance, we maintain $\lambda = 1.0$, and modulate the bank angle according to the following equations:

$$\mu = \mu_o - \delta\mu_o + \delta\mu = \mu + \delta\mu \tag{70}$$

where in Region 1:

$$\mu_o = \cos^{-1}(-M), \quad \delta\mu_o = \text{const.} > 0 \tag{71}$$

and in Region 2:

$$\mu_o = 90°, \quad \delta\mu_o = 0 \tag{72}$$

The nominal trajectory can be analytically predicted for $\delta\mu=0$, and using the approximations:

$$\cos\mu \simeq -M + \delta\mu_o \sin\mu_o, \quad \sin\gamma \simeq \gamma \tag{73}$$

the details of which can be found in [18]. The predicted heading change ($\Delta\psi_p$) for the exit maneuver is calculated at each integration step along the trajectory, and is used to both initiate the maneuver (when $\Delta\psi_p = \psi_{go}$), and to track the terminal constraint using a simple proportional control law,

$$\delta\mu = k(\psi_{go} - \Delta\psi_p) \tag{74}$$

Region 2 guidance is initiated when the present altitude satisfies the continuity constraint at the junction of the two regions.

4.3 Numerical Results

A numerical study was performed to evaluate the performance of the sub-optimal guidance algorithm described in the preceding section, using the same vehicle data as presented in [6] and in Section 3. Fig's 9 and 10 illustrate the guided altitude profiles and the corresponding bank angle profiles obtained for heading changes up to 40^o, in increments of 10^o. The λ profiles are very close to 1.0 throughout for all the maneuvers, and are not

illustrated. These results were generated for $\delta\mu_o = 25^o$, k = 50, however it was found that the general character of the solutions did not change as these guidance parameters were varied. Note from Fig. 10 that, following the initial perturbation, bank angle continues to decrease in Region 1. This is due to the variation in M that takes place as the altitude departs from the reduced solution profile. After completing Region 1, the bank angle remains very close to 90^o, or in other words, $\delta\mu$ in (24) is very close to zero, indicating the accuracy of the prediction algorithm.

In order to evaluate the optimality of the guidance algorithm, optimal solutions were obtained numerically using the multiple shooting algorithm [17]. Fig's. 11 and 12 illustrate the optimal altitude and bank angle profiles. The most remarkable characteristic in these solutions is that the final time is nearly independent of the final heading. Also note that the final bank angle is always 90^o, which is required by the necessary conditions. The corresponding λ profiles are shown in Fig. 13, which verifies that the optimal solution lies close to $\lambda = 1$. The flight path angle histories for all the cases in Fig. 9 and Fig. 12 are quite small, and close to zero at the final time.

Despite the fact that the final times are considerably different, the guided solution performance is not far from optimal. Table 2 illustrates the near optimality by comparing the energy loss of the guided solutions with that of the optimal solutions.

SECTION 5
CONSTRAINED AEROGLIDE

The constrained aeroglide problem is treated in this section. This is essentially the same problem addressed in Section 4 with the addition of a heating rate constraint, which amounts to a first order state variable inequality constraint.

5.1 Problem Formulation

For this problem it is necessary to consider the system of equations in (2-6), since the approximation that $\phi = 0$ is no longer valid. In this case, θ remains an ignorable coordinate, and (7) is used to define the change in inclination angle. It was also necessary to initiate the maneuver at a much higher altitude, since the starting condition for the results in Section 4 has a fairly high value of heating rate. Only numerically optimized solutions were considered, using the same multiple shooting method that was employed for the unconstrained solutions. First the touch point solution was considered, and the range of maximum allowable heating rate over which this solution applies was obtained for the same vehicle dynamics considered in Section 4. Then, the constrained arc solution was attempted for lower values of the heating rate limit. However, only a narrow range of solutions were found for this case. Unfortunately, all of these solutions violate the practical limits for heating rate. Hence, the optimal aeroglide problem remains an open research issue. It may be that very complex behavior results for lower values of heating rate limit, such as multiple touch point solutions combined with portions of a constrained arc.

The expression for heating rate employed in this study was:

$$dQ/dt = 17600[p/p_s]^{1/2}[V/V_s]^{3.15} \quad (BTU/sec/ft^2) \qquad (75)$$

5.2 Numerical Results

The vehicle characteristics are the same as those given in Section 3.3. The initial and terminal condition data are as follows:

$$h(0) = h(t_f) = 365{,}000 \text{ ft}, \quad V(0) = 25{,}746 \text{ ft/s}, \quad \gamma(0) = 0.55^{o}$$

$$i(t_f) = 18^{o}$$

The initial h, V and γ correspond to the same deorbit impulse employed in Sections 3 and 4.

Figures 14-16 illustrate the h, V and i profiles for the unconstrained solution and for the touch point solution corresponding to a maximum heating rate of 600 BTU/sec/ft^2. As the heating rate limit is decreased, the minimum altitude and flight time increase. Figures 17 and 18 show the corresponding control time histories. For the touch point solution, there is a slight jump in the normalized lift coefficient at the touch point. However, this is likely due to numerical inaccuracy in satisfying the touch point conditions. The bank angle history is continuous. Figures 19 and 20 illustrate the jumps that occur in the λ_h and λ_V at the touch point. All other costates are continuous. All of the state and costate histories can be found in [18]. Figure 21 compares the heating rate profiles. The peak heating rate for the unconstrained case was 729.3 BTU/sec/ft^2. In comparing these results it was found that the increase in energy loss due to the heating rate limit imposed was negligible. However lower heating rate limits will likely result in much greater energy loss.

Attempts to decrease the heating rate limit below 600 BTU/sec/ft^2 resulted in convergence failure. This failure was abruptly encountered at a heating rate limit of 599.3 BTU/sec/ft^2. Thus we suspect that either a conjugate point is encountered, or the nature of the optimal solution changes to either a constrained arc case or a multiple touch point case. The constrained arc case was investigated, and after many attempts (including reformulation in nondimensional variables) we were not able to obtain a converged solution.

SECTION 6
CONCLUSIONS AND RECOMMENDATIONS

The application of singular perturbation methods to optimal control problems related to aeroassisted orbit transfer vehicles has been investigated in this study. Two closely related problem formulations were addressed: optimal reentry of a hypersonic gliding vehicle, and optimal orbit plane change with aeroglide. In addition, an attempt was made to obtain numerical solutions for optimal aeroglide orbit plane change subject to a maximum heating rate constraint.

6.1 Conclusions

The major conclusions resulting from this research effort are as follows:

(1) Singular perturbation theory using energy state approximations can be used to reduce the model order to a single state equation, and a closed form solution for the reduced problem can be readily obtained. The solution for the reduced problem reasonably approximates the full order optimal solution, except near the initial and final conditions. By non-dimensionalizing the equations of motion a singular perturbation expansion parameter can be identified that depends on vehicle parameters and the required heading change.

(2) For the reentry problem, three guidance algorithms were derived, all of which are nearly optimal in terms of minimizing the energy loss for the maneuver. No terminal boundary layer correction was required for this problem formulation.

(3) A constraint on terminal altitude, required for the noncoplanar orbit transfer problem, results in a difficult boundary layer problem for which we were not able to obtain a tractable analytic solution. However, the optimal terminal maneuver was approximated

using a sub-optimal predictor/corrector guidance law. In general, optimization of the terminal maneuver (to satisfy terminal constraints) is not as critical as optimizing the initial (reentry) portion of the maneuver.

(4) The problem of optimal orbit plane change subject to a heating rate constraint results in a touch point extremal solution for a high (but narrow) range of heating rate limit. These trajectories and the corresponding control histories are similar to the unconstrained solution, with negligible increase in energy loss. This will not be true for lower values of the heating rate limit, where the constrained trajectory may ride the constraint boundary and/or contain multiple touch points. Unfortunately, the multiple shooting method could not be successfully used to find extremal solutions corresponding to the first order necessary conditions associated with this problem.

6.2 Recommendations

Based on the results of this research effort, the recommendations for further work along this line are:

(1) The numerical study of optimal aeroassisted orbit transfer with aeroglide, subject to a heating rate constraint, should be completed over a more practical range of heating rate limit. Along this line, alternative formulations of the necessary conditions, such as the transformation method in [19], should be explored. Another approach is to use a parameter optimization based method such as that employed in OTIS [20]. In this case, the constraint would be enforced indirectly through a penalty function approach. The resulting profiles are of interest for comparison to aerocruise solutions [12], and for further developing near optimal guidance algorithms based on singular perturbation theory.

(2) Further research is needed to develop methods of solving the terminal boundary layer problem associated with terminal

constraints. One such alternative, investigated in this study [18] (but not reported here), is a formulation in which the terminal altitude constraint was satisfied as a part of the reduced solution. This avoids the terminal boundary layer problem altogether.

(3) Parametric studies of the effect of initial and final orbit altitudes on the optimal orbit plane change maneuver should be conducted. This includes the possibility of optimizing the deorbit impulse, and including the use of multiple impulsive maneuvers for performing a part of the orbit inclination change outside the atmosphere.

(4) Robustness of the guidance algorithms resulting from this study was not investigated. In particular, the effect of uncertain atmospheric conditions at high altitudes should be evaluated.

(5) Extensions to problem formulations suitable for aerocapture and orbit plane change for future Mars missions should be explored.

6.3 Publications

The journal and conference publications that resulted from this research effort can be found in [18] and in [22-26].

REFERENCES

1. Bryson, A.E., Desai, M.N., and Hoffman, W.C., "Energy-State Approximation in Performance Optimization of Supersonic Aircraft," Journal of Aircraft, Vol. 6, Nov.-Dec. 1968.

2. Calise, A.J., "Singular Perturbation Methods for Variational Problems in Aircraft Flight," IEEE Trans. on A.C., Vol. AC-21, No. 3, June 1976.

3. Calise, A.J., "Extended Energy Management Methods for Flight Performance Optimization," AIAA Journal, Vol. 15, No. 3, May-June 1976.

4. Calise, A.J., "Singular Perturbation Techniques for On-Line Optimal Flight-Path Control," AIAA J. of Guid. and Cont., Vol. 4, No. 4, July-Aug. 1981.

5. Mapar, J., "Development and Comparison of Optimal Guidance Laws for Aeroassisted Orbital Transfer," MS Thesis, University of Texas at Austin 1984.

6. Hull, D.G., Giltner, J.M., Speyer, J.L. and Mapar, J., "Minimum Energy-Loss Guidance for Aero-Assisted Orbital Plane Change," AIAA J. of Guid., Cont., and Dyn., Vol. 8, No. 4, July-Aug. 1985.

7. Hull, D.G., "New Analytical Results for AOTV Guidance," AIAA GN&C Conf., Snowmass, CO, Aug. 1985.

8. Hull, D.G., McClendon, J.R., Speyer, J.L., "Aero-assisted Orbital Plane Change Using an Elliptic Drag Polar," Journal of the Astron. Sciences, Vol. 36, Nos. 1/2, Jan.-June 1988.

9. Hull, D.G., McClendon, J.R., Speyer, J.L., "Improved Aero-assisted Plane Change Using Successive Approximation," Journal of the Astron. Sciences, Vol. 36, Nos. 1/2, Jan.-June, 1988.

10. Speyer, J.L., Crues, E.Z., "An Approximate Atmospheric Guidance Law for Aeroassisted Plane Change Maneuvers," AIAA GN&C Conf., Minneapolis, MN, Aug. 1988.

11. Hull, D.G. Speyer, J.L., "Optimal Reentry and Plane-Change Trajectories," Journal of Astron. Sciences, Vol. 30, No. 2, April-June 1982.

12. Mease, K.D., Lee, J.Y., Vinh, N.X., "Orbital Changes During Hypervelocity Aerocruise," Journal of the Astron. Sciences, Vol. 36, Nos. 1/2 Jan-June 1988.

13. Lee, J.Y., Hull, D.G., "Maximum Orbit Plane Change with Heat-Transfer-Rate Constraints," AIAA J. of Guid., Cont. and Dyn., to appear.

14. Mease, K.D., "Optimization of Aeroassisted Orbital Transfer: Current Status," Journal of the Astron. Sciences, Vol. 36, Nos. 1/2, Jan.-June 1988.

15. Ardema, M.D., "Linearization of the Boundary Layer Equations of the Minimum Time-To-Climb Problem," J. of Guid. and Cont., Vol. 2, No. 5, Sept.-Oct. 1979.

16. Calise, A.J., "Optimization of Aircraft Altitude and Flight-Path Angle Dynamics," J. of Guid., Cont. and Dyn., Jan.-Feb. 1984.

17. Burlish, R., "The Multiple Shooting Method for Numerical Solution of Nonlinear Boundary Value Problems and Optimal Control Problems (in German), Carl-Cranz-Gessellchaft, Techn., Rep., Heidelberg, 1971.

18. Bae, Gyoung-Hyun, "Optimal Control of Aero-Assisted Orbit Transfer Vehicles, Ph.D. Thesis, Georgia Institute of Technology, December 1988.

19. Jacobson, D.H. and Lele, M.M., "A Transformation Technique for Optimal Control Problems with a State Variable Inequality Constraint," IEEE Trans. on A.C., Vol. AC-14, No. 5, Oct. 1969.

20. Paris, S.W., Hargraves, C.R., "Optimal Trajectories by Implicit Simulation - Vol's. I-IV," AFWAL-TR-88-3057, Flight Dynamics Lab., Air Force Wright Aeronautical Labs., WPAFB, November 1988.

21. Calise, A.J., Bae, G.H., "Singular Perturbation Analysis of AOTV-Related Trajectory Optimization Problems," Progress Report for 1 Sept. - 30 July, July 1987.

22. Calise, A.J., "Singular Perturbation Analysis of the Atmospheric Orbital Plane Change Problem," Journal of the Astron. Sciences, Vol. 36, Nos. 1/2, Jan.-June 1988.

23. Calise, A.J., Bae, G.H., "Optimal Guidance for Aeroassisted Orbit Transfer Vehicles," Americal Control Conf., Atlanta, Ga., June 1988.

24. Calise, A.J., Bae, G.H., "A Near Optimal Guidance Algorithm for Aeroassisted Orbit Transfer," AIAA Guidance, Navigation and Control Conf., Minneapolis, MN, August 1988.

25. Calise, A.J., Bae, G.H., "Aeroassisted Orbit Transfer with a Heating Rate Constraint," IEEE International Conf. on Cont. and Appl., Jerusalem, Israel, April 1989.

26. Calise, A.J., Bae, G.H., "Optimal Heading Change with Minimum Energy Loss for a Hypersonic Gliding Vehicle," AIAA J. of Guidance Dynamics and Control, to appear.

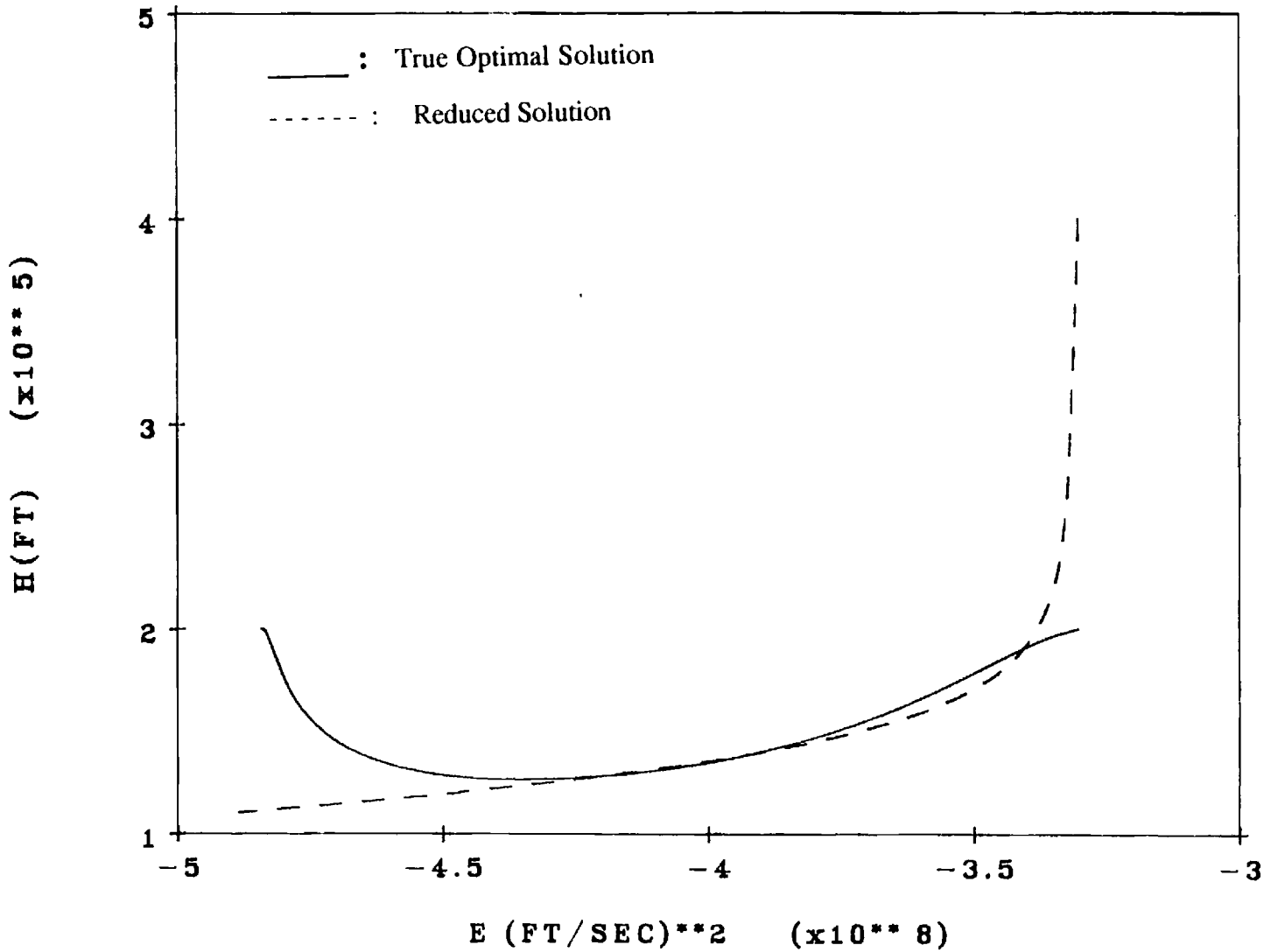

Figure 1. Comparison of the reduced solution altitude profile with an optimal profile for a 40^{o} heading change.

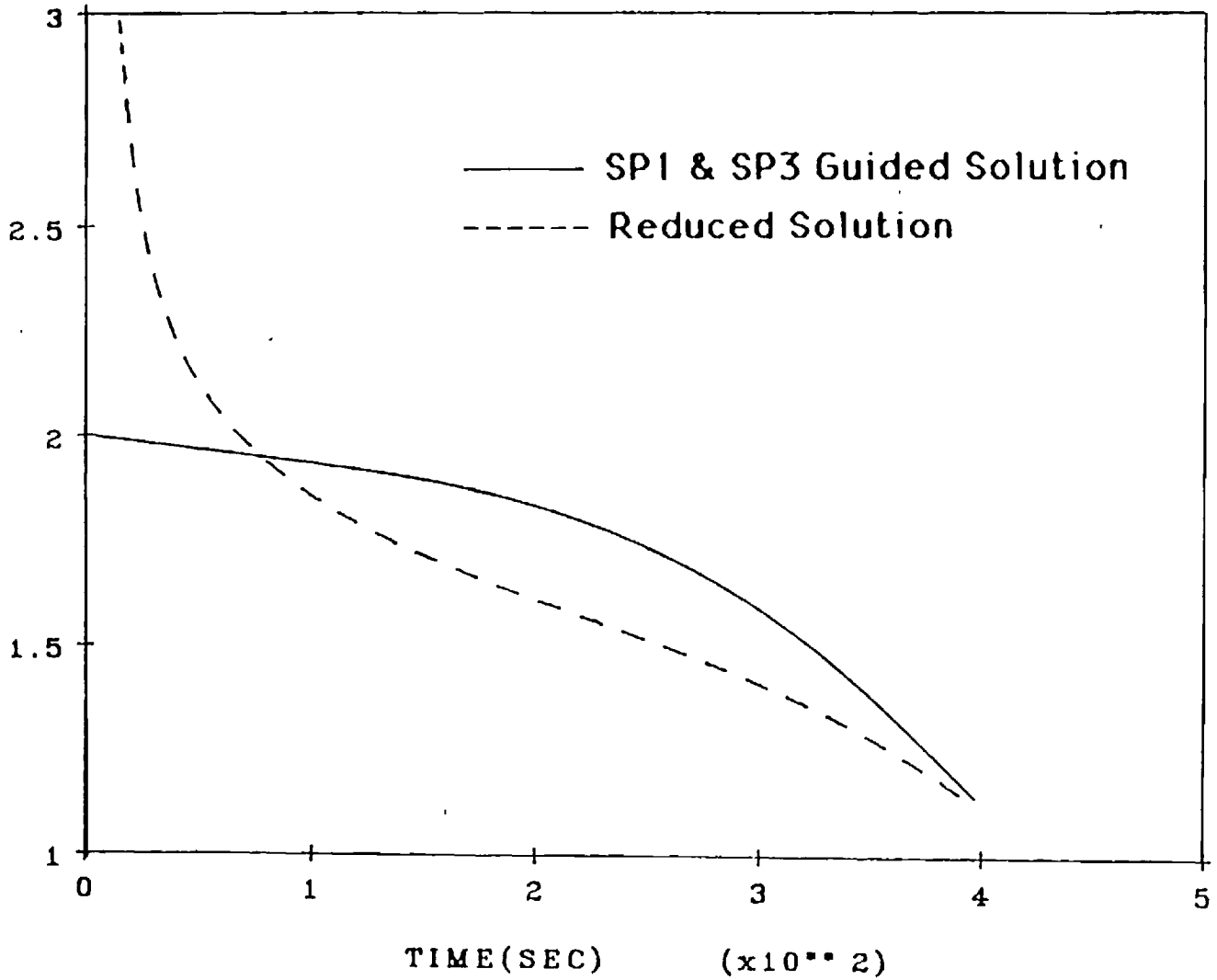

Figure 2. **Comparison of the SP1 and SP3 guided altitude profiles with the reduced solution.**

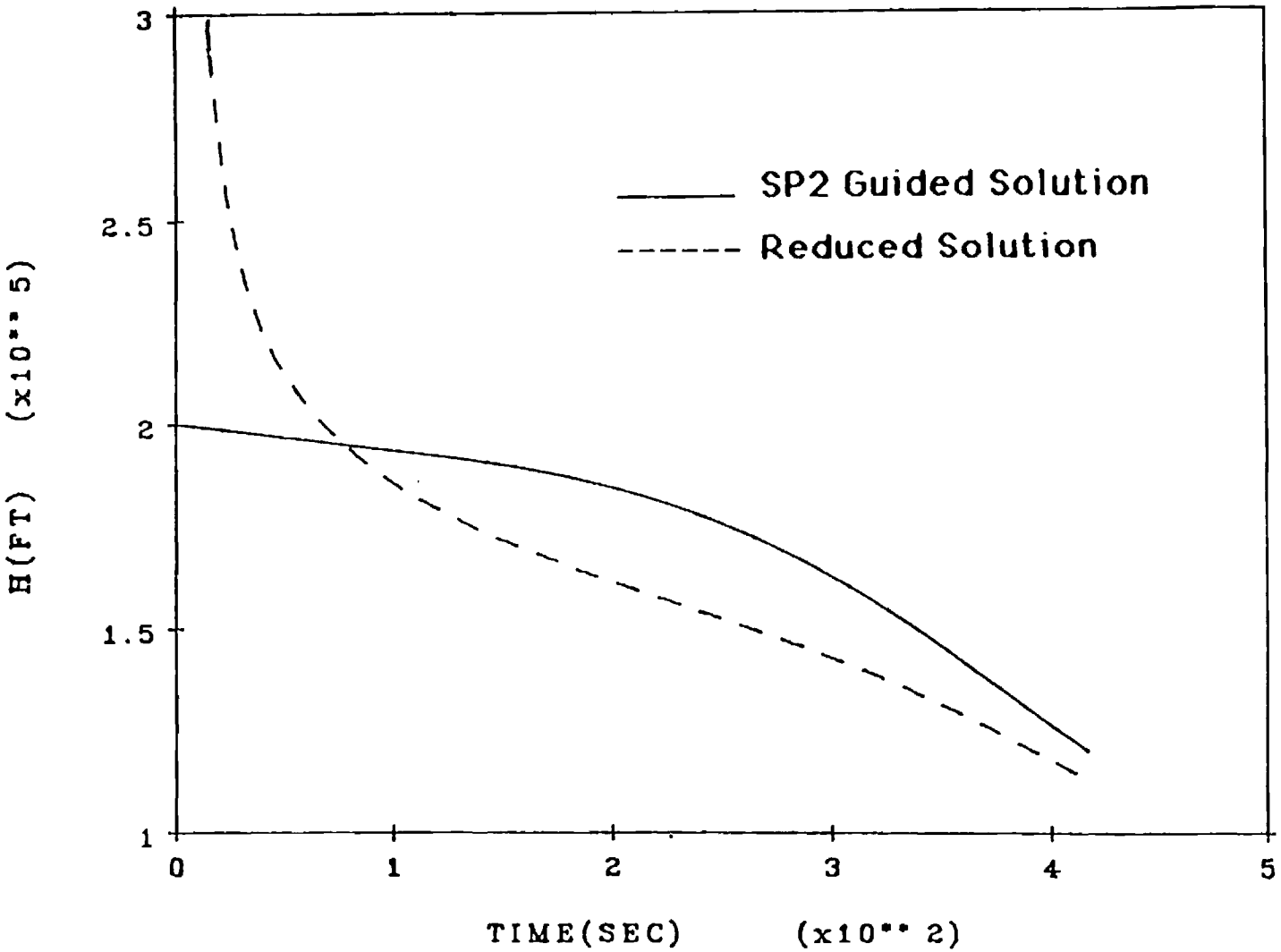

Figure 3. Comparison of the SP2 guided altitude profile with the reduced solution.

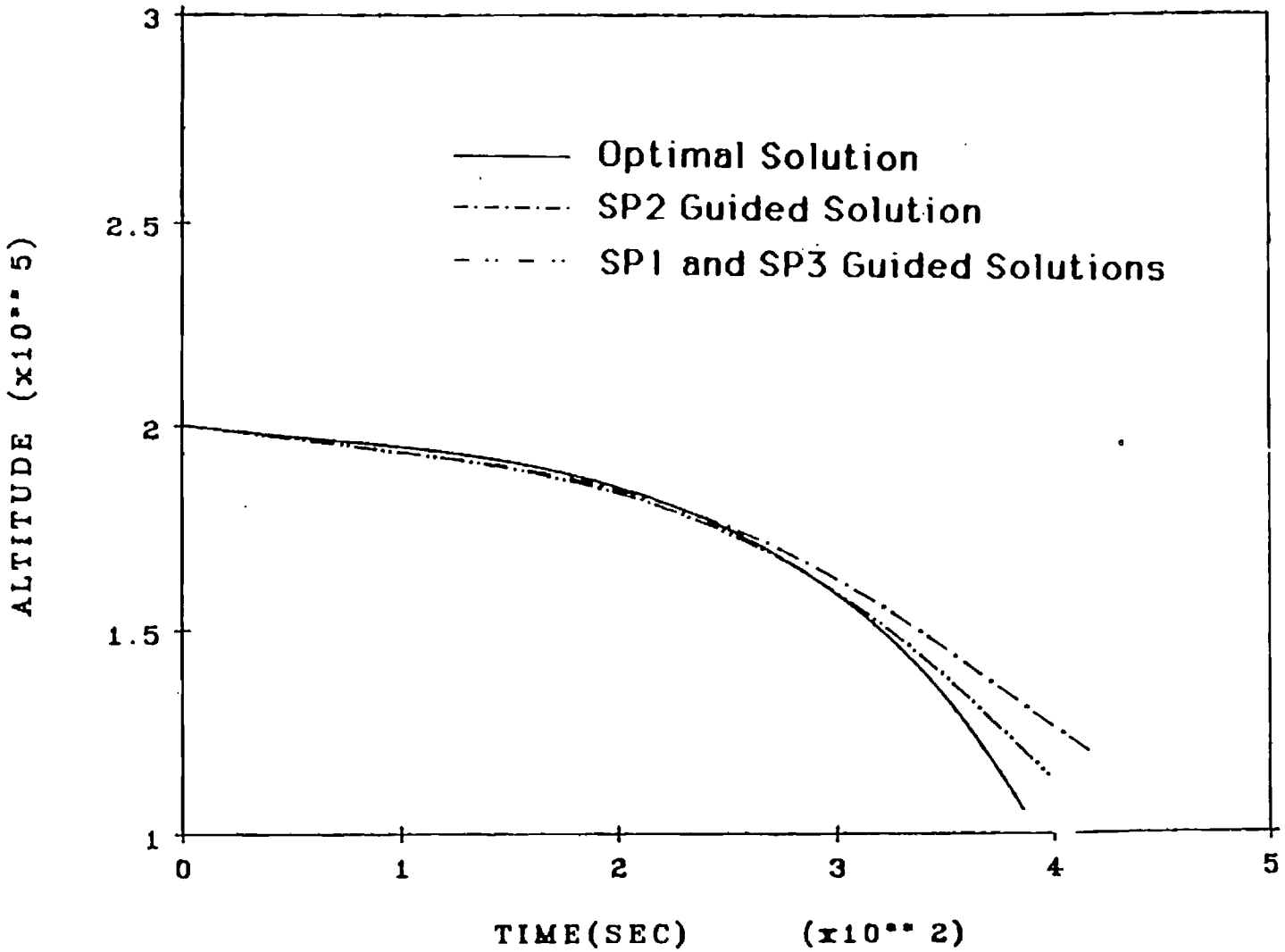

Figure 4. Comparison of the guided altitude profiles with the true optimal solution.

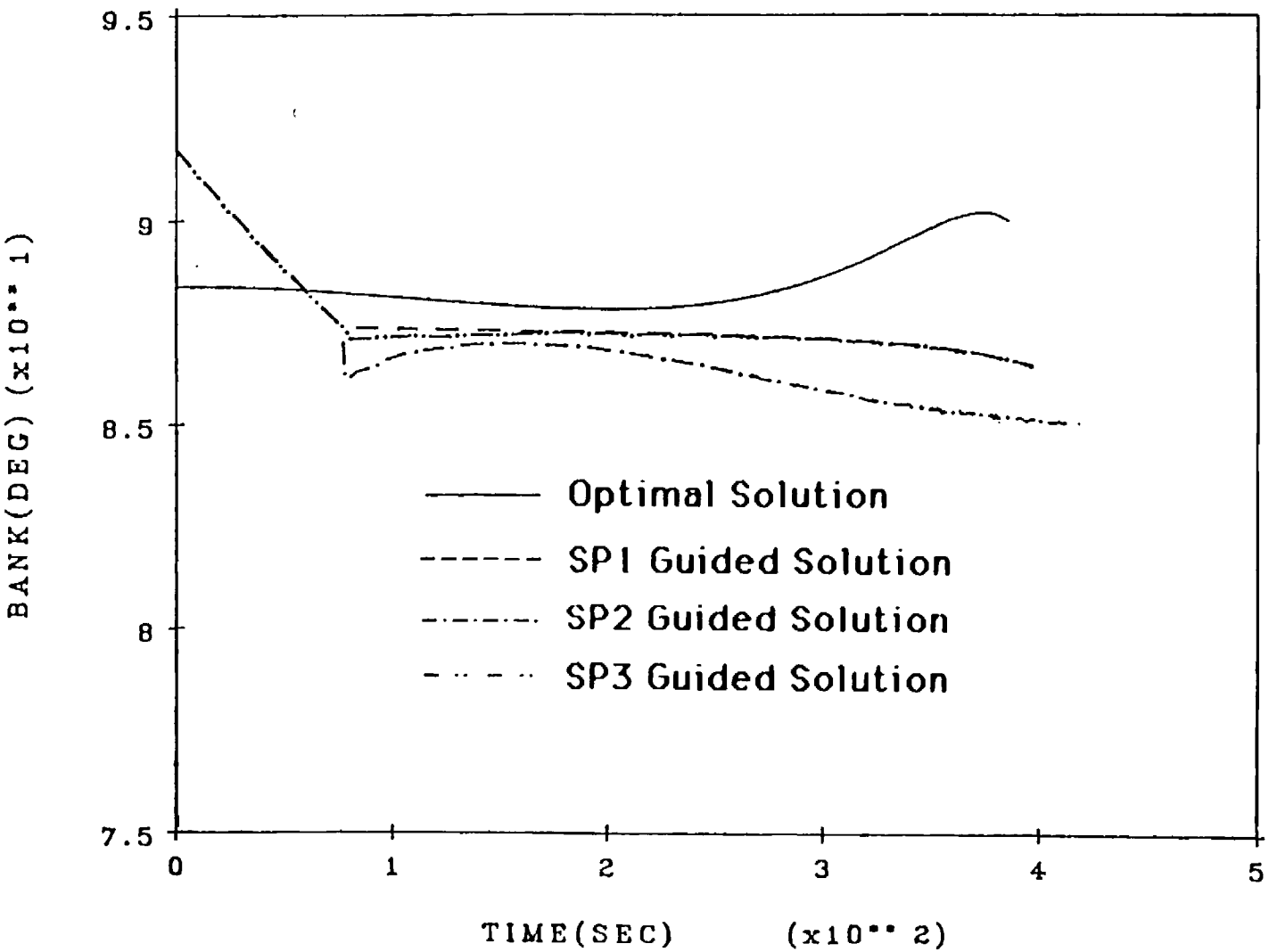

Figure 5. Bank angle profiles.

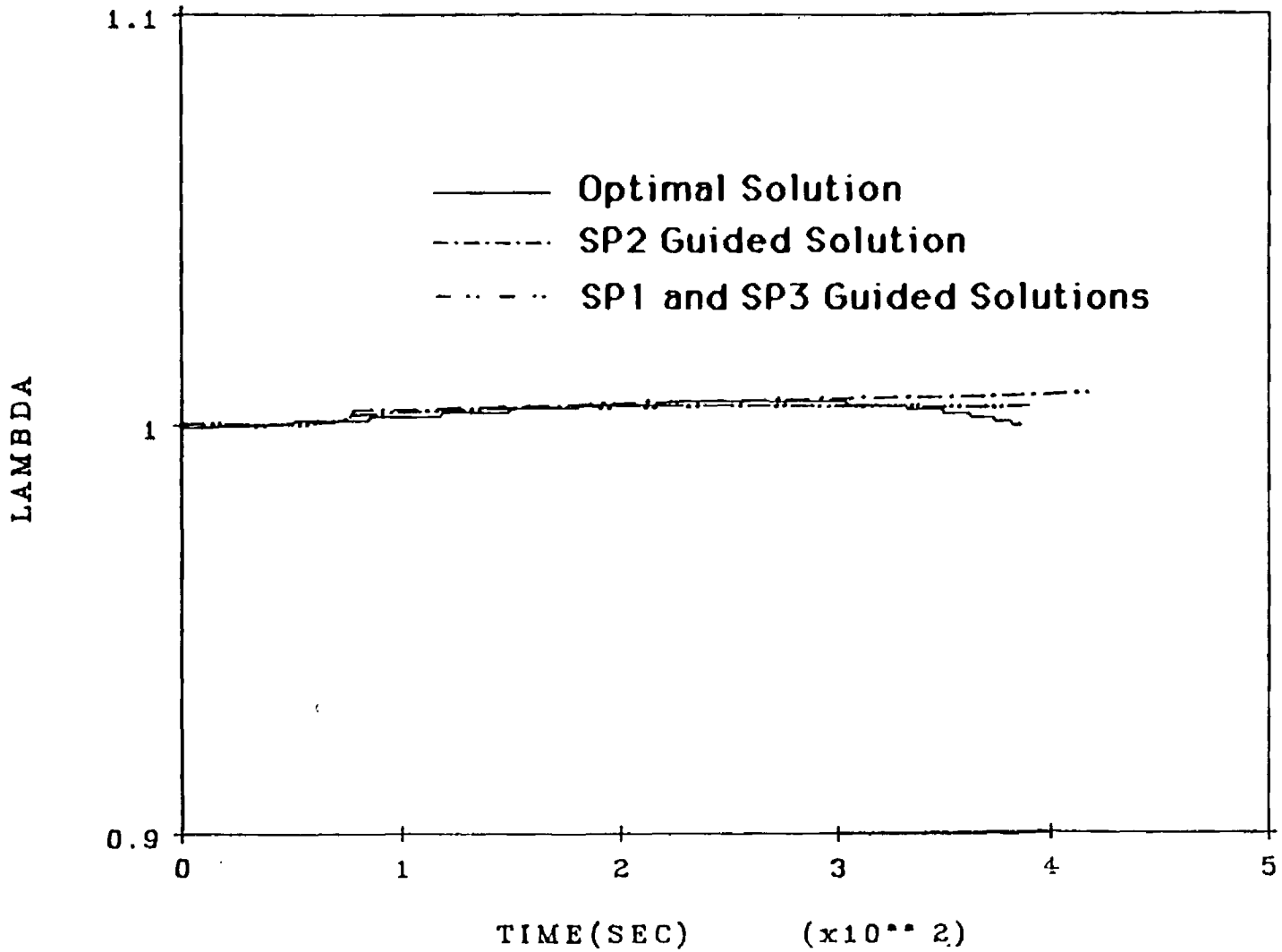

Figure 6. Normalized lift coefficient profiles.

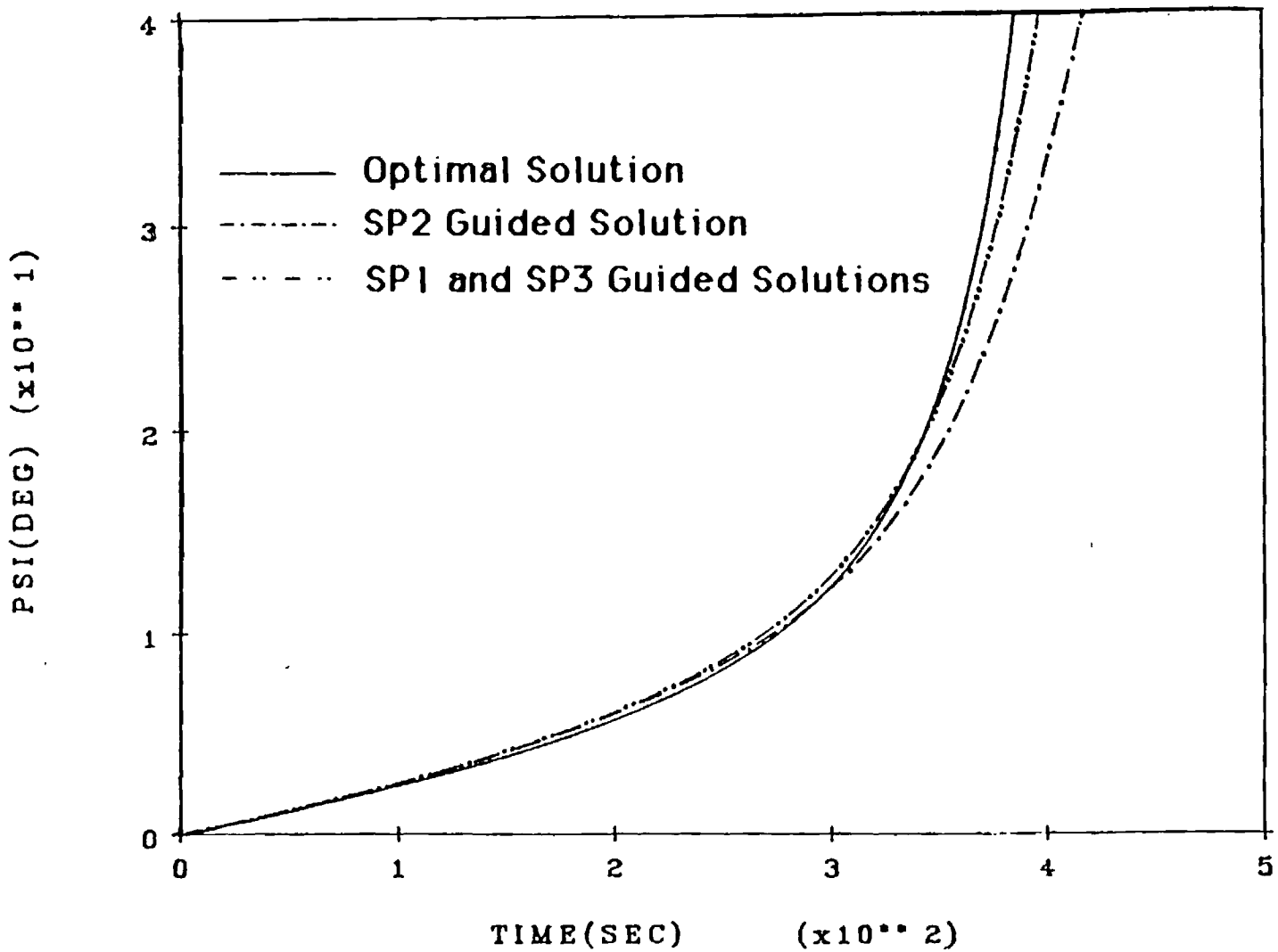

Figure 7. Heading profiles.

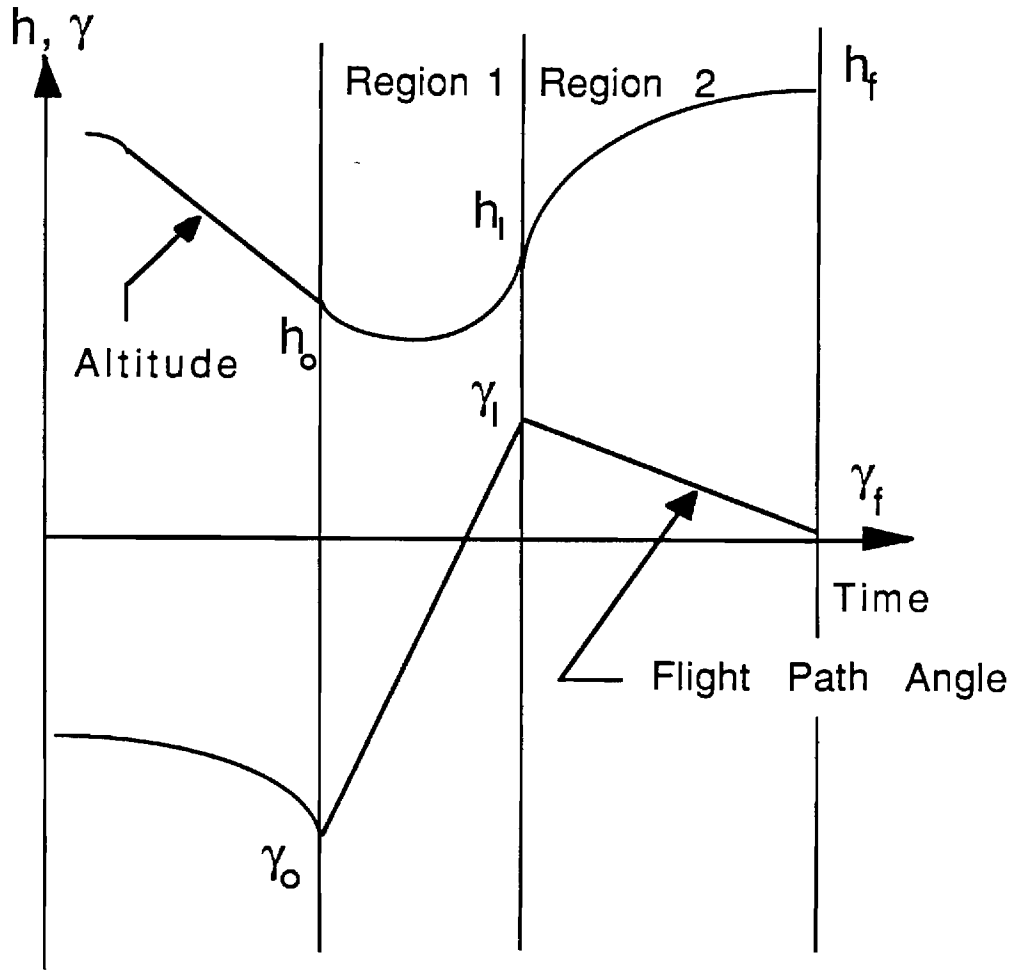

Figure 8. Depiction of the exit phase maneuver.

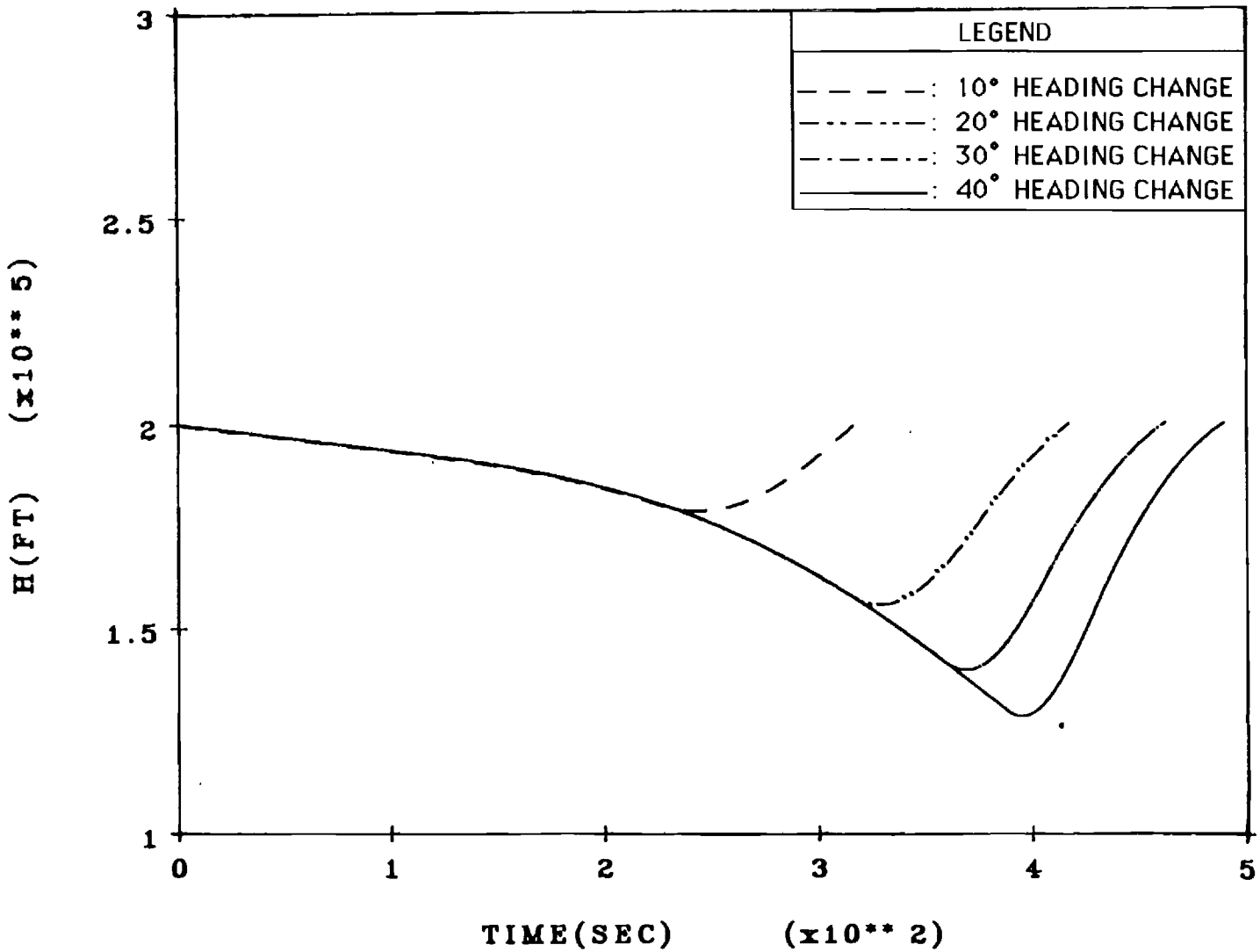

Figure 9. Guided solution altitude profiles.

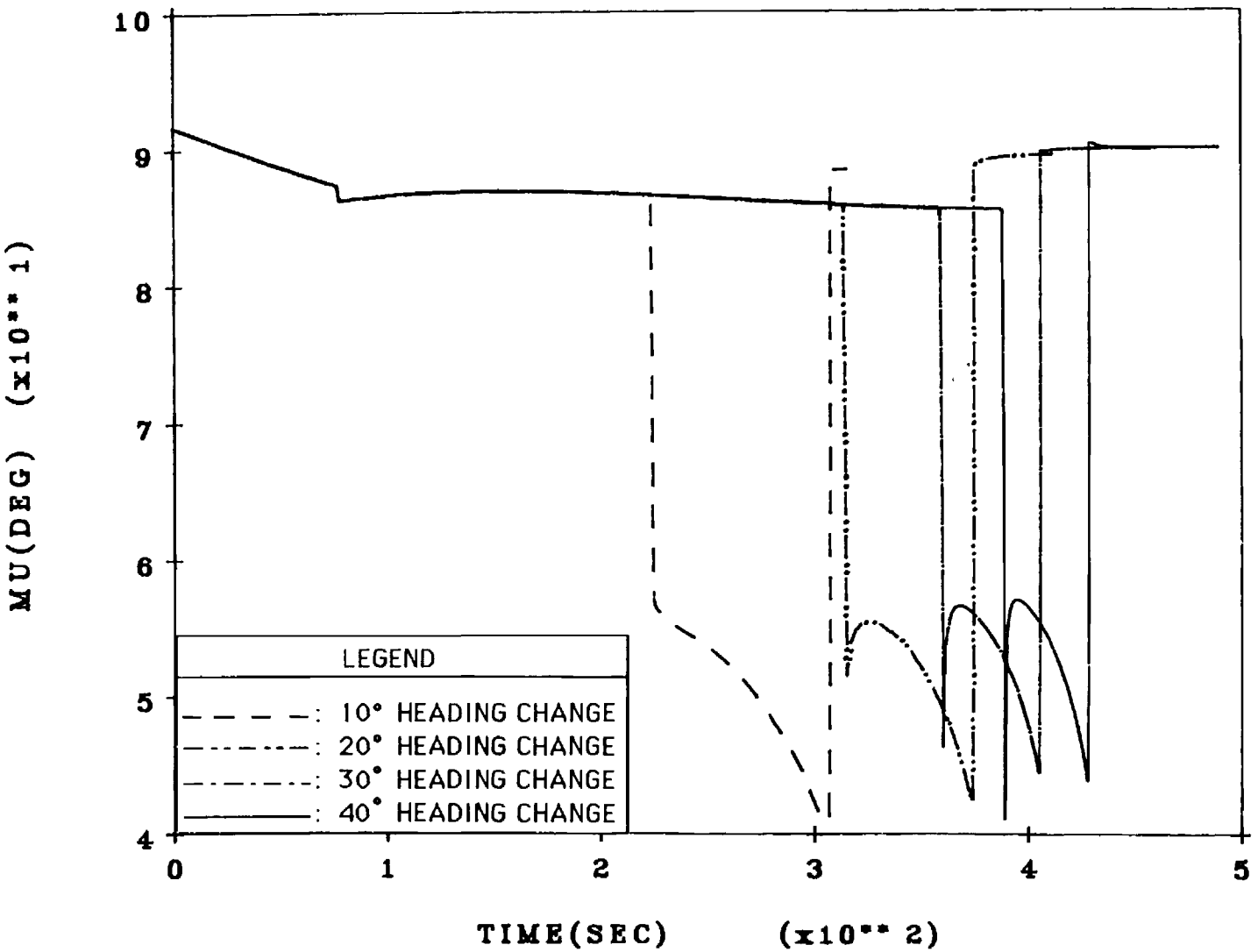

Figure 10. Guided solution bank angle profiles.

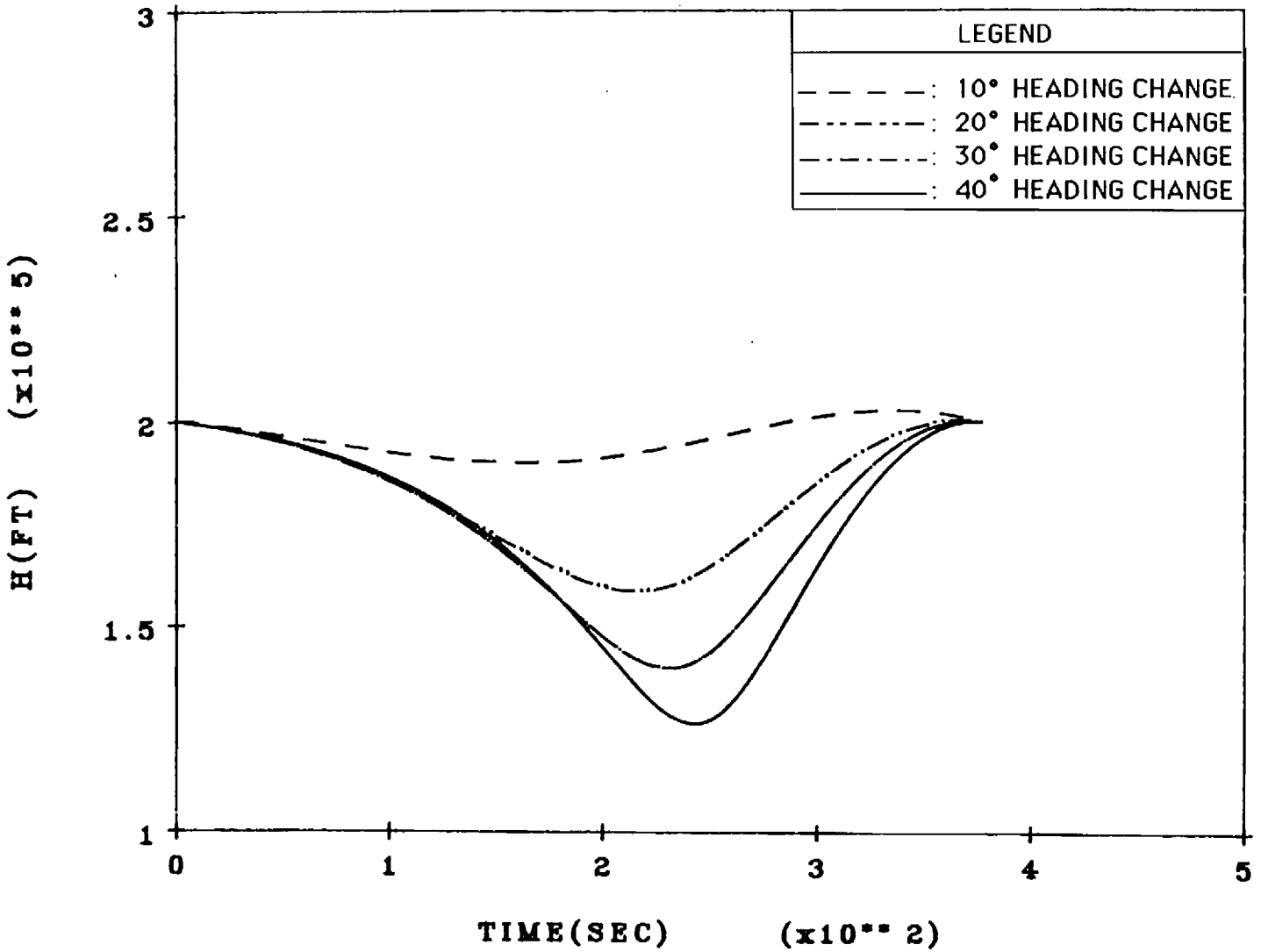

Figure 11. Optimal solution altitude profiles.

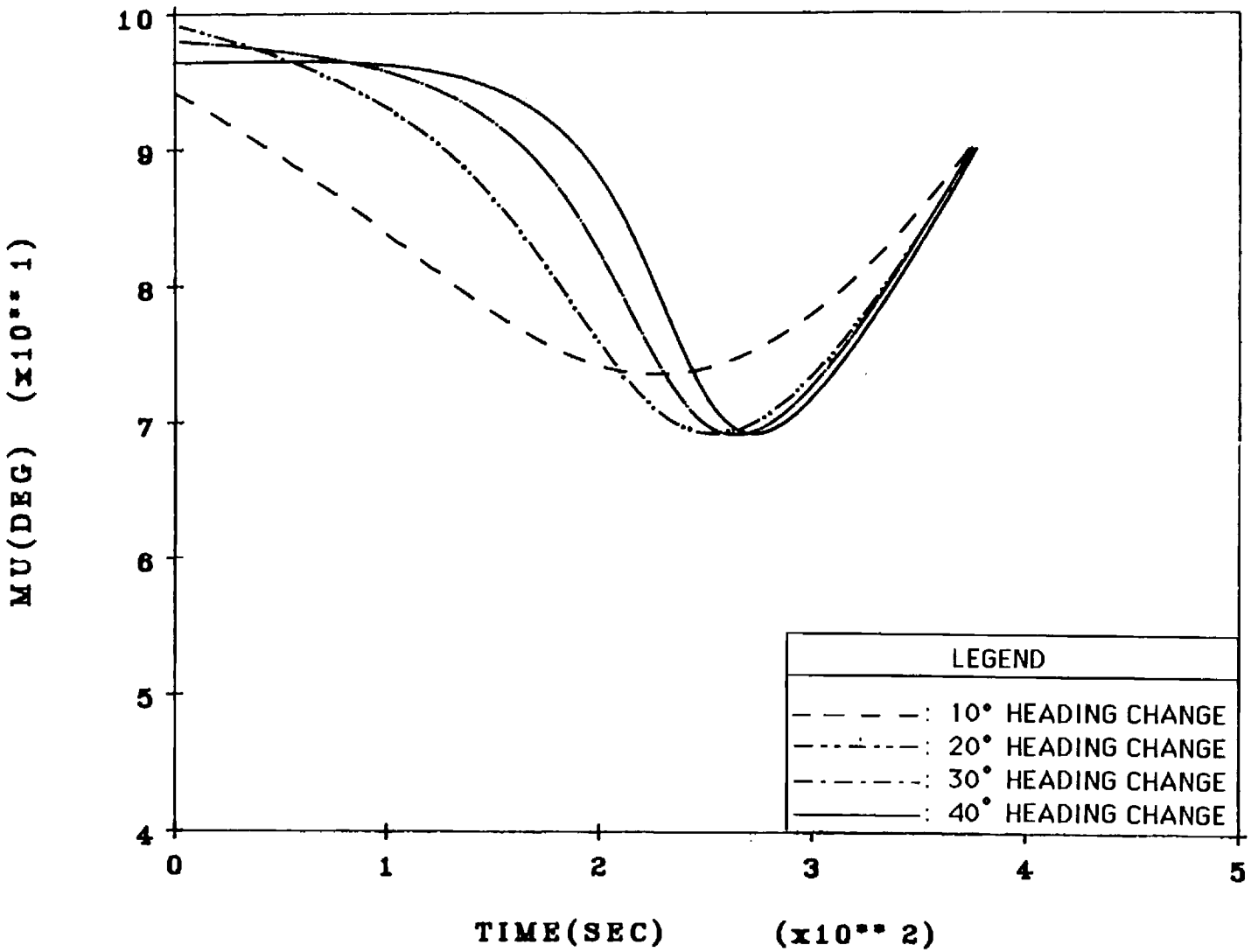

Figure 12. Optimal solution bank angle profiles.

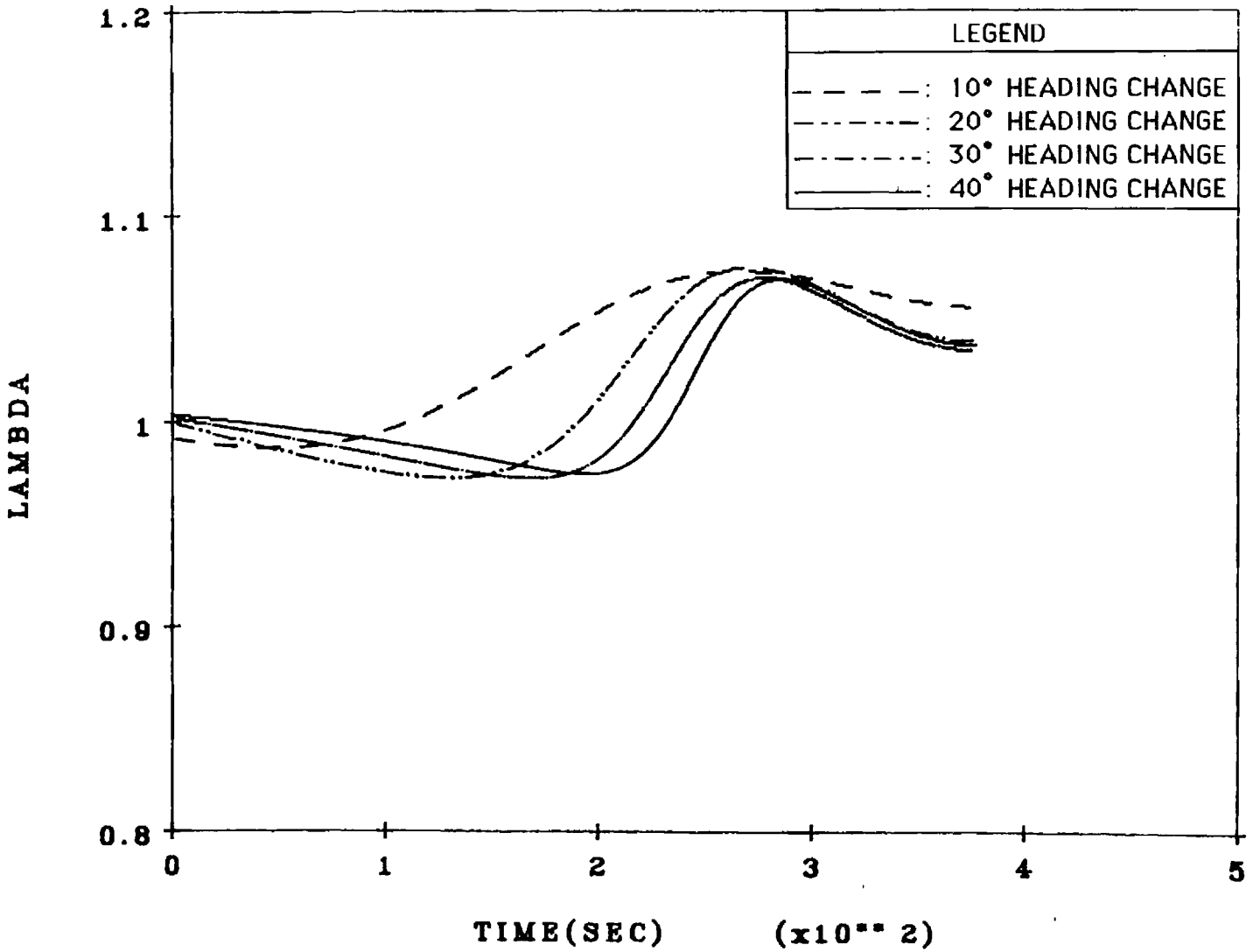

Figure 13. Optimal solution normalized lift coefficient profiles.

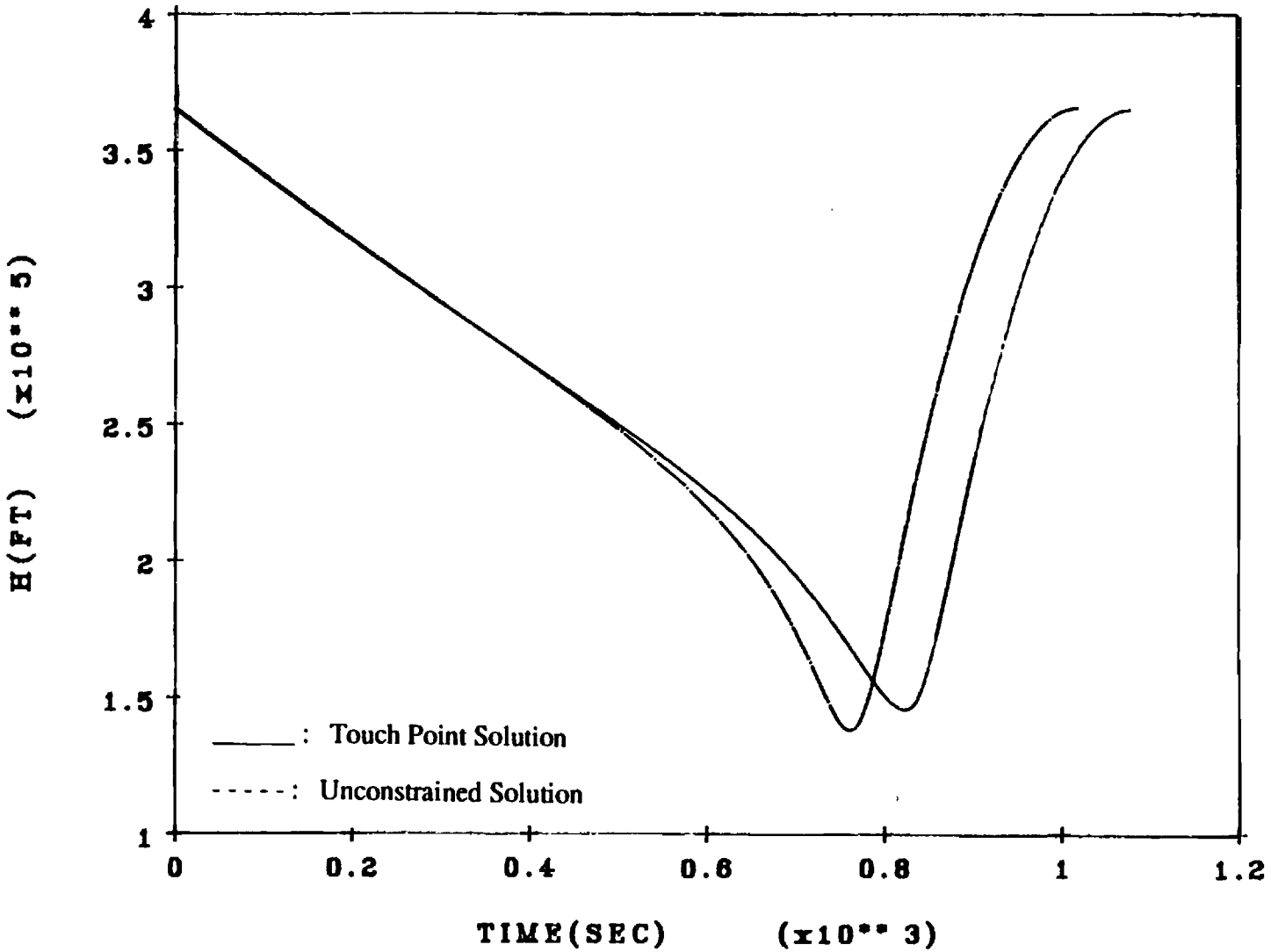

Figure 14. Altitude profiles for the unconstrained and touch point solutions.

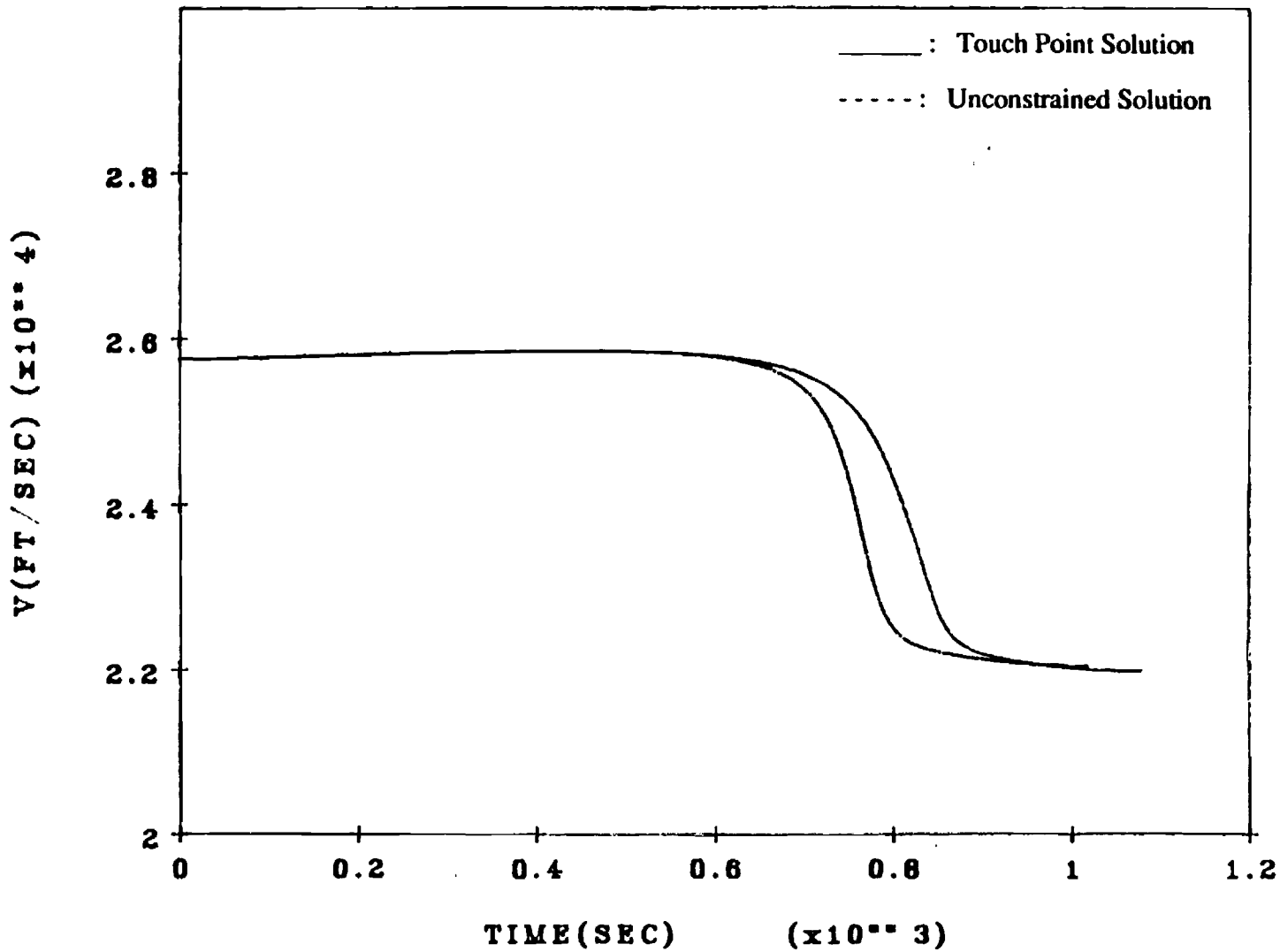

Figure 15. Velocity profiles for the unconstrained and touch point solutions.

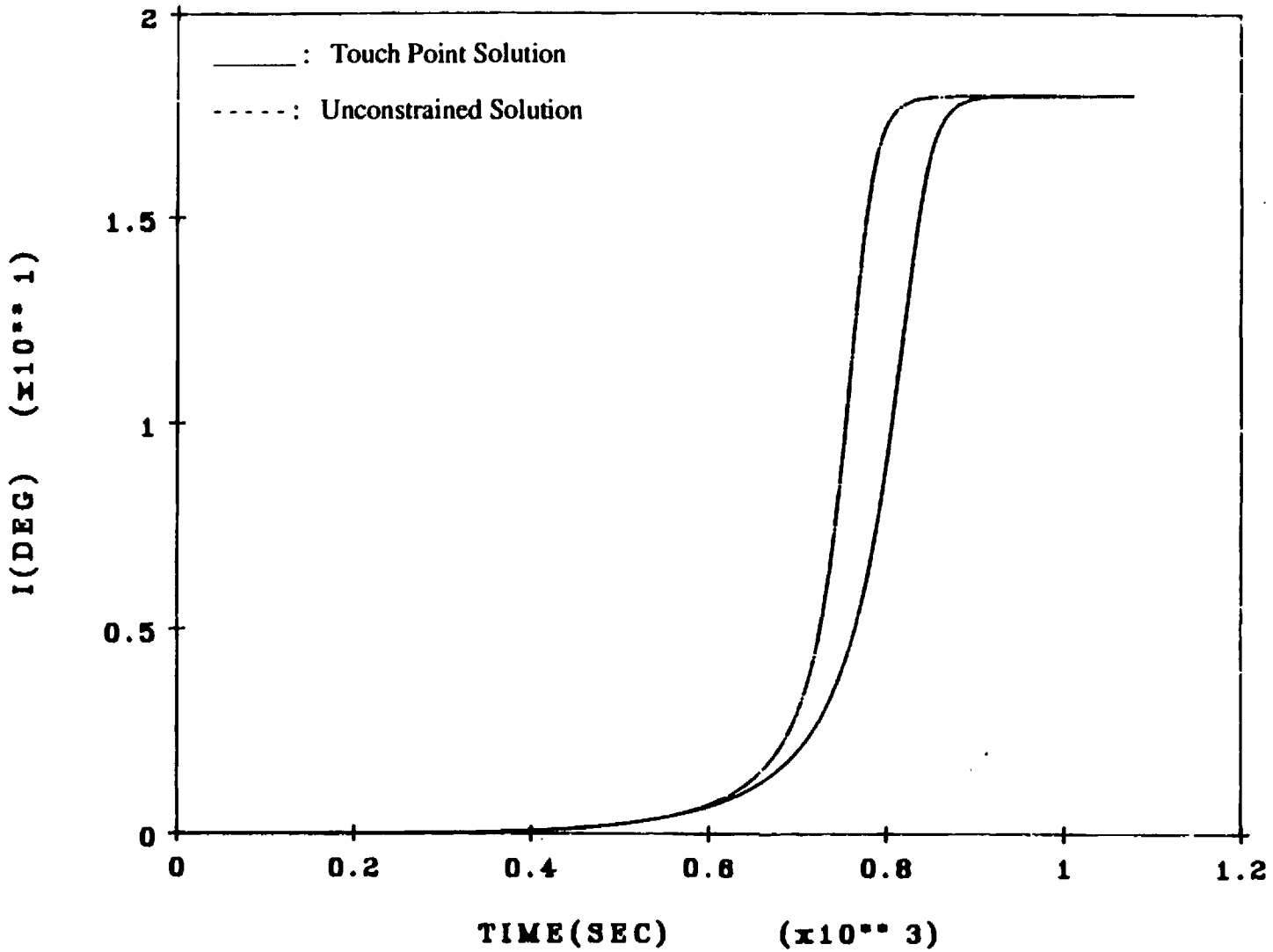

Figure 16. Inclination angle profiles for the unconstrained and touch point solutions.

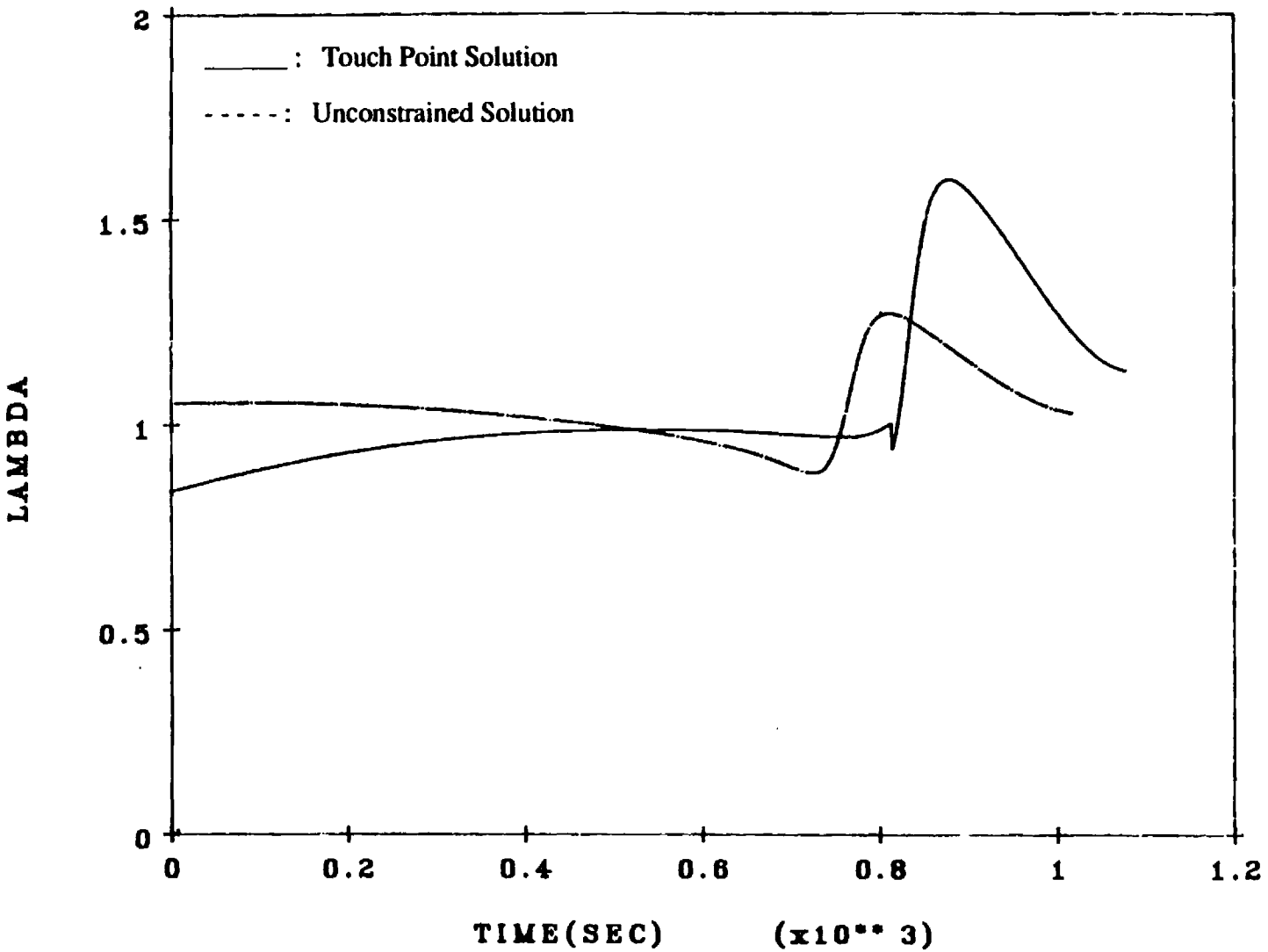

Figure 17. Normalized lift coefficient profiles for the unconstrained and touch point solution.

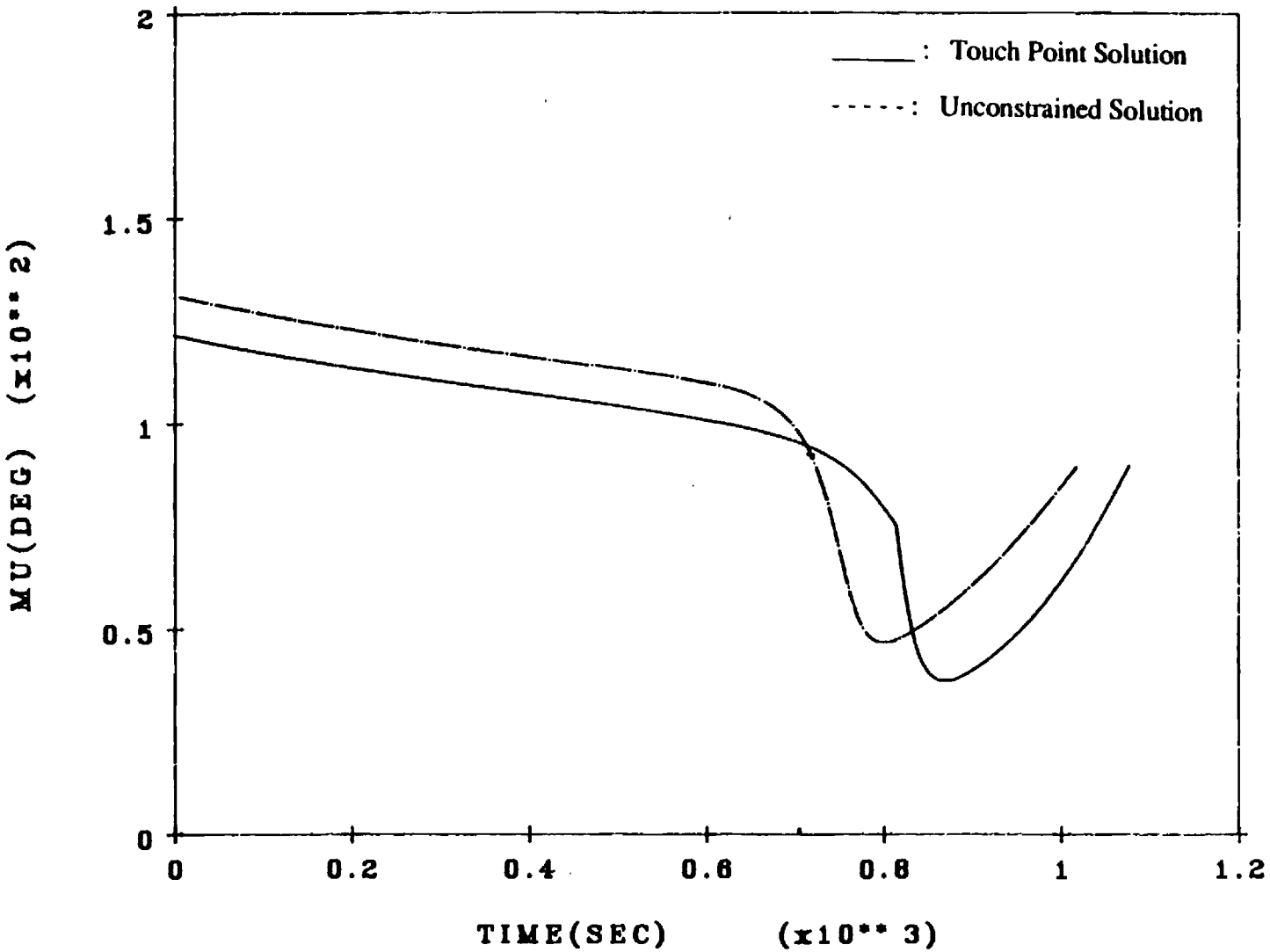

Figure 18. Bank angle profiles for the unconstrained and touch point solutions.

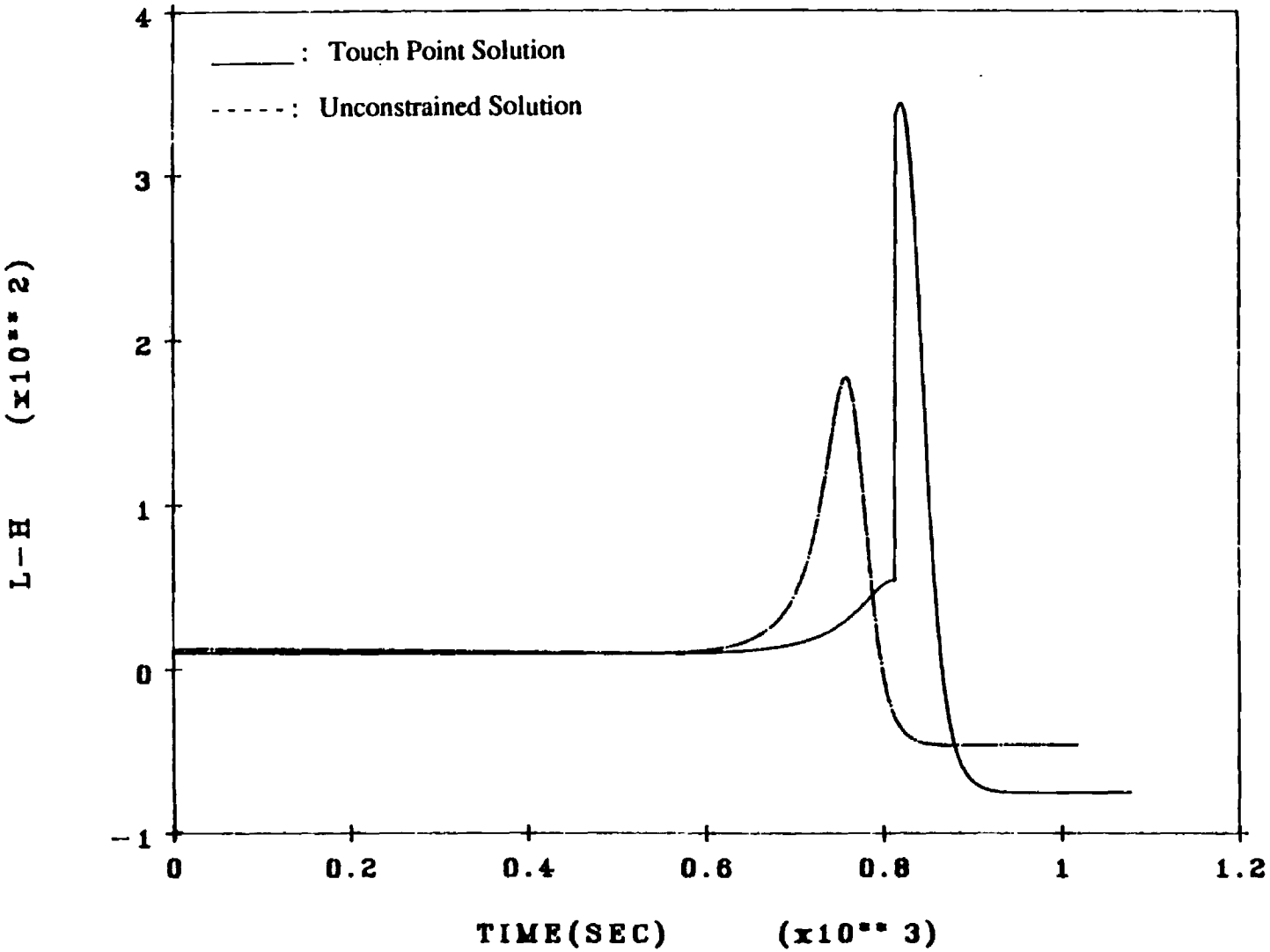

Figure 19. Altitude costate profiles for the unconstrained and touch point solutions.

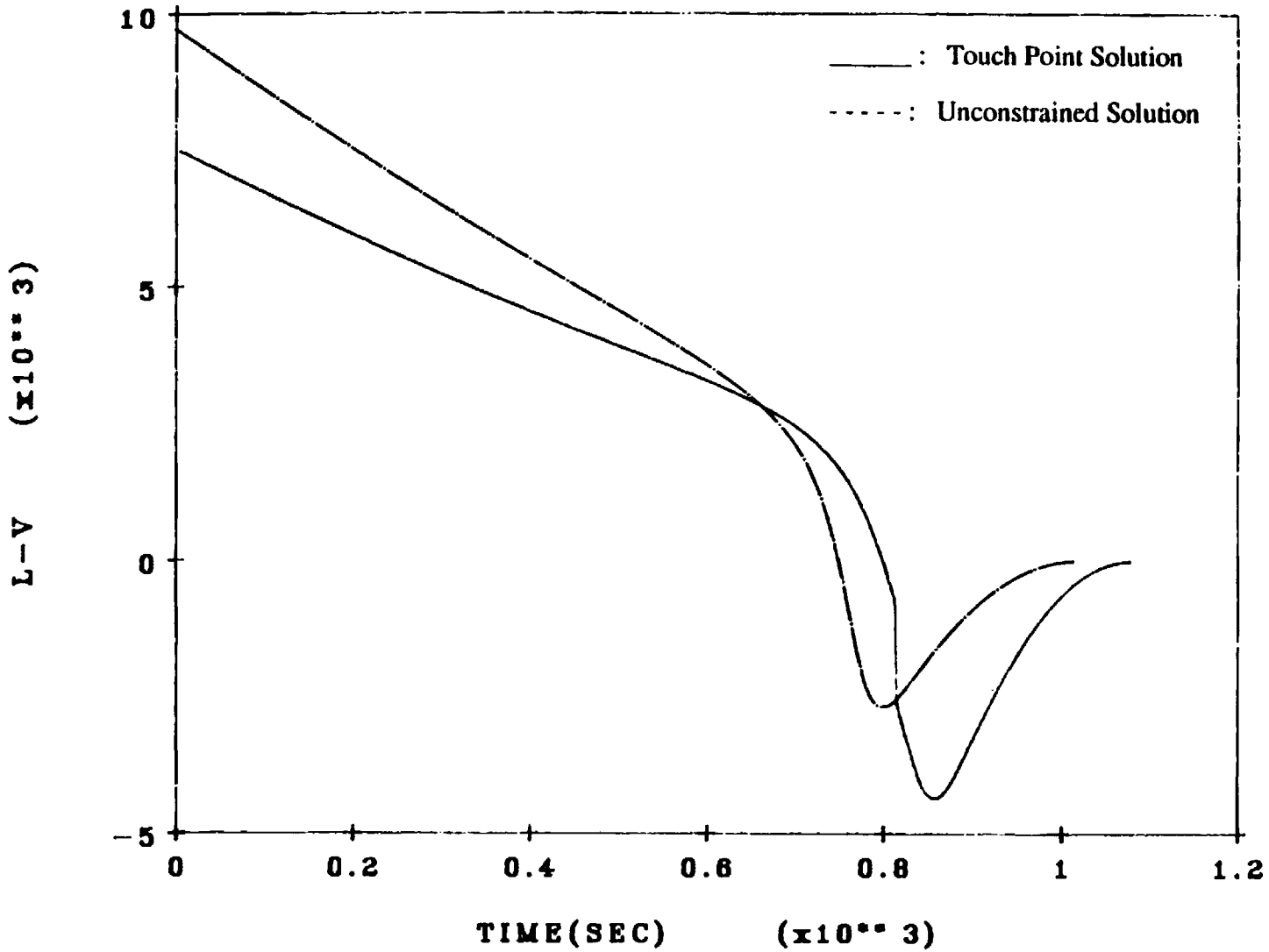

Figure 20. Velocity costate profiles for the unconstrained and touch point solutions.

Table 1
Comparison of Final Energies for the Reentry Problem

Guidance	Final Time	$E_f x10^8 (ft^2/sec^2)$	ΔE
Optimal	358.6	-4.813	1.510
SP1	397.0	-4.813	1.510
SP2	415.8	-4.814	1.511
SP3	398.0	-4.813	1.510

Table 2
Comparison of Energy Loss for the AOTV Problem

Heading Change	Optimal Solution $x10^7$	Guided Solution $x10^7$	%Error
10^o	4.713	4.971	5.47
20^o	8.858	9.109	2.83
30^o	12.38	12.63	2.04
40^o	15.40	15.66	1.69